HOST UNIVERSITY: Ghent University

FACULTY: Faculty of Engineering and Architecture

DEPARTMENT: Department of Flow, Heat and Combustion Mechanics

Academic Year 2016-2017

CFD Modeling of the Interaction between a Smoke plume and a Sprinkler Spray

Mohamed Beshir

Promoters: prof. dr. ir. B. Merci

dr. T. Beji

Master Thesis submitted in the Erasmus+ Study Program

International Master of Science in Fire Safety Engineering

Disclaimer

This thesis is submitted in partial fulfilment of the requirements for the degree of The International Master of Science in Fire Safety Engineering (IMFSE). This thesis has never been submitted for any degree or examination to any other University/programme. The author declares that this thesis is original work except where stated. This declaration constitutes an assertion that full and accurate references and citations have been included for all material, directly included and indirectly contributing to the thesis. The author gives permission to make this master thesis available for consultation and to copy parts of this master thesis for personal use. In the case of any other use, the limitations of the copyright have to be respected, in particular with regard to the obligation to state expressly the source when quoting results from this master thesis. The thesis supervisor must be informed when data or results are used.

Mohamed Beshir

Read and approved

30/04/2017

Abstract (English)

This thesis illustrates a detailed sensitivity analysis for the penetration capabilities of an Early Suppression Fast Response (ESFR) sprinkler spray over a smoke plume. The study was done by the Computational Fluid Dynamics (CFD) code namely Fire Dynamics Simulator (FDS) and the sensitivity analysis was based on the sprinkler flow rate, spray angle, droplet size, spray momentum, ceiling height, target area and the hot air plume momentum.

A hot air plume is assumed to represent a real heptane pool fire. Three different convective heat release rates (500 kW, 1000 kW and 1500 kW) were analyzed. Two hot air models (namely model A and model B) were investigated in this research. Where model A was proposed by O Mégret et al. and model B was developed in this research based on empirical correlations. The early hot air simulations showed the need to add synthetic turbulence at the boundary conditions. This was done by using the Synthetic Eddy Model (SEM). This synthetic turbulence helped the hot air plumes to act like real fire plumes by increasing the dissipation along the height. When comparing the velocity and temperature profiles along the heights of the pool fire simulations and the hot air plume simulations, the results were found to be promising, especially for model B in the region above the flame height.

The interaction between hot air plumes and water spray simulations were done under two different ceiling heights (6.0 and 3.0 m), where, three different heat release rates (500 kW, 1000 kW and 1500 kW) and six different water flow rates (1.9, 3.16, 4.42, 6.26, 7.58 and 9.48 l/s) were analyzed. The results are showing that, the drop size and the spray angles are the most effective parameters on the penetration capabilities. It was also indicated that (despite some exceptions) for a given sprinkler there is an optimal water flow rate corresponding to the highest penetration ratio within a practical range of fire sizes and water flow rates. In this research it was found to be 6.26 l/s for the 6.0 m ceiling case and 4.42 l/s for the 3.0 m ceiling case.

Abstract (Arabic)

خلاصه

تعرض هذه الرسالة العلمية تحليل حساسية مفصل لقدرات اختراق مرش مياه من نوع (ESFR) فوق عمود من الدخان. وقد تم إجراء الدراسة باستخدام برنامج حاسوبي لديناميكا الموائع (CFD) يسمى محاكي ديناميكا الحريق (FDS), و قد استند تحليل الحساسية على معدل تدفق الرش، زاوية الرش، حجم القطرات، قوه اندفاع القطرات، ارتفاع السقف، منطقة الهدف و قوه اندفاع عمود الهواء الساخن.

يفترض أن يمثل عمود الهواء الساخن حريقا حقيقيا لحوض من وقود الهيبتان. حيث تم تحليل ثلاثة معدلات إطلاق للطاقة حراريه (500 كيلوواط، 1000 كيلوواط و 1500 كيلوواط). تم في هذا البحث دراسة نموذجين للهواء الساخن (هما النموذج A والنموذج B), حيث طور O Mégret et al. النموذج (A) وقد تم تطوير النموذج(B) في هذا البحث بناء على بعض الارتباطات التجريبية. أظهرت عمليات محاكاة الهواء الساخن في بدايه البحث الحاجة إلى إضافة الاضطرابات الاصطناعية في ظروف بدايه تدفق الهواء وقد تم ذلك باستخدام نموذج(SEM). ساعد هذا الاضطراب الاصطناعي أعمدة الهواء الساخن على التصرف مثل أعمدة النار الحقيقية من خلال زيادة التبديد على طول الارتفاع. عند المقارنة بين ملامح السرعة ودرجة الحرارة على طول ارتفاعات نتائج محاكاة النار ومحاكاة الهواء الساخن، وجد أن النتائج واعدة، وخاصة بالنسبة للنموذج (B) في المنطقة فوق ارتفاع اللهب.

تمت دراسه محاكاة التفاعل بين أعمدة الهواء الساخن و مرشات المياه تحت ارتفاعين مختلفين للسقف هما (6.0 و 3.0 م)،لحالات تشمل علي ثلاثة معدلات مختلفة لإطلاق الطاقه الحراريه (500 كيلوواط، 1000 كيلوواط و 1500 كيلوواط) وستة معدلات تدفق مياه مختلفة (1.9، 3.16، 4.42، 6.26، 7.58، 9.48 لتر / ثانية). وقد اظهرت النتائج أن حجم القطرات وزوايا الرش هي أكثر الخصائص تأثيرا على قدرات الاختراق. وأشير أيضا إلى أنه (على الرغم من بعض الاستثناءات) لمرش مياه معين هناك معدل تدفق امثل للمياه, هذا التدفق يكون مقابل لأعلى نسبة اختراق ضمن نطاق معين من أحجام النار ومعدلات تدفق المياه. في هذا البحث وجد أن المعدل يكون تقريبا 6.26 لتر / ثانية في حاله ان ارتفاع السقف 6.0 م و 4.42 لتر / ثانية في حاله ان ارتفاع السقف 3.0 م.

Table of Contents

List of figures

List of tables

1. Introduction and Methodology

Sprinklers are the most widely spread fire control and suppression tool; it showed effective and reliable performance in firefighting in the last decades e.g., according to some statistics sprinklers can provide around 75% reduction in death rate within residential structures [1]. Based on that, many experimental and numerical studies were done to investigate, validate and test the ability of different types of sprinklers to deal with different fire scenarios (e.g., [2], [3], [4,[6],[24]).

There is no doubt, that the cost of testing the sprinklers' performance has been one the main barriers in front of developing and validating new sprinklers or the ability of the current sprinklers to deal with new fire scenarios, in addition to the cost, the long preparation times engaged to these experiments were always an obstacle. The Computational Fluid Dynamics (CFD) models –with its alternatively low cost- are considered as the main alternative to the experimental testing. The CFD models, however, needs to be well validated with benchmark experiments. With validated CFD models, the performance of different types of sprinklers can be tested and also it can be used to prove the safety of the new performance based designs in order to get the authority`s acceptance.

Being cheaper than the experimental approach, the CFD modeling approach still has its noticeable cost due to the large computational times. However, by understanding how these models are working, we still can by-pass some of its complexity and decrease the computational times in order to get cheaper and faster simulations. The turbulence, combustion and radiation are considered as the main three complicated processes and are requiring most of the computational time; therefore, the distinction patterns between the different models are mainly on how they solve these three obstacles [3]. Due to the fact that the modeling of the water sprays in interaction with fires is considered a physically complex process [5], there is a persistent need to decrease the complexity of this process while doing the CFD simulations.

As the main focus is usually on the sprinklers' performance, it was decided in this research to keep the water phase (sprinkler's water sprays) without any changes, however, the fires was substituted by hot air plumes. Recently, many studies were done using hot air plumes instead of the fires [2, 6, and 24] to decrease the simulations' times by avoiding modeling the combustion process and also to validate the CFD models with simple hot air experiments rather than real fires. Yet, to our knowledge, none of the previous hot air interaction with water sprays' computational studies simulated specific real fires by these hot air plumes. Therefore, in the first part of this work, numerical simulations that attempt to reproduce the same velocity and temperature profiles as in real fires using hot air plumes will be investigated, these trials will be based mainly on empirical and semi-empirical models.

The first study to develop a semi-empirical model for the determination of the physical characteristics of fires was done by O. Mégret et al. [7]. O. Mégret's model was based on few empirical correlations in addition to mathematical equations to define the heat release rate, smoke flow rate and smoke temperature (initial smoke characteristics) for heptane pool fires based on the pool diameter. Mégret also claims that this model could be used for any other liquid pool fires without difficulties. In this research, in addition to the procedure developed by Mégret et al.[7], we developed and tested another method to predict smoke characteristics. This method is based on the average temperatures and gas velocity on the centerline of

axisymmetric buoyant diffusion flames that have been measured by McCaffrey in 1979 [8] and by Kung and Stavrianides in 1982 [9]. For simplicity, through the whole document Mégret's model will be named as model A, while the other model will be named as model B.

In the second part of this research, a study will be done for the Large Eddy Simulations of Early Suppression Fast Response (ESFR) sprinklers' water sprays with respect to the ceiling height, spray angle, droplets mean diameter size, velocity of the spray flow rate (momentum), the grid size and the number of tracked particles in the Lagrangian approach, in addition to that, the trend of the results of this section will be compared to the trends found in [3 and 4].

In the third part, a study will be done for the interaction of the hot air plumes and the ESFR sprinklers' water sprays. This study will be done under two different ceiling heights (3.0 m and 6.0 m), six sprinklers flow rates (1.90, 3.16, 4.42, 6.26, 7.58 and 9.48 l/s) and three different convective heat release rates (500, 1000 and 1500 kW) from the hot air plumes. Additionally, a sensitivity analysis will be done based on the spray angle, a third ceiling height (8.0 m), target area, droplet mean size and the spray momentum. The trend of the results in this section will also be compared to the trends found in [3, 4].

To summarize, the research carried out herein is threefold:

(i) Modeling heptane pool fires using hot air plumes to give comparable results to the pool fire simulations, these simulations will be done for heptane pool fires of 500, 1000 and 1500 kW convective Heat Release Rates (HRR).
(ii) Modeling water sprays only without fires for Early Suppression Fast Response (ESFR) sprinklers and comparing it to the experimental results in [3 and 4].
(iii) Combine the two models of the hot air (gas phase) with the water sprays (water phase) to study the interaction between the hot air plume and the water sprays, then to compare these results to those found in [3 and 4].

All the CFD simulations in this research were done using the CFD package namely Fire Dynamics Simulator (FDS 6.1.2).

2. Gas phase simulations

2.1. Gas phase LES

The Fire Dynamic Simulator (FDS) is considered a Computational Fluid Dynamics (CFD) model, usually used to model buoyancy driven fluid flows (fires). The FDS works basically by solving numerically a set of Navier -Stokes Equations (NSE) of thermally driven and low speed flows. FDS is a free online source that was developed by the National Institute of Standards and Technology (NIST) and the smoke view is the visualization program used to display the FDS outputs. FDS is consists of Navier- stokes solver, turbulence model, combustion model, radiation model and boundary heat transfer.

Where, the Navier – Stokes Equations are [25]:

- Mass conservation equation:

$$\frac{\partial \rho}{\partial t} + \nabla.(\rho \boldsymbol{u}) = \dot{m}_b''' \quad \textbf{(}\textit{Equation 1)}$$

Where t is time, ρ is the air density and u is the velocity. The source term ($\dot{m}_b'''$) is representing the added mass from evaporating droplets or other sub-grid scale particles that represent e.g. sprinklers' sprays and fuel sprays. These are assumed by the FDS to occupy no volume, yet they are represented by the governing equations as point sources of mass, momentum and energy. It is also important to note that, for example, even though the water vapor is a product of the combustion process, it also could be evaporated from the sprinklers droplets and there must be one for which an explicit transport equation is solved. So, in this case, an explicit transport equation for water vapor is needed to distinguish between that which was produced by combustion and that produced by the evaporated water droplets.

- Energy conservation equation:

$$\frac{\partial(\rho h_s)}{\partial t} + \nabla.(\rho h_s \boldsymbol{u}) = \frac{D\bar{p}}{Dt} + \dot{q}''' - \dot{q}_b''' - \nabla.\dot{q}'' \quad \textbf{(}\textit{Equation 2)}$$

Where h_s is the sensible enthalpy, $\bar{p}$ is the background pressure, $\dot{q}'''$ is heat release rate per unit volume from a chemical reaction, $\dot{q}_b'''$ is the energy transferred to subgrid scale droplets and particles and the term $\dot{q}''$ represents the conductive, diffusive and radiative heat fluxes.

- Momentum conservation equation:

$$\frac{\partial \boldsymbol{u}}{\partial t} - \boldsymbol{u} \times \boldsymbol{\omega} + \nabla H - \tilde{p}\nabla\left(\frac{1}{\rho}\right) = \left(\frac{1}{\rho}\right)[(\rho - \rho_o)\boldsymbol{g} + \boldsymbol{f_b} + \nabla.\boldsymbol{\tau}] \quad \textbf{(}\textit{Equation 3)}$$

Where, H is the stagnation energy per unit mass, ω is the vorticity vector, $\tilde{p}$ is the perturbation pressure, f_b represents the drag force exerted by the sub-grid scale particles and droplets, τ is the viscous stress

and is closed via gradient diffusion with turbulent viscosity by the Deardorff eddy viscosity model (Will be discussed later).

The radiative source term and the combustion source term are needed to be modeled. The FDS uses sub models to model these terms. However, due to the limited number of the pages of this thesis these models will not be discussed here and it can be checked into details in [25].

The practical flows are mostly turbulent and it is also important to note that the FDS uses the Large Eddy Simulations (LES) to describe a turbulent flow (where turbulent energy contained in largest scales). LES approach means that only the large scales of motion will be solved and the effect of the smallest scales of motion will be modeled, it is also important to note that, the default turbulent model used in FDS 6 is the Deardroff turbulence model. All in all, the FDS only solve the large energy scales and model the small energy scales (sub-grid scales) which is assumed to be only a small portion of the turbulent kinetic energy.

2.2. Hot air models

The gas phase in this document refers to the hot air plume models. The methodology of the hot air plumes and smoke that results from burring of fuels at the fuel bed is to rise up governed by buoyancy and momentum, where the buoyancy and momentum are governed by the hot air velocity and temperature. Basically, any fire is just an exothermic chemical reaction that will create air with hot temperature (buoyancy) and high velocity (momentum) at the fuel bed. The velocity and temperature of the air can affect the life safety in the building, it can create radiation which can highly affect the occupancy and also can help in the flame spread to the surrounding, it can also -if reached the ceiling- create ceiling jets which will activate the ceiling detectors. In addition to that, the hot air plumes can also affect the ability of the sprinklers sprays or the water mist to deal with the fire, where the velocity can affect the momentum factor and the temperature can affect the vaporization of the water droplets. Based on that, many experimental and computational works were done to investigate the hot air plumes [2, 6, and 24].

It was found that the main factors that affect the turbulent plumes simulated by the LES approach are the Sub Grid Scale (SGS) turbulent viscosity models and the inflow boundary conditions [24]. In this work the simulation of the hot air plumes using the LES approach will be done by the FDS 6, which by default is using the Deardroff turbulent viscosity model variation [25]:

$$\boldsymbol{\mu_t = \rho\, C_v \Delta \sqrt{k_{sgs}}\,;\; k_{sgs} = \frac{1}{2}\left((\bar{u} - \hat{u})^2 + (\bar{v} - \hat{v})^2 + (\bar{w} - \hat{w})^2\right)} \quad \textit{(Equation 4)}$$

Where, μ_t is turbulent viscosity transport coefficient, C_V is constant set to 0.1, ρ is the density, $\bar{u}$ is the average value of u at the grid cell center and $\hat{u}$ is a weighted average of u over the adjacent cells:

$$\boldsymbol{\bar{u}_{ijk} = \frac{u_{ijk} + u_{i-1,jk}}{2}\;;\; \hat{u}_{ijk} = \frac{\bar{u}_{ijk}}{2} + \frac{\bar{u}_{i+1,jk}}{4}} \quad \textit{(Equation 5)}$$

Where $(\hat{v},\hat{w})$ and $(\bar{v},\bar{w})$ are defined in the same way.

As mentioned in the introduction, the aim of the first part in this research is to provide comparisons between the average velocities and temperatures along the axis of the plume of the simulations done by the combustion and simulations using hot air plumes. The main interest will be the smoke part of the plume. So, while using any upcoming defined models; the main concern will be given to the plume part above the flame height. For simplicity, it is explained in Figure 1, the diagram on the left is for the pool fire case and the diagram on the right is for the hot air case. During our analysis in this research, we focus on the ability of the hot air plumes to give similar temperature and velocity profiles to that of the combustion simulations along the plume axis in region B, where the average flame height is noted as region A.

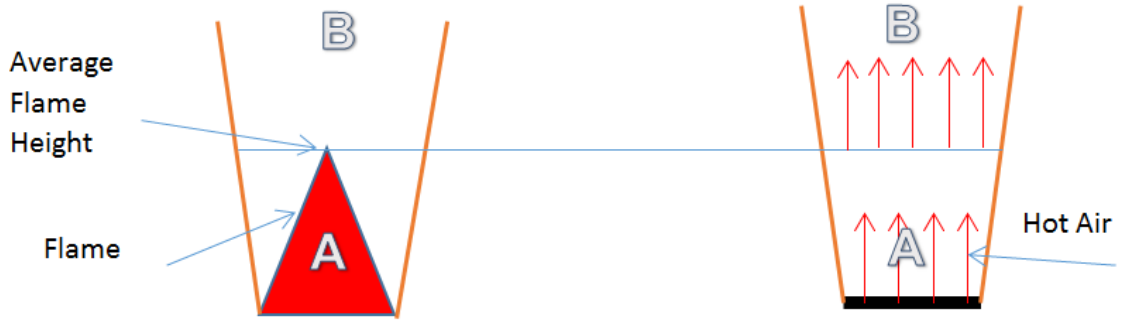

Figure 1 simple sketch for the pool fire (left) and the hot air plume (right)

Two models will be used to quantify for a given convective Heat Release Rate (HRR) and diameter of a pool fire, the smoke flow rate and the temperature along the axis of the plume, as mentioned in the introduction the two models will be named as model A and B.

2.2.1. Model A

Model A is the semi-empirical model proposed by O. Mégret [7]. Model A is based on the concept of choosing the pool fire diameter and the type of the fuel and based on the nominating pool fire diameter, a sequence of equations can be followed to calculate the HRR, flow rate and the temperature along the axis. Mégret et al. based their model on Heptane pool fires and their main goal was to estimate the temperature and flow rate of heptane pool fires in tunnels, however, the model could be extended to any other liquid pool fires without difficulties.

2.2.1.1. Pool fire chemistry

For sake of simplicity, only one global reaction is considered herein:

$$\text{Fuel} + \text{Oxidizer} \longrightarrow \text{Products} \quad \text{(R1)}$$

In reality, the combustion process involves complex mechanisms and hundreds of sub-reactions with thousands of intermediate species [10]. However, in fire applications the complex combustion process can be simplified into one step reaction (R1).

To follow Mégret model, one should be able to balance a stoichiometry combustion equation. Stoichiometry means that the fuel in the combustion process have got the exact amount of oxidizer needed for complete combustion and there is absolutely no excess or less amount of oxidizer in the process. For complete stoichiometric combustion reaction there is usually two ways to balance the equation depending on the oxidizer itself, whether it is pure oxygen or oxygen mixed with another component (e.g. nitrogen for oxygen in air), in this case we only care about the complete combustion when the oxidizer is the oxygen in the air (Assuming that the air available consists exactly of 21 % O_2 and 79 % N_2 by volume). The general equation of complete combustion will be written as the following [11, 7]:

$$C_xH_y + \left(x+\frac{y}{4}\right) O_2 + \frac{79}{21}\left(x+\frac{y}{4}\right) N_2 \longrightarrow x\ CO_2 + \frac{y}{2} H_2O + \frac{79}{21}\left(x+\frac{y}{4}\right) N_2 \quad (R2)$$

In addition to the previously mentioned outputs in R2, there will be heat released from this exothermic equation.

Based on R2, the stoichiometric combustion reaction for the heptane will be as the following:

$$C_7H_{16} + 11(O_2 + 3.76N_2) \longrightarrow 7\ CO_2 + 8\ H_2O + 41.36N_2 \quad (R3)$$

In real fires, the combustion reaction is never stoichiometric. It is whether fuel rich which means that there is too little oxidizer or fuel lean which means there is excess of oxidizer. In our case we will be studying fires in open environment, so the fires will be always fuel lean which means that the complete combustion reaction should be written by adding up the amount of air used to stoichiometry burn the heptane to the excess amount of the entrained heated air.

Therefore, the amount of the air (Nitrogen and Oxygen) in R.3 will depend on the amount of air entrained. Based on that, the nitrogen and oxygen at the output of R.3 can be written like that:

$$n(O_2+3.76N_2)_{To} \longrightarrow n(O_2+3.76N_2)_T \quad (R.4)$$

Where, T_o is the ambient temperature, T is the heated air temperature and n is the air entrainment ratio (mol air/mol heptane).

2.2.1.2. Heat release rate (HRR)

For complete reactions for pool fires, the HRR by complete reaction as that mentioned in (R.2) can be calculated using the following equation:

$$\dot{Q} = X\dot{m}''A\Delta Hc \quad (Equation\ 6)$$

Where $\dot{Q}$ is the heat release rate (kW), X is the combustion efficiency (in this research it is assumed to be 1), $\dot{m}''$ is the burning rate per unit area (kg/m^{2}s), A is the heptane pool fire area, ΔHc is the net calorific value at 298 K (kJ/kg of combustible). The total heat released by the fires is usually distributed into two

parts, the first part is the convective heat release rate which is the amount of heat released and carried by smoke, the other part is the HRR lost by radiation from the fire to the surrounding.

The amount of the heat lost from the fire by radiation can be estimated from the radiative fraction which is a global parameter and is fuel-dependant. For heptane the radiative fraction (X_R) is assumed to be 0.3 [11]. Therefore the convective HRR ($\dot{Q}_C$) can be calculated using the following equation:

$$\dot{Q}c = (1 - X_R)\dot{m}''\text{A}\Delta\text{Hc} \quad (\textit{Equation 7})$$

2.2.1.3. Smoke flow rate

To calculate the smoke volume flow rate, first the smoke induced volume for a given mass of fuel should be calculated. Based on (R.3), it is possible to calculate the smoke induced volume by inserting the molecular weight of the combustion products and the equilibrium coefficients in the following equation:

$$\boldsymbol{Vs} = \frac{\boldsymbol{\nu_m} \sum_{\boldsymbol{products}} \boldsymbol{a_i}}{\boldsymbol{a_c M_C}} \boldsymbol{m_c} \ (\textit{Equation 8})$$

Where, V_s is the volume of smoke (m^3), ν_m is the molecular volume at (298 K, 1 atm) (m^3/mol), a_i is the product of combustion's equilibrium coefficient (mol), a_c is the combustible's (heptane) equilibrium coefficient (mol), M_c is the molecular weight of combustible (kg/mol) and m_c is the combustible mass (kg).

Using the following values in Equation.8:

Table 1 Equation.8 variables' values

$\boldsymbol{\nu_m}$	24.46 l/mol
$\mathbf{a_{CO2}}$	7 mol
$\mathbf{a_{H2O}}$	8 mol
$\mathbf{a_{N2}}$	41.36 + 3.76n
$\mathbf{a_{o2}}$	N mol
$\mathbf{a_c}$	1 mol
$\mathbf{M_c}$	0.1 kg/mol

Then for heptane pool fire:

$$V_s = (13.8+1.2n)\text{Ax}\rho_c \quad (\textit{Equation 9})$$

Where, x is the thickness of the heptane layer in the pool fire (m) ρ_c is the density of the combustible (kg/m^3). To calculate the smoke volume flow rate of the heptane pool fire, the volume of smoke should be divided by the combustion time. To calculate the combustion time in seconds (t_c), the following equation will be used:

$$t_c = \frac{(\text{x}.\rho_c)}{\dot{m}''} \quad (\textit{Equation 10})$$

Therefore, the smoke flow rate at ambient conditions (q_o) in m^3/s can be calculated with the following equation:

$$q_o = \frac{V_s}{t_c} \quad \textit{(Equation 11)}$$

The pervious equation calculated the smoke flow rate without including the heating expansion effect on the smoke, so to take it into account the ideal gas law was used (where "o" refers to ambient conditions and "s" refers to smoke):

$$\rho_o \, q_o = \rho_s q_s \quad \textit{(Equation 12)}$$

Therefore the final equation to calculate the volume flow rate of smoke:

$$q_s = [13.8+1.2n] \, A\dot{m}'' \frac{T_s}{T_0} \quad \textit{(Equation 13)}$$

Where, T is temperature.

2.2.1.4. Smoke temperature

Assuming that all the heat released in the combustion reaction will be produced as sensible heat and transfer with the smoke, the smoke temperature can be calculated by integrating the summation of the specific heat of each combustion product species multiplied by its equilibrium coefficient as the following:

$$\Delta H_c = \int_{To}^{Ts} \sum a_i \, C_{pi} \, dT \quad \textit{(Equation 14)}$$

Where, C_{pi} is the specific heat at constant pressure (J/kg.K) for products

Assuming that 0.3 of this heat is lost by radiation, the integral equation will lead to second order polynomial equation which depends mainly on the amount of air entrained.

$$(30.7+2n)10^{-3}T_S^{\,2}+(407+32n)\,T_S-(8.77\,10^5+9.9\,10^3 n)=0.0 \quad \textit{(Equation 15)}$$

2.2.1.5. Mass Loss Rate Per Unit Area (MLRPUA)

In order to estimate the combustion time, we need to calculate the burning rate which is the MLR for a given amount of fuel. The MLRPUA is a function of (D) the pool fire diameter (m) as the following:

$$\dot{m}'' = \dot{m}''_{\infty}\left(1 - e^{-k\beta D}\right) \quad \textit{(Equation 16)}$$

Where, $\dot{m}''_{\infty}$ the limiting burning rate of Heptane is taken = 0.101 kg/m^2s [13]

$$k\beta = 0.8 \ m^{-1} \ [12]$$

2.2.1.6. Air entrainment ratio

The air entrainment ratio which is noted as the coefficient n, is the amount of air entrained by natural convection, in other words it is the ratio between the numbers of moles of the entrained air to the number of moles of the fuel. Some experimental studies were done before in [13] to investigate the amount of air entrainment into heptane pool fires, with diameters ranging from 0.3 to 6 m. In [13] Koseki and Yumoto, ended up with an empirical correlation between the amount of air entrained, the radius of the pool fire and the height above the pool as the following:

$$n= 11(2.13(h/R)^{0.53} -1) \text{ where } h/R > 0.5 \quad \textit{(Equation 17)}$$

Where, h is the height above the pool (m) and R is the heptane pool fire radius (m).

2.2.1.7. Flame height

To calculate the amount of air entrained using equation 17, it is essential to calculate the flame height. Mégret used Thomas's classical equation [14] to calculate the flame height as the following:

$$\frac{Z}{D} = 42\left[\frac{\dot{m}''}{\rho_o (gD)^{0.5}}\right]^{0.61} \quad \textit{(Equation 18)}$$

Where, Z is the flame height (m), D is the heptane pool diameter (m) and g is the gravitational acceleration (m^2/s).

2.2.1.8. Summary

Mégret Model:

Based on the equations' sequence mentioned before and the values proposed for heptane fuel, Mégret's model can be summarized in the following simple sequence for heptane pool fires:

Megret`s model is composed of two sets of equations that leads to the main fire characteristics of a heptane pool fire based on the value of the diameter:

- Convective heat release rate.
- Smoke flow rate.
- Temperature of smoke.

The set of main equations:

1. $\dot{Q}_C = (1 - X_R)\dot{m}''A\Delta Hc$
2. $q_S = [13.8 + 1.2n]\, A\dot{m}''\frac{T_S}{T_0}$
3. $(30.7+2n)10^{-3}T_s^{\,2}+(407+32n)T_S-(8.77\ 10^5+9.9\ 10^3\ n)=0.0$

The set of secondary equations:

1. X_R= 0.3.
2. $\dot{m}'' = \dot{m}''_{\infty}(1 - e^{-k\beta D})$
3. n= 11(2.13($\frac{h}{R}$)$^{0.53}$-1)
4. $\frac{Z}{D} = 42[\frac{\dot{m}''}{\rho_o(gD)^{0.5}}]^{0.61}$

2.2.2. Model B

Model B is proposed to evaluate the boundary conditions of the hot air plume at the pool fire bed's level. Model B is much simpler than model A, it is only based on two simple equations.

2.2.2.1. Temperature

The first equation is to calculate the temperature at boundary condition using McCaffrey's empirical correlation [8] (which will be discussed further later in 2.3.3.1) to calculate the temperature at the flame region, which will be always independent on the HRR and is approximated to be 870 ℃ independent on the type of the hydrocarbon fuel or the diameter of the pool fire [14].

Where:

$$\frac{2g\Delta T}{T_o} = (\frac{k}{C})^2 (\frac{h}{\dot{Q}^{2/5}})^{2\eta-1} \quad \textit{(Equation 19)}$$

Where, ΔT is (T_S -T_0), T_S is smoke temperature (℃) and T_0 is the ambient temperature (℃).

At the flame region the values of the constants are as the following:

k= 6.8 $m^{1/2}$/s

C= 0.9

η= ½ (so the term where the HRR is mentioned will be raised to the power zero)

2.2.2.2. Velocity

As the first boundary condition for the hot air temperature is the 870℃. To maintain the same convective HRR, the following equations [10] should be followed:

$$\dot{Q}c = \dot{m}\, C_p\, (T_s - T_o) \quad \textit{(Equation 20)}$$

Where,

$$\dot{m} = \rho\, \dot{v} \quad \textit{(Equation 21)}$$

$$\dot{v} = W_S \,.A \quad \textit{(Equation 22)}$$

$$\boldsymbol{\rho_s} = \left(\frac{\mathbf{353}}{\boldsymbol{T_s}}\right) \textit{(Equation 23)}$$

Therefore,

$$\dot{Q}c = \left(\frac{353}{T_s}\right) W_s \, A \, C_p \, (T_s - T_o) \quad \textit{(Equation 24)}$$

Where, W_S is the smoke velocity (m/s) and $\dot{v}$ is the volume flow rate. Based on equation 24, since the convective heat release rate and smoke temperature are known, the velocity of the smoke can be easily calculated. For example, for convective HRR equal to 1500 kW, C_p = 1 kJ/kg.k and area equal to 1 m^2, the velocity of the hot air at the boundary condition should be 5.7 m/s. Using the following proposed simple graph as shown in Figure 2 , by knowing the Heat Release Rate Per Unit Area (HRRPUA) for the simulated fire, the velocity of the boundary condition can be expected.

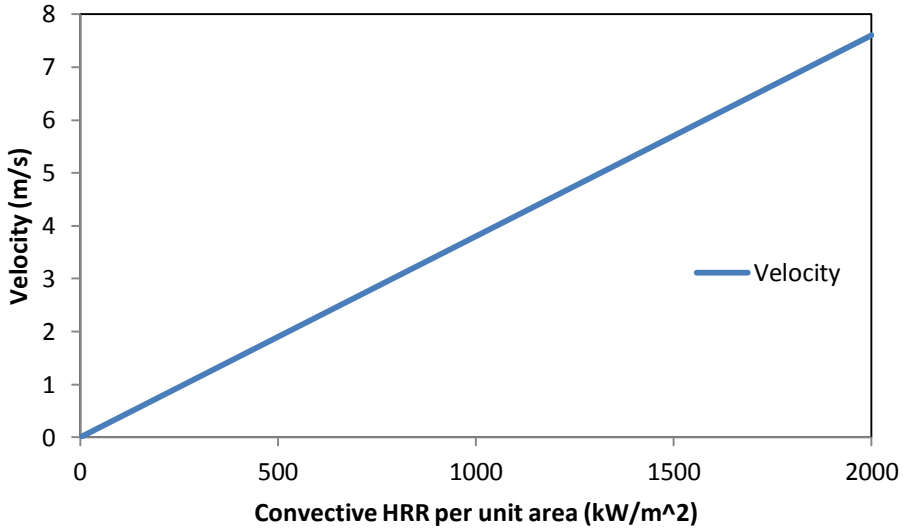

Figure 2 Velocity - HRRPUA relation for model B

2.2.3. Set up and boundary conditions

The computational domain (which was used for both the hot air and the combustion simulations) is set as the following: 5 m × 5 m × 10 m (width × depth × height) and with open boundary conditions at the sides and the top as shown in Figure 3. The boundary conditions (which will be injected in the domain at the same level and area of the pool fire's bed in the combustion simulations) for the hot air plumes are presented in table 2, which also shows that all the hot air plumes (especially model B)were buoyancy driven flows (like real fires) not momentum driven as the Froude number was around 1 in most of the cases [24].Where, Froude number in general is a dimension less number used in hydrodynamics to indicate how well a particular model works in relation to reality, in our case it is a measure of the importance of momentum and buoyancy in the system and for natural fires (buoyancy driven flows) is

usually around 1, however, in case of momentum driven jets, it could go to up to 10 000. So, the lower the Froude number the more the buoyancy is dominating the flow [24]. The densimetric Froude number can be calculated by the following equation:

$$\mathrm{Fr} = \frac{T_o V_i^2}{\Delta T\, g D} \quad (Equation\ 25)$$

Where Fr is the densimetric Froude number, V_i is for the inlet to the velocity and D is the hydraulic diameter.

Table 2 Boundary Conditions

Model	Convective HRR (kW)	Inlet Temperature ℃	Inlet Velocity (m/s)	Froude Number	Area (m^2)
A	500	531	2.18	0.278	1
A	1000	435	4.8	1.61	1
A	1500	387	7.6	4.7	1
B	500	873	2	0.131	1
B	1000	873	3.8	0.49	1
B	1500	873	5.78	1.172	1

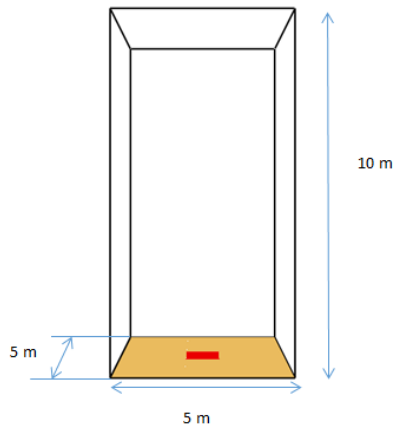

Figure 3 the computational domain used for the hot air and the combustion simulations

A uniform and structured mesh has been used in the whole domain with a cell size of 0.1 m. For fire plumes, it is recommended by Baum, McGrattan & Rehm [15] that the burner surface should be covered

by at least 10 × 10 cells. In all of our simulations, the burner surface or the vent surface (in case of hot air) is covered by at least 10 × 10 cells. Also to ensure having small enough cell sizes to get computationally accepted results, the mesh resolution index R^* should be calculated using the following equations:

$$R^* = \frac{\max(\Delta x, \Delta y, \Delta z)}{D^*} \quad \textit{(Equation 26)}$$

Where:

$$D^* = \left(\frac{\dot{Q}}{\rho_0 T_o C_p \sqrt{g}}\right)^{\frac{2}{5}} \quad \textit{(Equation 27)}$$

According to Ma & Quintiere [16] the plume dynamics can be simulated accurately only when the R^* = 0.1 or less, in most of the simulations the R^* was less than 0.1.

2.3. Gas phase results

2.3.1. Turbulent boundary conditions

The default turbulent viscosity model Deardorff is used and as it is shown in Figure 4 (a and b) using Deardorff model only, did not give a sufficiently turbulent flow at the inlet that gives reasonable and realistic flow pattern comparable to that of the simulation with a combustion pool fire.

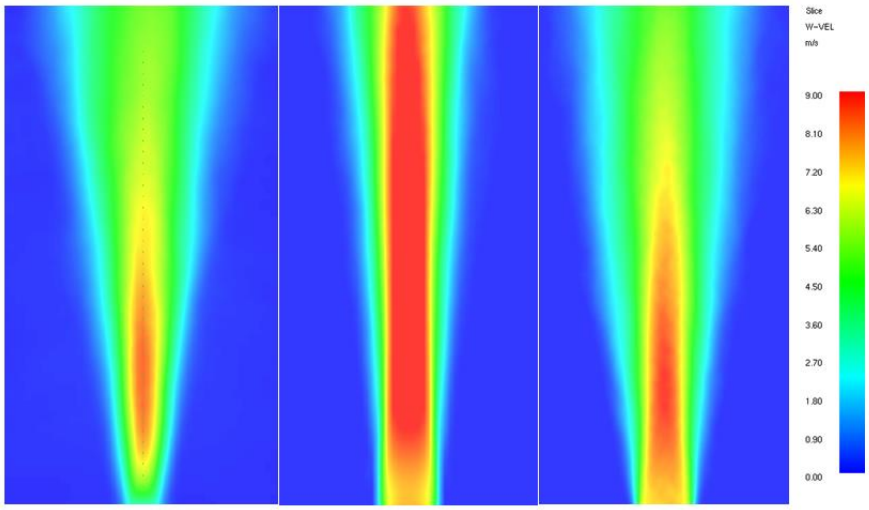

(a) (b) (c)

Figure 4 the average velocity pattern for (a. Heptane combustion pool fire, b. Hot air simulation using the default Deardorff model only, c. Hot air simulation using SEM)

This raises the importance of the turbulent inflow boundary condition. The turbulence inflow boundary condition is one of the most important inlet boundary conditions for the buoyancy driven flows (e.g. smoke). As the main aim in the hot air simulations was to reproduce the same temperature and velocity

realistic patterns along the plume z-axis, there was a persistent need to generate realistic turbulence boundary conditions.

Jarrin [17] gave an overview of different ways to change the turbulence boundary conditions for the LES and (Direct Numerical Simulations) DNS. Jarrin distributed these ways into three groups; recycling methods, synthetic turbulence methods and forcing techniques, where in this research we used the synthetic turbulence method. To use the synthetic turbulence method in FDS, we used the Synthetic Eddy Method (SEM) with eddy length scale$l_{eddy} = 0.1\,m$, where the eddy length scale was calculated to be (D/10), number of eddies = 1000 [10] and the velocity root mean square value was calculate from the following equation [18]:

$$\text{RMS} = \sqrt{\boldsymbol{w'^2}} = \mathbf{0.5}\,\dot{\boldsymbol{Q}}^{\mathbf{1/5}} \quad \textit{(Equation 28)}$$

Figure 4 (c), presents how does the SEM affect the velocity flow pattern. The hot air flow breaks up earlier and closer to the boundaries (inlet) because of the synthetic added turbulence which emulated the turbulence boundary conditions of the hot smoke and causes dissipation, which made the hot air behavior more toward the combustion simulations. After involving the SEM at the boundary conditions, the hot air simulations are giving acceptable and realistic trends that could be compared to the real fires' simulations. Next step is to examine –to what extent- could the previously explained models capture the velocity and temperature profiles along the axis that corresponds to the values obtained from the combustion simulations.

In this section, a comparison will be done between the numerical data from the hot air simulations and the pool fire simulations to expect the velocity and temperature along the axis of the plume. Three sets of comparisons were done in this research for the heptane pool fires based on the value of the convective HRR as the following: Set.1: 500 kW, Set.2: 1000 kW and Set.3: 1500 kW.

It is good to note that, based on the output signals from the simulations in this research; the steady state is assumed to start after 20 seconds from the beginning of the simulations for both the hot air and combustion simulations. Therefore, the average taken for both of the velocity and temperature along the axis for 40 seconds, specifically after 20 seconds from the beginning till 60 seconds.

2.3.2. Sensitivity analysis

2.3.2.1. Cell size sensitivity analysis for hot air simulations

A sensitivity analysis for the cell size was done to ensure that a reasonable cell size is used, three simulations were done using three different cell sizes varying descending as 0.25 m, 0.10 m and 0.06 m respectively. As it is shown in Figure 5, the cell size of 0.25 was too coarse and the cell size of 0.10 seems to be fine enough as by going further with the finer mesh of 0.06 m the results is almost the same. In all the cell size sensitivity analysis in this research, the cell size will be assumed as fine enough when the difference in the results' values between this cell size and the finer cell size is less than 10%.

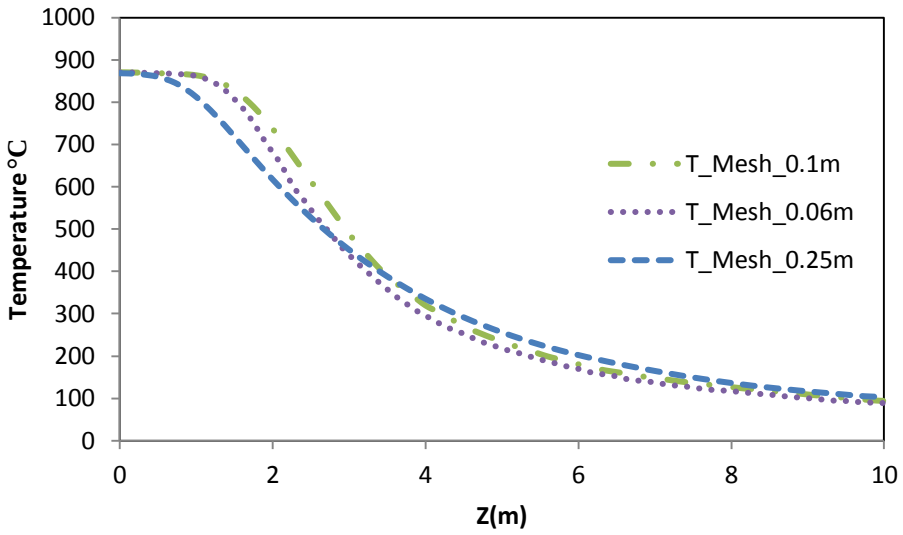

(a)

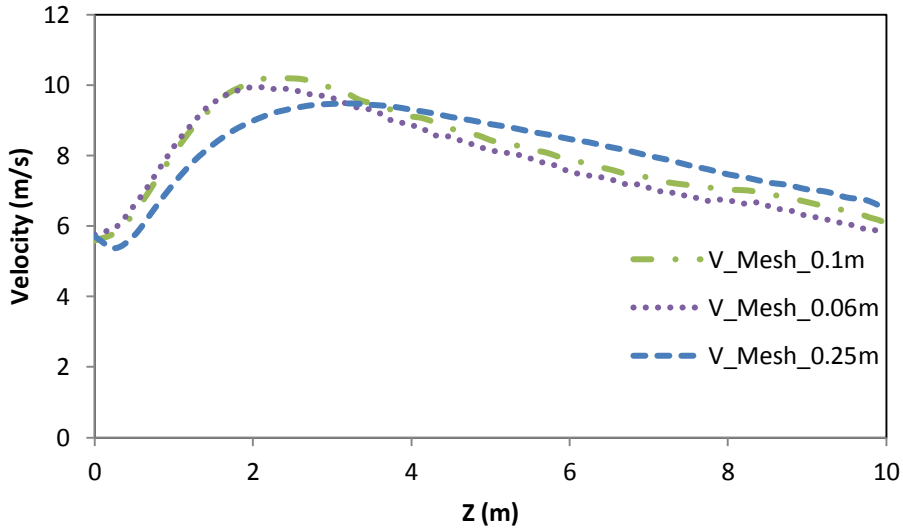

(b)

Figure 5 temperature (a) and velocity (b) average patterns along the plume axis with cell size = 0.25, 0.10 and 0.06 m

2.3.2.2. Cell size sensitivity analysis for the combustion simulations

For the combustion simulations we compared between the cell size of 0.2 m 0.1 m and 0.05 m. We did the cell size sensitivity analysis for the three heat release rates and we found that the 1500 kW is showing the most deviation when comparing the 0.1 m cell to the 0.05 m. However, it was still reasonable enough to be considered as independent on the cell size. As shown in Figure 6 Cell size sensitivity analysis

combustion simulation 1500 kW, the results are matching for both the temperature and velocity (with a maximum error of 8% at the far field of the velocity).

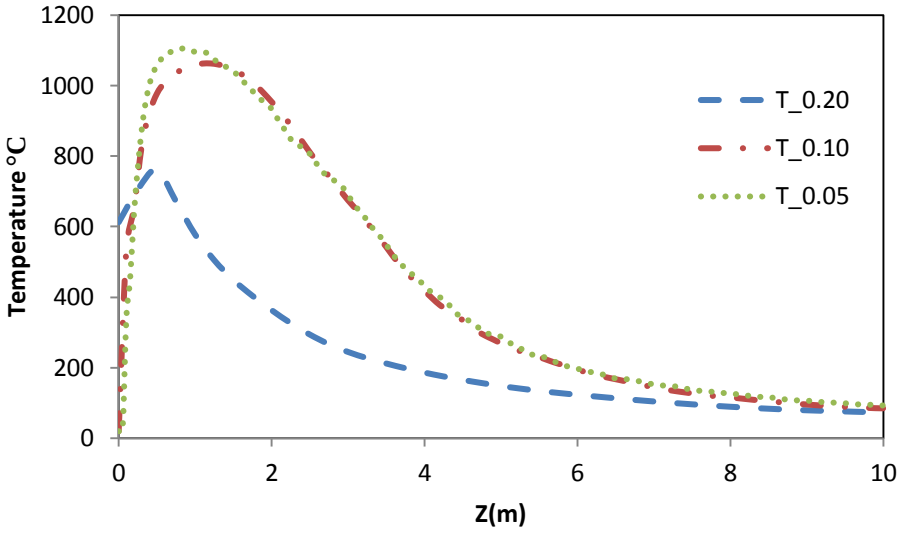

(a)

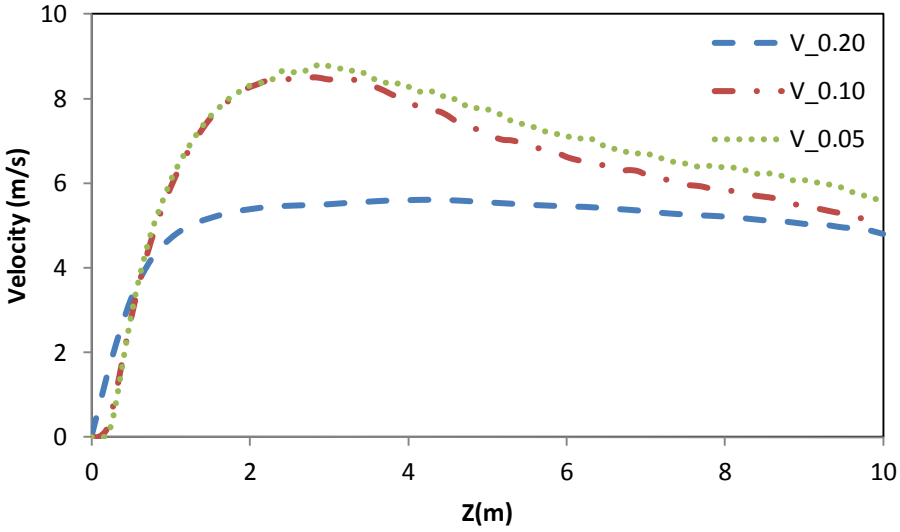

(b)

Figure 6 Cell size sensitivity analysis combustion simulation 1500 kW (a) Temperature and (b) Velocity

2.3.2.3. Number of eddies

The number of eddies was found to have slight effect on the computational time, e.g. when the number of eddies used was 100 eddies instead of 1000 eddies there was a 10 % decrease in the computational time,

therefore, simulations using 100 eddies, 1000 eddies and 15000 eddies were done to investigate the effect of the number of eddies on the data and to recommend decreasing it in case it is possible.

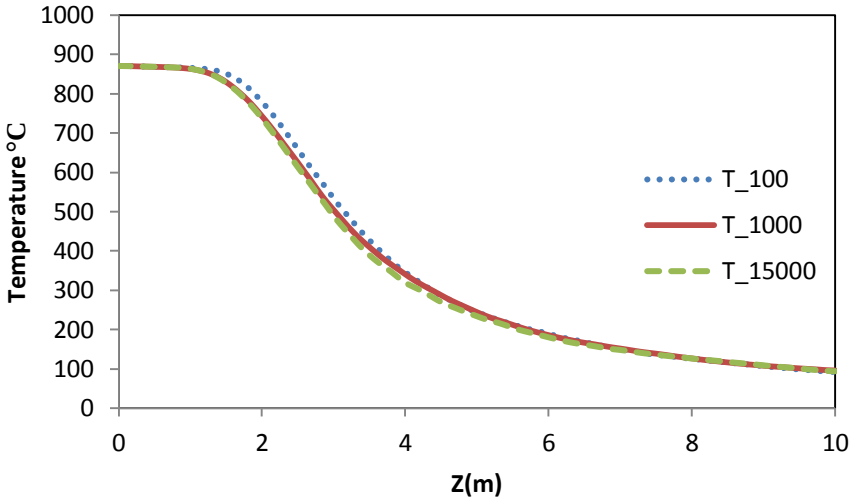

(a)

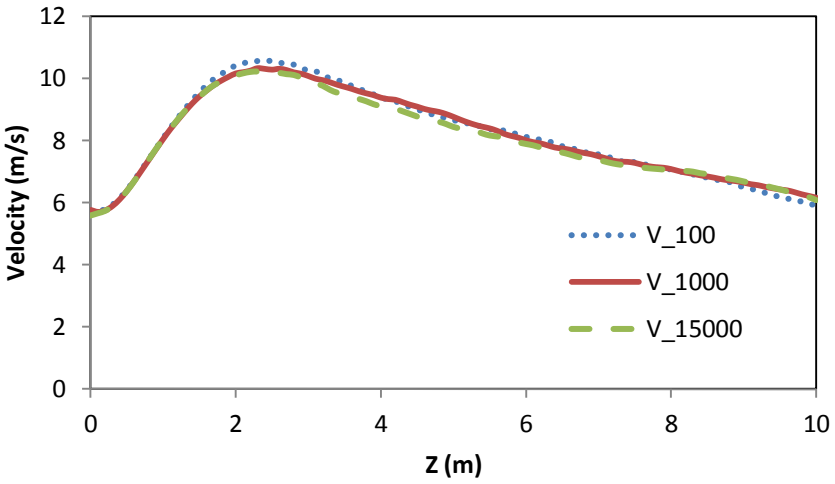

(b)

Figure 7 Temperature (a) and Velocity (b) average patterns along the plume axis with number of eddies = 100, 1000 and 1500 eddies

As it is shown in Figure 7 for both the temperature and velocity respectively, the number of eddies has very small and negligible effect on the data. It is therefore recommended to use 100 eddies instead of 1000 to decrease the computational time. Note: Both of the two previously mentioned sensitivity analyses were done for the 1500 kW simulations. Sensitivity analyses were done also for the 1000 and 500 kW simulations and gave the same results, so it is not shown here.

2.3.3. Empirical correlations, Combustion and hot air simulations

2.3.3.1. Combustion simulations vs. McCaffrey empirical correlations

First, the combustion simulations were compared to the empirical correlations proposed by McCaffrey to show the deviation between our combustion simulations' profiles and the expected empirically based profiles. Where the combustion simulations' parameters used in this research are shown in Table 3.

Table 3 Combustion simulations' parameters

Convective HRR (kW)	MLRPUA (kg/s.m^2)	Heat of Combustion (kJ/kg)	Area (m^2)
500	0.0160	44580	1
1000	0.0319	44580	1
1500	0.0479	44580	1

McCaffrey measured the average temperatures and gas velocities on the centerline of axisymmetric buoyant diffusion flames for methane as a fuel with a burner of 0.3 m square, also Kung and Stavriandes did the same for hydrocarbon pool fires with a wide range of diameters (1.22, 1.74 and 2.42 m)[14]. McCaffrey then proposed that there are three regions of the fire plume namely (Flame, Intermittent and Plume) as shown in Figure 8. Where for each of which there were specific correlations between temperature and gas velocity as presented in table 4.

It is clear in Figure 8, that the average temperature is almost constant in the flame part and is independent on the convective heat release rate of the fire, the flame temperature at the flaming part can be approximated to 870 ℃ as mentioned before. The temperature then decreases in the intermittent part to reach around 320 ℃ at the boundary of the buoyant plume. Based on that, the temperature at the flame height will probably be between 500 to 600 ℃.

For the velocity profile, McCaffrey noticed that the velocity at the near filed is not dependent on the value of the convective heat release rate and it increases with the increase of the Z (height) till it reaches the maximum value before the intermittent part starts, where the velocity will be constant and independent on the Z value. However, McCaffrey noticed that the value of the maximum velocity reached in the flame part is directly dependent on the value of $\dot{Q}_C{}^{1/5}$, which means that, when the fire size is too large, the downward momentum of the sprinkler spray might not be able to overcome the strong momentum generated by the fire and won't be able to penetrate the plume to reach the fuel bed. It was also noted that after the constant value of the intermittent part, the velocity will start to decrease as shown in Figure 9 Temperature (a) and velocity (b) profiles comparisons for combustion pool fires and McCaffrey correlation.

The calculations for McCaffrey correlations for both the temperature and velocity were done for the heat release rates of (500, 1000 and 1500 kW) fires and compared to the results from the combustion pool fires by the FDS.

Table 4 Summary of centerline data for a buoyant methane diffusion flame [14]

Centreline velocity: $\frac{u_0}{Q^{1/5}} = k\left(\frac{z}{Q^{2/5}}\right)^{\eta}$

Centreline temperature: $\frac{2g\Delta T_0}{T_0} = \left(\frac{k}{C}\right)^2\left(\frac{z}{\dot{Q}^{2/5}}\right)^{2\eta-1}$

Region[a]	k	η	$z/\dot{Q}^{2/5}$ (m/kW$^{2/5}$)	C
Flame	6.8 m$^{1/2}$/s	1/2	<0.08	0.9
Intermittent	1.9 m/kW$^{1/5}$·s	0	0.08–0.2	0.9
Plume	1.1 m$^{4/3}$/kW$^{1/3}$·s	−1/3	>0.2	0.9

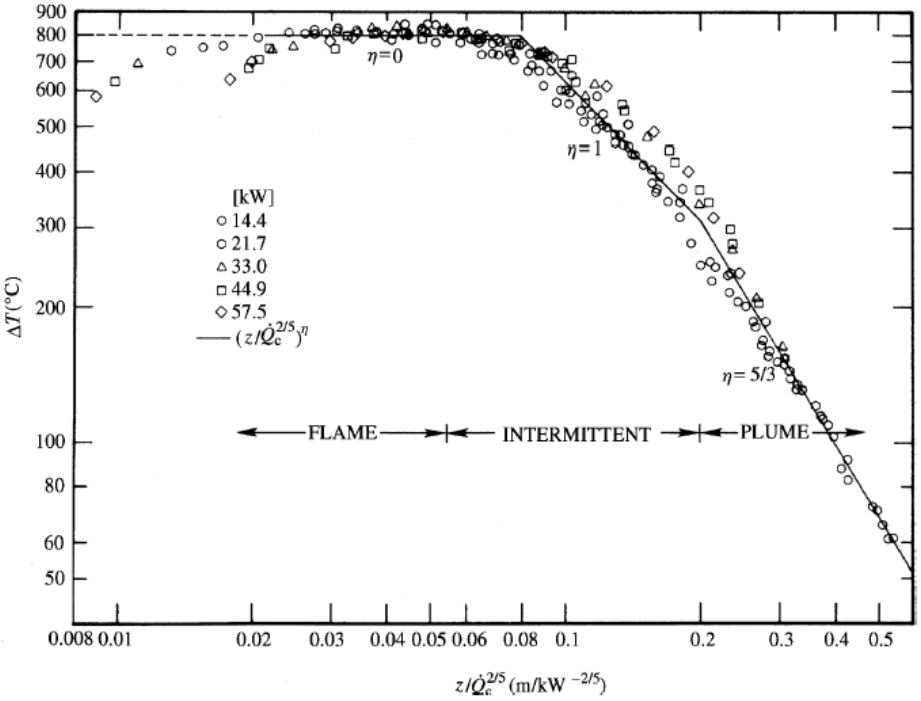

Figure 8 Variation of centerline temperature rise with height in a buoyant methane diffusion flame [14]

- Temperature profiles:

As it is presented in Figure 9(a) for the heat release rate of 500 kW, the temperature is expected perfectly by the combustion pool fire simulation for both the intermittent and plume regions, in addition to the maximum temperature in the flame part. In Figure 10(a) for the 1000 kW, the temperature was over estimated by the pool fire simulation with an average deviation of 15 % in the intermittent part; however, it is well expected in the plume region. In Figure 11(a) for the 1500 kW, the temperature was overestimated by the pool fire simulation with an average deviation of 20 % in the intermittent region; yet, it was well expected in the plume region. So it can be concluded that, for the temperature profiles, the FDS simulations well expected the values in the plume region for the three fire sizes and slightly over estimated the values in the intermittent part where the deviation increased with the increase of the fire size.

- Velocity profiles:

As noticed by McCaffrey, the maximum velocity value increased with the increase of the fire size. As presented in Figure 9, Figure 10 and Figure 11 (b) the maximum velocity was approximately 7, 8 and 9 m/s for the fire sizes 500, 1000 and 1500 kW respectively. It was also noted that, the FDS simulations underestimated the velocity values for the three fires sizes by around 5 % in the intermittent region and by around 15 % in the plume region.

- 500 kW:

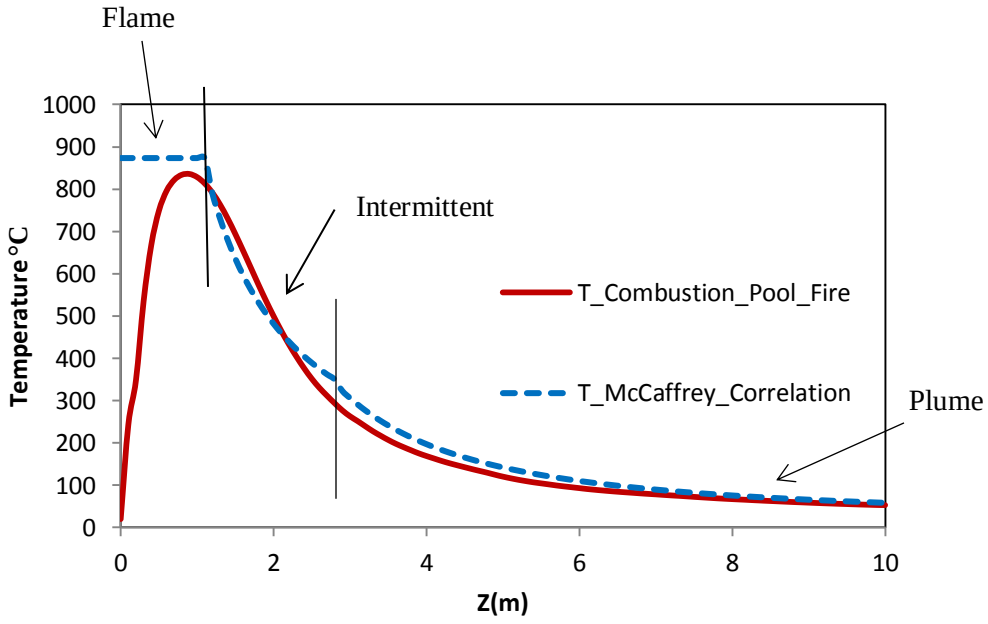

(a)

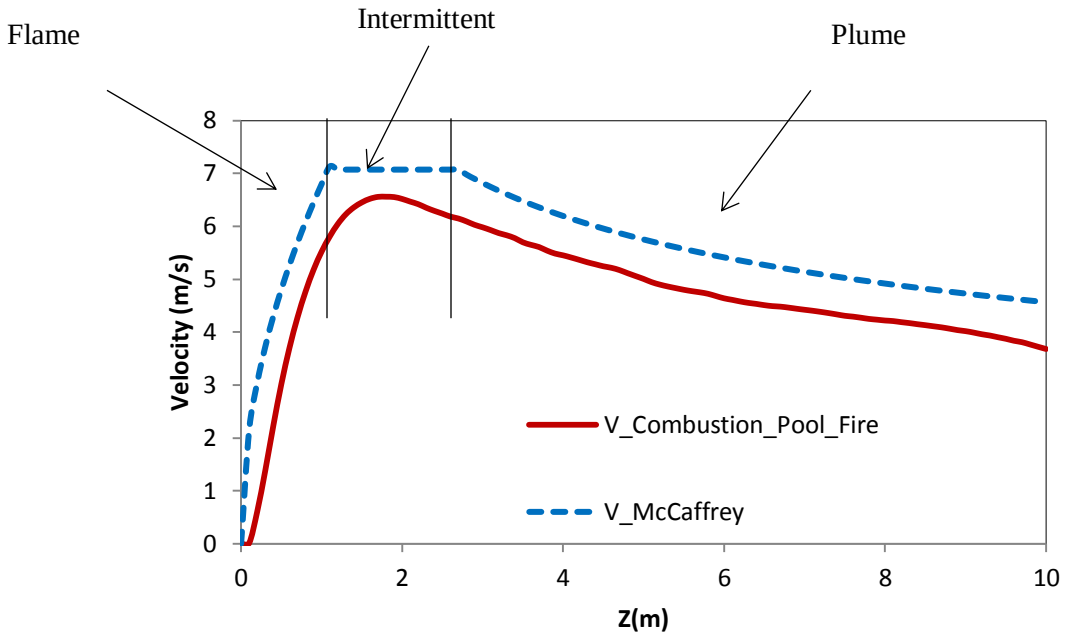

(b)

Figure 9 Temperature (a) and velocity (b) profiles comparisons for combustion pool fires and McCaffrey correlation (500 kW)

- 1000 kW:

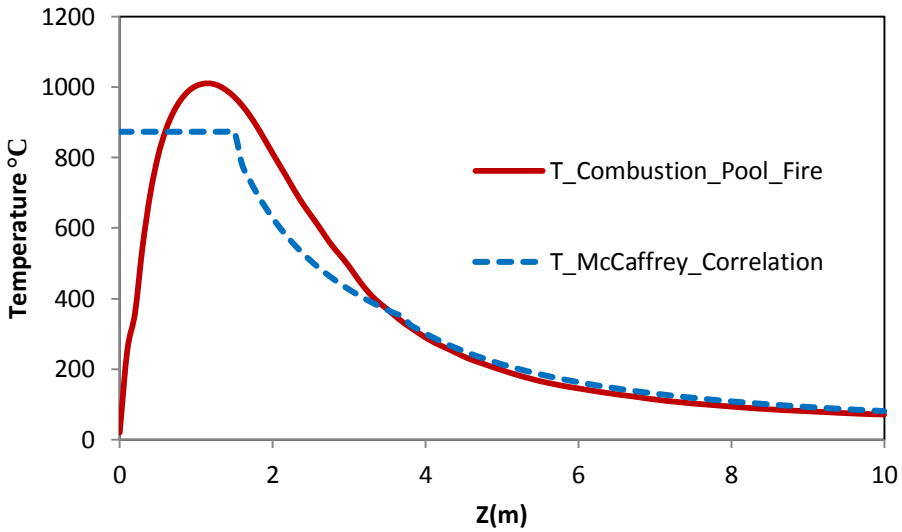

(a)

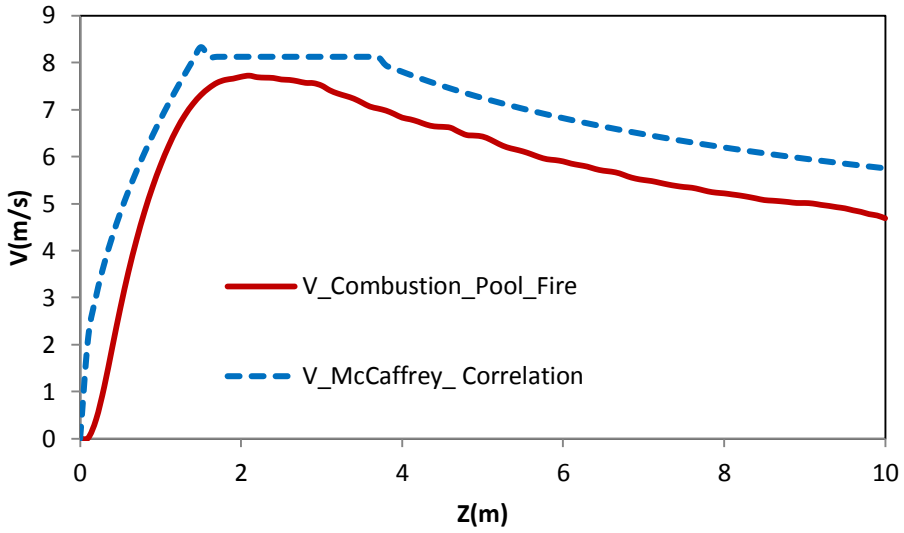

(b)

Figure 10 Temperature (a) and velocity (b) profiles comparisons for combustion pool fires and McCaffrey correlation (1000 kW)

- 1500 kW:

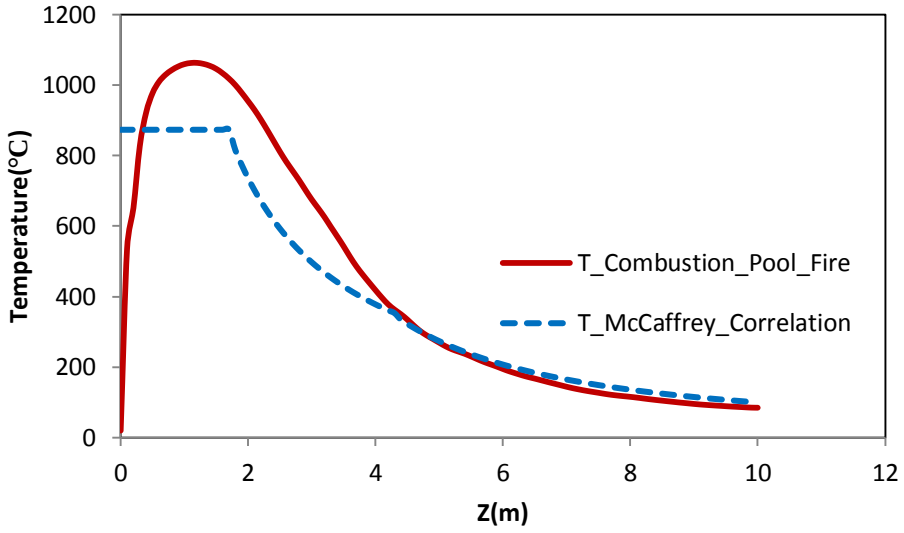

(a)

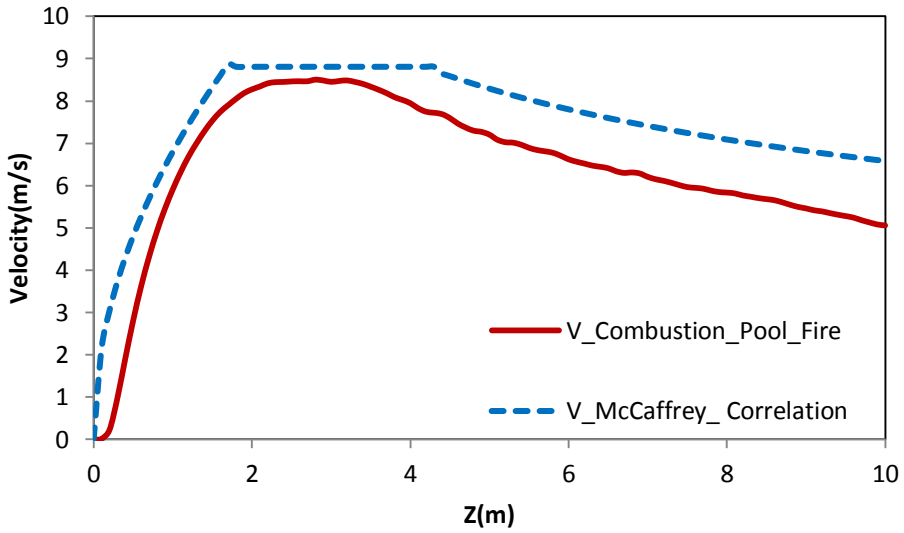

(b)

Figure 11 Temperature (a) and velocity (b) profiles comparisons for combustion pool fires and McCaffrey correlation (1500 kW)

2.3.3.2. Combustion simulations vs. hot air simulations

In this section, the hot air simulations using the two previously mentioned models will be compared to the combustion pool fire simulations and the flame height value, where the flame height was calculated using the empirical correlation proposed by Zukoski[19]:

$$Z = 0.23\ \dot{Q}_c^{2/5} - 1.02\ D \quad \textit{(Equation 29)}$$

Where, Z is the flame height (m)

The main parameters for the combustion simulations were provided in Table 3and the main parameters for the hot air simulations are presented in Table 5.

Table 5 Hot air simulations input parameters

Model	Convective HRR (kW)	Inlet Temperature (℃)	Inlet Velocity(m/s)	Area(m^2)	N_Eddy	L_Eddy(m)
A	500	531	2.18	1	1000	0.1
A	1000	435	4.8	1	1000	0.1
A	1500	387	7.6	1	1000	0.1
B	500	873	2	1	1000	0.1
B	1000	873	3.8	1	1000	0.1
B	1500	873	5.78	1	1000	0.1

- Temperature profile:

As presented in Figure 12(a), Figure 13(a) and Figure 14(a), the combustion pool fire simulations are showing a temperature of 600 ℃ at the expected flame height depend less on the fire size. Also the deviation between model A and model B decreased too much at the flame height and vanishes around 1 m from the flame height. Model B underestimated the temperature at the flame height with a deviation of 15 % from the combustion simulations for all the fire sizes. However, for model A underestimated the temperature at the flame height with deviation depending on the fire size, where, it was 35, 38 and 45 % for the fire sizes 500, 1000 and 1500 kW, respectively. Both model A and B matches exactly with the combustion simulations after around 2 m from the flame height depend less on the fire size.

For the region before the flame height, there were bigger deviations noted for both model A and model B from the combustion simulations, where the average underestimation deviation for model A before the flame height was increasing by the increase of the fire size as it was around 30, 50 and 60 % for the fire size 500, 1000 and 1500 kW respectively. However, model B was showing better results with an average underestimation deviation less than 20 % when compared with the combustion simulations before the flame height for the three fire sizes.

- Velocity profile:

Figure 12(b), Figure 13(b) and Figure 14(b) illustrates that model A and model B are achieving the same velocity value at the flame height for all the fire sizes. From the flame height onwards for the 500 kW, both of the two models are showing almost exact results as those of the combustion simulations. However, for the 1000 and 1500 kW cases, there is a constant overestimation deviation after the flame height between the hot air simulations and the combustion simulations, where the hot air simulations are overestimating the velocity by 18 and 13 % for the 1000 and 1500 kW fire sizes respectively.

Before the flame height, at the 500 kW case, the results of the hot air simulations are still showing good matching with the combustion simulations till 0.4 m from the fuel bed to the flame height. For the 1000 kW, model A is matching the combustion simulations with a very slight deviation from 0.5 m to the flame height, while model B is over estimating the velocity by 18 % deviation from 0.9 m to the flame height. For the 1500 kW, both model A and model B are overestimating the velocity by 14 and 20 % respectively from 0.9 m to the flame height when compared to the combustion simulations' results.

All in All, for the temperatures profiles, model B estimated the temperature better than model A at the flame height and both models matched together after 1.0 m from the flame height and with the combustion simulations after 2.0 m from the flame height. Generally, Model B was showing less deviation from the combustion simulations before the flame height than that of model A. For the velocity simulations, there were very good matching results in the 500 kW case for both of the two models in the two regions before and after the flame height. While, for the 1000 and the 1500 kW cases the two models are almost showing the same results after the flame height and also are showing a constant overestimation from the combustion simulations. Before the flame height, model A is showing good matching with the combustion simulations at the fire size of 1000 kW and slight deviation of 14 % at the fire size of 1500 kW, while model B is showing slightly higher deviation values.

For sack of completeness, comparison graphs between the combustion simulations, hot air simulations and McCaffrey correlations for the three fire sizes were provided in the appendix to give an overview of the performance of the hot air simulations when compared to McCaffery correlations.

- 500 kW:

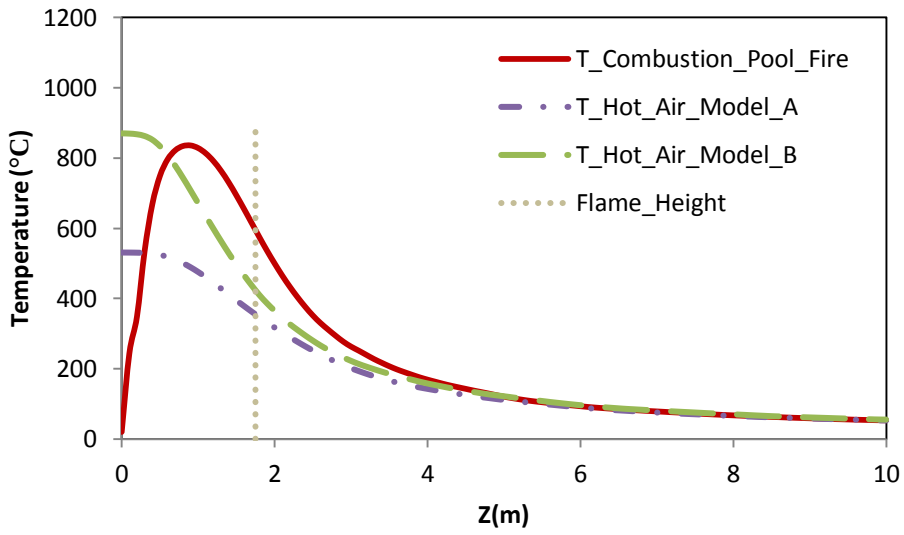

(a)

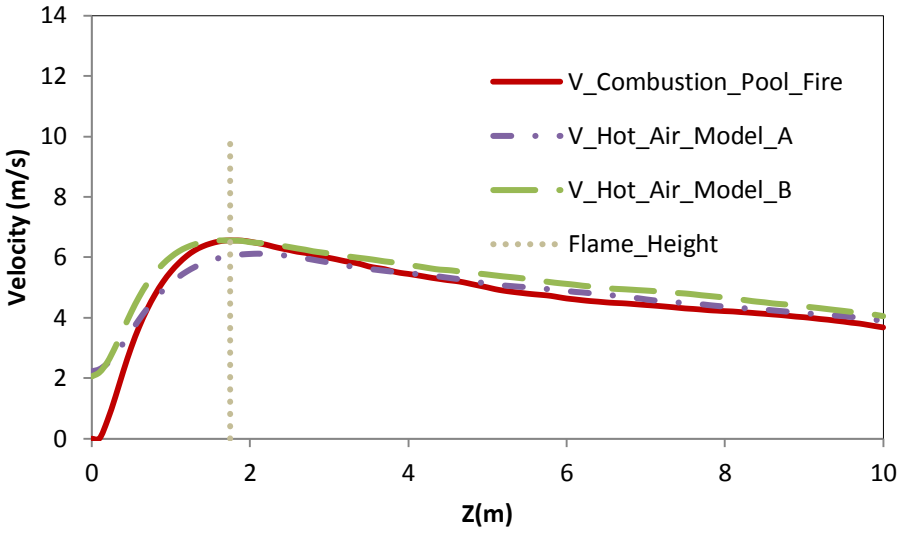

(b)

Figure 12 Temperature (a) and velocity (b) profiles comparisons for combustion pool fires and hot air models (500 kW)

- 1000 kW:

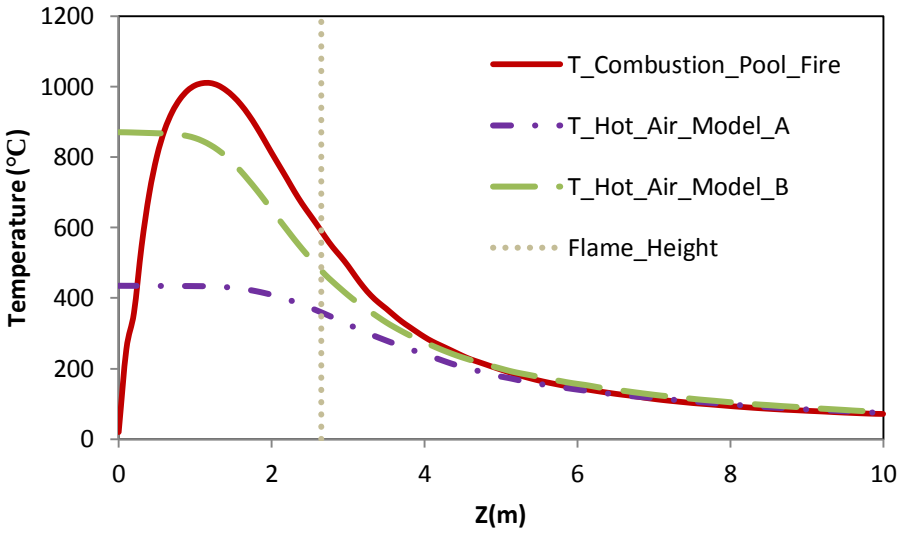

(a)

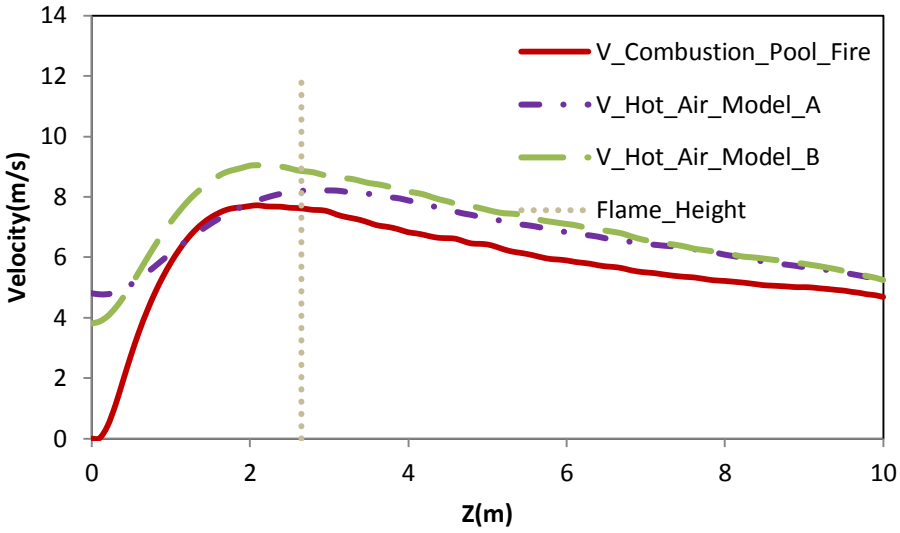

(b)

Figure 13 Temperature (a) and velocity (b) profiles comparisons for combustion pool fires and hot air models (1000 kW)

- 1500 kW:

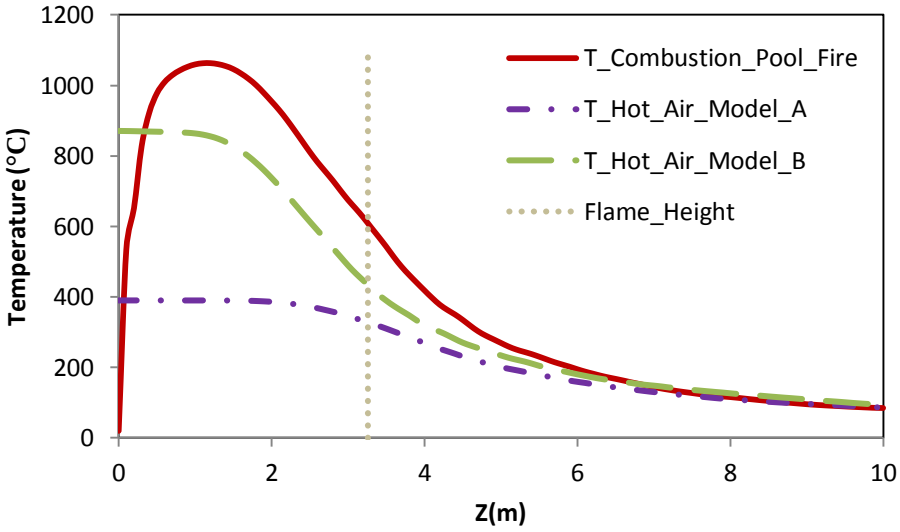

(a)

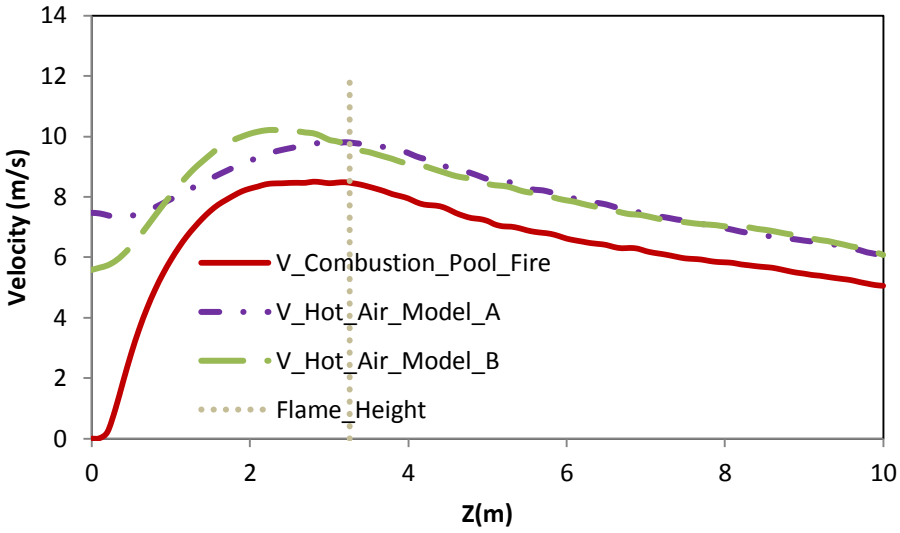

(b)

Figure 14 Temperature (a) and velocity (b) profiles comparisons for combustion pool fires and hot air models (1500 kW)

2.3.3.3. Experimental measurements for propane burner vs. hot air simulation

Based on the findings of the last section, we assumed that model B is giving more promising results than that of model A especially for the velocity after the flame height and the temperature before and after the flame height, one of the expected reasons behind the good performance of model B over model A is that it has less Froude numbers, which means that model B tends more toward the buoyancy driven flows which is more like real fires.

To ensure that, it was interesting to compare the results of model B with experimental data. In this section we compared some experimental data done by Gengembre et al [18] on a medium scale propane flames with a heat release rate of 37.9 kW. The burner was 30 cm diameter with 2000 vertical tubes, with measurement's expected error of 60 K in the region where the mean temperature is high. The error is expected due to the deposition of soot on the thermocouples.

As shown in Figure 15, model B is showing good results when compared to the experimental temperature and velocity measurements at the flame height (0.5m) and up to a height of three times the flame height (1.5m). After the 1.5 m height model B underestimated the temperature and overestimated the velocity, however, this deviation from the experimental data did not exceed the 30 % at any height.

This quick validation of the proposed model B seems to be promising and that means more validations should be done with a wide variety of different fuels to put hands on the main limitations of this model. It is good to note that at this simulation, the effect of the number of eddies was noticed and in order to get better data for the velocity it was found (after examining five different number of eddies) that around

150000 eddies are needed. However, this sensitivity analysis was only based on five different number of eddies (100, 1000, 10000, 15000 and 150000) so there might be another optimum number of eddies.

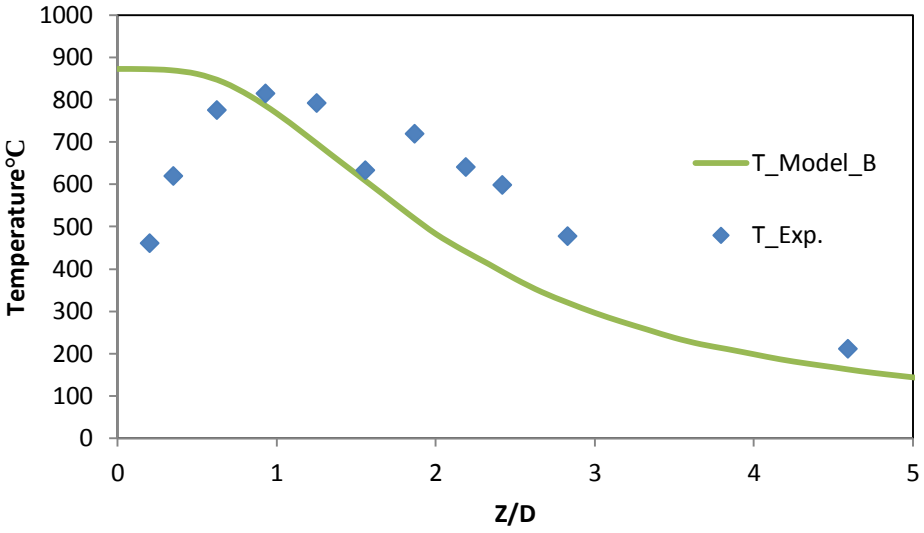

(a)

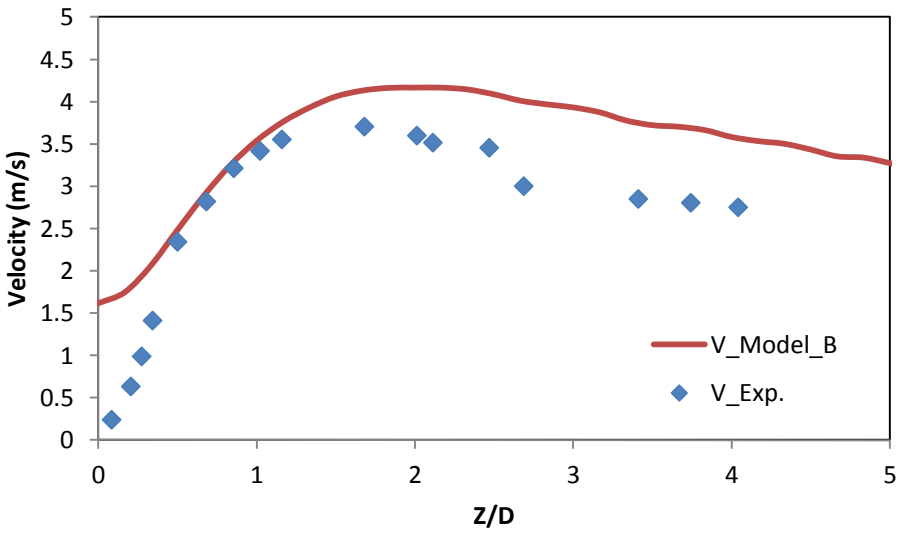

(b)

Figure 15 Temperature (a) and Velocity (b) patterns vs. normalized center line axis

2.3.3.4. Radial distribution

It was also important to ensure that we are getting reasonable radial velocity distribution when comparing the hot air simulations (model B) to the combustion simulations. The distribution was done at two fields,

the near field and far field. The near field is assumed to be at 2.5 m from the floor and the far field is assumed to be 5.0 m from the floor.

- 500 kW:

As shown in **Figure 16**, the velocity is well expected by the hot air when compared to the combustion at both of the far and near fields. Where R is the radial distance and the center of the plume is at R = 2.5m.

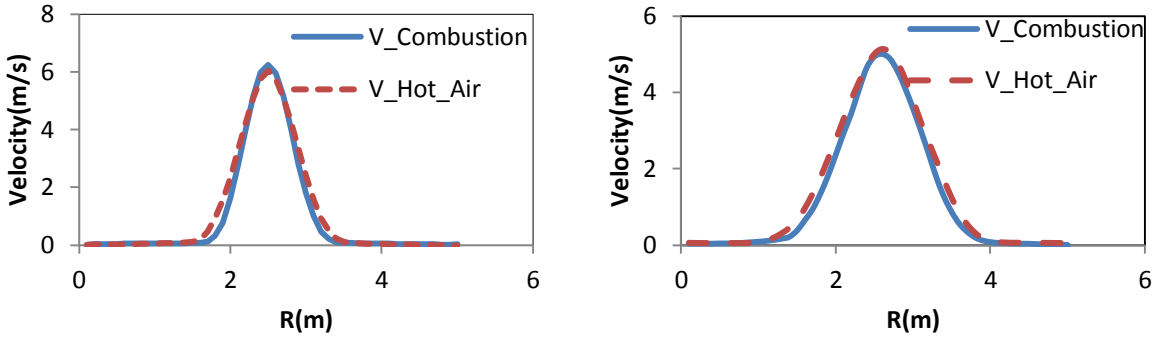

(a) (b)

Figure 16 Radial velocity distributions at near field (a) and far field (b)

- 1000 Kw:

As presented in Figure 17, the radial velocity distribution at the near field is expected perfectly by the hot air model, however there is a very small deviation from the combustion simulation at the far field.

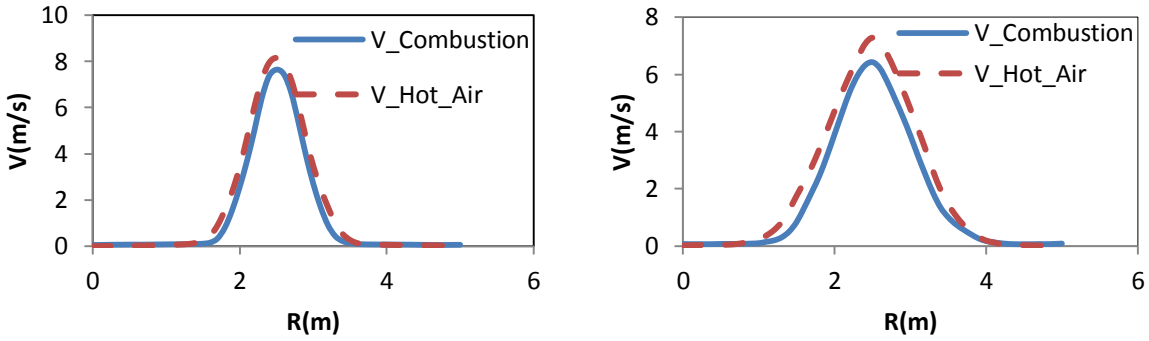

(a) (b)

Figure 17 Radial Velocity distribution at near field (a) and far field (b)

- 1500 Kw:

As shown in Figure 18, there is a small deviation near the axis of the plume for both of the near and far field, yet, the results seems promising to expect the velocity distribution along the radial distance.

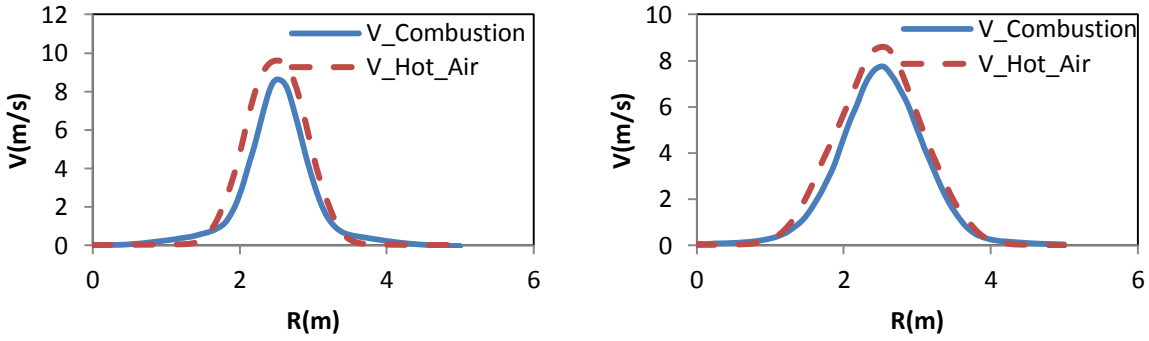

(a) (b)

Figure 18 Radial Velocity distribution at near field (a) and far field (b)

All in all, the velocity distribution for the hot air simulations along the radial distance seems to be quite similar to that of the combustions simulations. This is also a good finding which adds high value to the hot air model B developed in this research.

2.4. Future Work

1. Sensitivity analysis for the different models used in model A. Another model could be proposed by changing the method Mégret used to calculate the temperature and use the correlations of McCaffrey and to change the equation used to calculate the flame height by using for example Zukoski `s equation. The temperature equation is based on the heptane stoichiometric equation, amount of air entrained, the radiative fraction and the heat of combustion of heptane, so it needs to be changed based on the type of fuel and that could end up with a lot of calculations' errors. Therefore, it is better to calculate the temperature using McCaffrey`s correlations which showed in this research application to be much reasonable and is giving realistic outputs.

2. In this research work we did some trials to start the hot air simulations at the calculated flame height in order to decrease the computational domain. However, due to the high temperature and velocity at the inlet (Boundary conditions) the decay in temperature and velocity was not well predicted in the simulations using the SEM. Therefore, it is also recommended to try other methods to generate turbulence at the boundary conditions, e.g. recycling methods and forcing techniques [10].

3. Some comparisons between the hot air models simulations to expect the velocity under the ceiling vs. the empirical co-relations of Alpert and Heskestad [24] should be studied.

4. Doing some modifications to model B to prevent using the SEM, this will definitely decrease the computational time. In this research we did some simulations on a wider range of heat release rates using model B without the SEM and there was some promising data that should be later investigated.

5. Using different turbulent models other than the default Deardroff, e.g. Smagorinsky Model without adding the SEM and monitor the performance.

3. Water phase simulations

3.1. Water phase LES and methodology

The main interest when studying the interaction between the water sprays and the hot air plume computationally is to be able to expect the Actual Delivered Density (ADD) and the Penetration Ratio (PR) of a sprinkler with a known fire case. In that case, the FDS can be used in later studies to investigate the ability of different types of sprinklers to fight fires. To compute the PR capabilities of the sprinklers in case of fires, it was essential to first simulate the sprinklers' performance without fire. In this section, a sprinkler almost similar to the type (B) Early Suppression Fast Response (ESFR) sprinkler mentioned in [3] was simulated using the FDS and then the data's trends and founding were compared to those found in [3 and 4].

The ESFR sprinkler is a ceiling mounted downward flow sprinkler that is usually used in warehouses instead of the in-rack systems. ESFR sprinkler is known with its high flow rates and high pressure heads, the ESFR sprinkler is also known with its small drop sizes compared to the other sprinklers with comparable operating pressures. The ESFR rely mainly on discharging high amount of water at the early stages of the fire to decrease the chances for the fire to grow. So generally speaking, the ESFR sprinklers rely mostly on the momentum of the flow with small droplet sizes to quickly penetrate the fire plumes before it grows and become uncontrollable [4].

It is important to briefly describe how the FDS model the sprinkler spray; the FDS is briefly a CFD model which is based on the finite difference technique to solve the partial differential equations of conservation of mass, momentum and energy [20, 23]. The FDS model the spray droplet using the droplet distribution model and the droplet transport model:

- The Droplet distribution model:

The FDS uses a sample of droplets to calculate the distribution pattern. The initial drop size distribution is presented in terms of the Cumulative Volume Fraction (CVF) which uses a combination of log-normal and Rosin-Rammler distributions as the following:

$$F = \begin{cases} (2\pi)^{\frac{-1}{2}} \int_0^{D_{CVF}} (\sigma D)^{-1} e^{\frac{\left[\ln\left(\frac{D}{D_m}\right)\right]^2}{2\sigma^2}} \mathrm{dD} & (D_{CVF} \leq D_m) \\ 1 - e^{-0.693\left(\frac{D_{CVF}}{D_m}\right)^{\gamma}} & (D_{CVF} > D_m) \end{cases} \qquad \textit{(Equation 30)}$$

Where D_m is the median droplet diameter and it is a function of the orifice diameter, operating pressure and geometry. σ and γ are empirical constants used for curve fitting of distribution pattern.

- Droplet transport model:

FDS uses the Lagrangian approach to model the water droplets transport, to calculate the velocity and expect the position of each droplet; the FDS uses the theory of conservation of momentum, where the position and velocity is calculated by the following equations:

$$\frac{d}{dt}\left(mv_p\right) = mg - \frac{1}{2}\,\rho C_d \pi r^2 \left(v_p - v_a\right)|v_d - v_a| \quad \textit{(Equation 31)}$$

$$\frac{dx_p}{dt} = v_p \quad \textit{(Equation 32)}$$

Where, v is velocity, r is droplet radius, d/p is for droplets, a is for air and equation 32 is the position equation. C_d is the drag coefficient and it depends on the Reynolds number (Re) based on the droplet-air relative velocity and it can be calculated using the following equation:

$$C_d \begin{cases} \frac{24}{Re} & Re < 1 \\ \frac{24\left(0.85 + 0.15Re^{0.687}\right)}{Re} & 1 < Re < 1000 \\ 0.44 & Re > 1000 \end{cases} \quad \textit{(Equation 33)}$$

And the Reynolds number (Re) of droplet can be calculated by:

$$Re = \frac{\rho|v_d - v_a|\,2r}{\mu(T)} \quad \textit{(Equation 34)}$$

Where $\mu(T)$ is the dynamic viscosity of air at temperature (T).

The angle of the spray in the FDS is defined by two angles measured from the axis of the orifice, the inner angle where there is no flow and the outer angle which represent the outer boundary of the flow. In all of our simulations the inner angle is set to zero (if nothing else mentioned) so we have a full cone water spray.

Also it is good to note that both the parameters (β) and(μ) are used as the default values (check [23]). Where β is the spread parameter = 5 and μ is the parameter that gives the location in the spray at which most of the water is released, by default it is zero so most of the water is released in the core region (axis) of the spray.

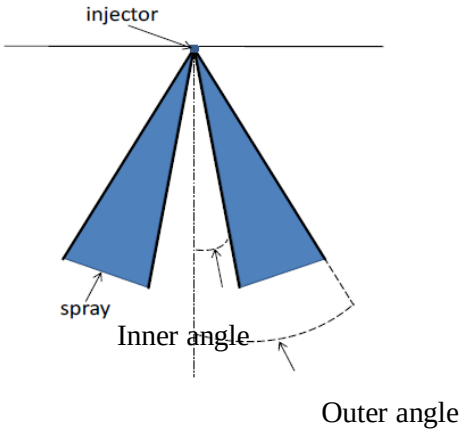

Figure 19 Spray angle (taken from [24])

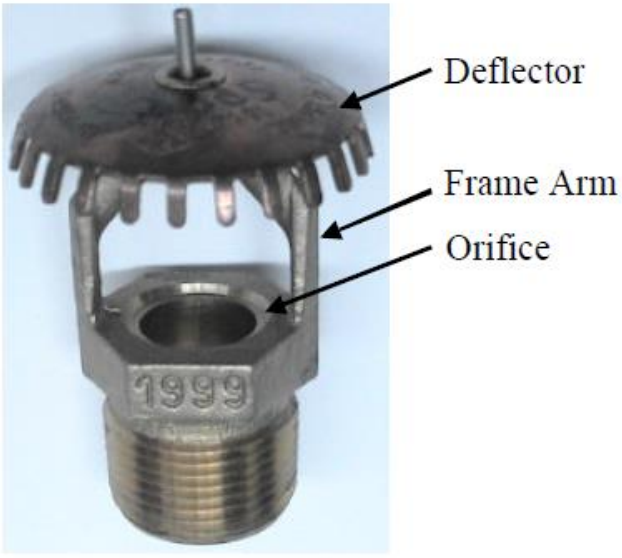

Figure 20 Typical sprinkler design [22]

The sprinkler was described by its input parameters e.g. volume median diameter D_{v50} (D_{v50} can be defined where any volume of the water spray can be distributed into two halves with half has a diameter less than D_{v50} and half has a diameter of more than D_{v50}), discharge speed, discharge angle and water flow rate as given in [3 & 4] and as shown in table 6. The D_{v50} used for each flow rate was extrapolated between the Cumulative Volume Fraction (CVF) of 0.45 and 0.55 as marked in table 6 and used as an input in the FDS file.

Nam et al. mentioned in [4] that each set of CVF is considered as 25 trajectories (with a total of 275 to describe the sprinkler) and the discharge angle and velocity of each set was presented in table 7.

It is important to note that Nam et al. found that there was a solid water stream near the axis of the flow which was a collection of large water drops. It was decided by Nam et al. while doing the computational

simulations to assign 25 trajectories near the axis with larger drop size of 3.7 mm to compensate the water jet flows and also the flow rate was increased by up to 20 % near the axis.

In Table 7, the first three rows are for the volume flow rate representing the water streams along the axis, the speed of the water streams along the axis and the uniform speeds of the rest of the trajectories respectively. The fourth row is for the discharge angle near the axis (25 trajectories) and the other 10 rows are representing the other 250 trajectories with 25 each.

Table 6 water particle diameter distribution [4]

CVF[a]	1.90 l/s d (mm)	3.16 l/s d (mm)	4.42 l/s d (mm)	6.26 l/s d (mm)	7.58 l/s d (mm)	9.48 l/s d (mm)
0.05	0.65	0.47	0.37	0.29	0.26	0.22
0.15	0.88	0.63	0.50	0.40	0.35	0.30
0.25	1.06	0.76	0.60	0.48	0.42	0.36
0.35	1.22	0.87	0.69	0.55	0.49	0.42
0.45	1.39	1.00	0.79	0.63	0.55	0.48
0.55	1.57	1.12	0.89	0.71	0.63	0.54
0.65	1.76	1.26	1.00	0.79	0.70	0.61
0.75	1.97	1.41	1.12	0.89	0.78	0.68
0.85	2.24	1.60	1.27	1.01	0.89	0.77
0.95	2.70	1.94	1.53	1.22	1.08	0.93

[a]Cumulative volume fraction.

Table 7 Discharge speed and discharge angles used in the spray models

1.90 l/s	3.16 l/s	4.42 l/s	6.26 l/s	7.58 l/s	9.48 l/s
$\bar{V}_0 = 0.057$ l/s	$\bar{V}_0 = 0.088$ l/s	$\bar{V}_0 = 0.13$ l/s	$\bar{V}_0 = 0.22$ l/s	$\bar{V}_0 = 0.27$ l/s	$\bar{V}_0 = 0.33$ l/s
$\lvert V_0\rvert = 8.5$ m/s	$\lvert V_0\rvert = 13.0$ m/s	$\lvert V_0\rvert = 16.0$ m/s	$\lvert V_0\rvert = 21.0$ m/s	$\lvert V_0\rvert = 25.5$ m/s	$\lvert V_0\rvert = 31.8$ m/s
$\lvert V\rvert = 7.5$ m/s	$\lvert V\rvert = 12.0$ m/s	$\lvert V\rvert = 15.0$ m/s	$\lvert V\rvert = 19.0$ m/s	$\lvert V\rvert = 23.0$ m/s	$\lvert V\rvert = 28.8$ m/s
$0 \leqslant \theta_0 \leqslant 4$	$0 \leqslant \theta_0 \leqslant 4$	$0 \leqslant \theta_0 \leqslant 4$	$0 \leqslant \theta_0 \leqslant 4$	$0 \leqslant \theta_0 \leqslant 4$	$0 \leqslant \theta_0 \leqslant 4$
$4 \leqslant \theta_1 \leqslant 65$	$3 \leqslant \theta_1 \leqslant 67$	$3 \leqslant \theta_1 \leqslant 70$	$0 \leqslant \theta_1 \leqslant 72$	$0 \leqslant \theta_1 \leqslant 72$	$0 \leqslant \theta_1 \leqslant 72$
$4.5 \leqslant \theta_2 \leqslant 65$	$3 \leqslant \theta_2 \leqslant 67$	$3 \leqslant \theta_2 \leqslant 70$	$0.75 \leqslant \theta_2 \leqslant 72$	$0.75 \leqslant \theta_2 \leqslant 72$	$0.75 \leqslant \theta_2 \leqslant 72$
$5 \leqslant \theta_3 \leqslant 65$	$3 \leqslant \theta_3 \leqslant 67$	$3 \leqslant \theta_3 \leqslant 70$	$1.5 \leqslant \theta_3 \leqslant 72$	$1.5 \leqslant \theta_3 \leqslant 72$	$1.5 \leqslant \theta_3 \leqslant 72$
$5.5 \leqslant \theta_4 \leqslant 65$	$3 \leqslant \theta_4 \leqslant 67$	$3 \leqslant \theta_4 \leqslant 70$	$3 \leqslant \theta_4 \leqslant 72$	$3 \leqslant \theta_4 \leqslant 72$	$3 \leqslant \theta_4 \leqslant 72$
$6.5 \leqslant \theta_5 \leqslant 65$	$3 \leqslant \theta_5 \leqslant 67$	$3 \leqslant \theta_5 \leqslant 70$	$6 \leqslant \theta_5 \leqslant 72$	$6 \leqslant \theta_5 \leqslant 72$	$6 \leqslant \theta_5 \leqslant 72$
$9 \leqslant \theta_6 \leqslant 65$	$3 \leqslant \theta_6 \leqslant 67$	$3 \leqslant \theta_6 \leqslant 70$	$10 \leqslant \theta_6 \leqslant 72$	$10 \leqslant \theta_6 \leqslant 72$	$10 \leqslant \theta_6 \leqslant 72$
$11 \leqslant \theta_7 \leqslant 67$	$11 \leqslant \theta_7 \leqslant 71$	$11 \leqslant \theta_7 \leqslant 74$	$16 \leqslant \theta_7 \leqslant 72$	$16 \leqslant \theta_7 \leqslant 72$	$16 \leqslant \theta_7 \leqslant 72$
$56 \leqslant \theta_8 \leqslant 70$	$50 \leqslant \theta_8 \leqslant 74$	$50 \leqslant \theta_8 \leqslant 75$	$22.5 \leqslant \theta_8 \leqslant 72$	$22.5 \leqslant \theta_8 \leqslant 72$	$22.5 \leqslant \theta_8 \leqslant 72$
$56 \leqslant \theta_9 \leqslant 72$	$54 \leqslant \theta_9 \leqslant 76$	$54 \leqslant \theta_9 \leqslant 76$	$30 \leqslant \theta_9 \leqslant 72$	$30 \leqslant \theta_9 \leqslant 72$	$30 \leqslant \theta_9 \leqslant 72$
$56 \leqslant \theta_{10} \leqslant 77$	$58 \leqslant \theta_{10} \leqslant 78$	$56 \leqslant \theta_{10} \leqslant 76$	$38 \leqslant \theta_{10} \leqslant 72$	$38 \leqslant \theta_{10} \leqslant 72$	$38 \leqslant \theta_{10} \leqslant 72$

Based on table 6 and table 7 and according to Nam et al., the angle of the total number of 275 trajectories are 77°, 78°, 76°, 72°, 72° and 72° for the flow rates (1.90, 3.16, 4.42, 6.26, 7.58 and 9.48) l/s respectively. It was not clear if Nam et al. used the previously mentioned angles to describe the whole spray or just half of it. So we investigated both of the two possibilities, first it was assumed that Nam et al. used the previously mentioned angles to describe the whole cone of the sprinkler, which means that the angle calculated from the axis of the sprinkler to each side (outer boundaries) was 38.5°, 39°, 38°, 36°, 36° and 36° for the flow rates (1.90, 3.16, 4.42, 6.26, 7.58 and 9.48) l/s respectively and then assumed that Nam et al. used 77°, 78°, 76°, 72°, 72° and 72° for the flow rates (1.90, 3.16, 4.42, 6.26, 7.58 and

9.48) l/s respectively to describe just half of the cone from the axis to the boundaries. In further discussions in case of using the following angles (77°, 78°, 76°, 72° , 72° and 72°) to describe the half of the spray cone we will call it angle set 1 and when using it to describe the whole spray cone we will call it angle set 2.

We found that, to get the same ADD (on a 1.29 m radius annulus placed directly below the spray angle) as that for the experimental and computational work done in [3 & 4] we need to use angle set 2 when we do the simulations under the 6.0 m ceiling and angle set 1 when we are doing the simulations under 3.0 m ceiling. However, to get the same radial distribution for the water flux under the 3.0 m ceiling it is better to use angle set 2-That will be shown in the later discussions-. Yet, when using the Angle set 2 in our simulations we found that we get too high PRs, so we were not able to capture the effect of changing the parameters of the sprinklers or the fire size on the PR values. Therefore, we did our research with the spray angles were assumed to be angle set 1 to decrease the momentum of the water sprays on the target (fire) to be able to capture the effect of the parameters changes and to get more significant notes on our data.

Another thing to note about the research done in [3 & 4]; the Fire used in the experimental part was modified by injecting air with high velocity (9.5 m/s) in the middle of the fire to simulate the air flow in rack-storages. Based on that, for the 3.0 m ceiling if we used angle set 2 and get the same high flow rates at the axis as in [4], with the normal pool fires, the penetration rate will be too high because of the high water momentum compared to that of the smoke (hot air) from the normal pool fires without injecting high speed air and in most of the simulations the water spray was extremely dominating the two phases interaction.

Also it is good to note that the parameters of the simulated sprinklers and pool fires in [3] were changed to tune the experimental results without giving much information on all the modifications done, which make any trials to get the exact values found in [4] doesn't make much sense according to the sake of our research. However, it was found to be interesting to investigate the ability of our simulations to capture the same trends/concepts of the experimental and computational data in [3 & 4] and to understand what are the main factors affecting the PR of the ESFR sprinklers. Also we kept the simulations done with angle set 1 and angle set 2 to compare the effect of changing the spray angle on the results, while keeping the angle set 1 as the default.

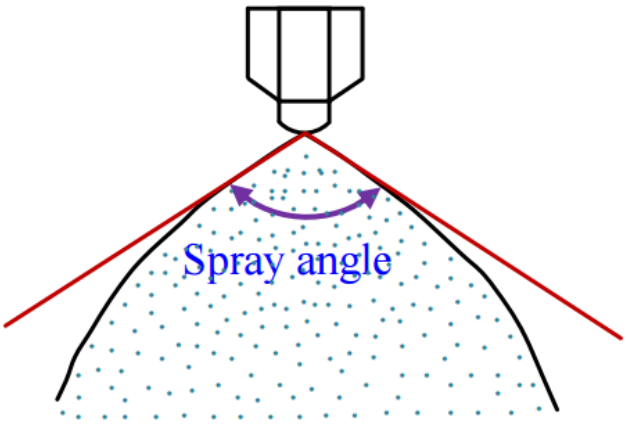

Figure 21 Spray angle [20]

The computational simulations were done under two ceiling heights (3.0 m and 6.0 m) and six flow rates with properties as shown in table 6 and table 7.

The simulations carried out herein are threefold:

(i) The radial water flux distribution of the sprinkler with flow rates (1.88 l/s, 3.15 l/s, 4.25 l/s and 6.23 l/s) with both angles under 3.0 m ceiling.

(ii) The ADD on a 1.29 m radius annulus with its center exactly under the spray axis with flow rates (1.88 l/s, 3.15 l/s, 4.25 l/s, 6.23 l/s, 7.58 l/s and 9.48 l/s) under 6.0 m and 3.0 m ceilings with both angles.

(iii) The ADD of the sprinkler with flow rate (3.16 l/s) with larger droplet mean diameters (Do, 1.25 Do and 1.5 Do) at ceiling heights of 6.0 m and 3.0m, where Do is the default diameter as shown in table.6.

(iv) Ratios of the ADDs between 3.0 m ceiling and 6.0 m ceiling heights with respect to the flow rates (1.88 l/s, 3.15 l/s, 4.25 l/s, 6.23 l/s, 7.58 l/s and 9.48 l/s).

3.2. Numerical modeling of the sprinklers and setup

The computational domain used for the 3.0 m ceiling simulations was as the following: 10 m x 10 m x 3 m (width x depth x height). While that for the 6.0 m ceiling simulations was as the following: 10 m x 10 m x 6 m (width x depth x height) where the sprinkler was placed exactly at the center of the ceiling. The computational area was open to flow on the sides and bottom of the domain. The domain of the 6.0 m ceiling simulations is shown in Figure 22:

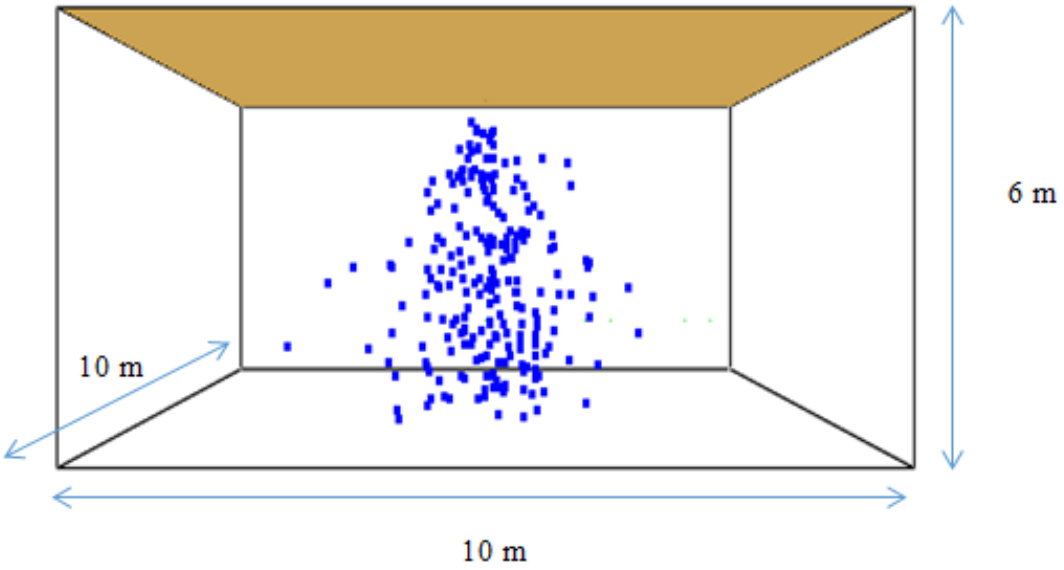

Figure 22 Water spray simulations domain. 6m height ceiling

To calculate the radial values of the water flux at the floor level and compare it to the measured experimental data for specific flow rates in [4], the water flux was calculated in the FDS by Phase Doppler Particle Analysis (PDPA) on an annulus with a radius of 0.15 m placed at the following positions (0, 0.4, 0.8, 1.2, 1.6, 2.0, 2.4, 2.8, 3.2, 3.6, 4.0, 4.4 and 4.8 m), a simple sketch showing the methodology is presented in Figure 23.

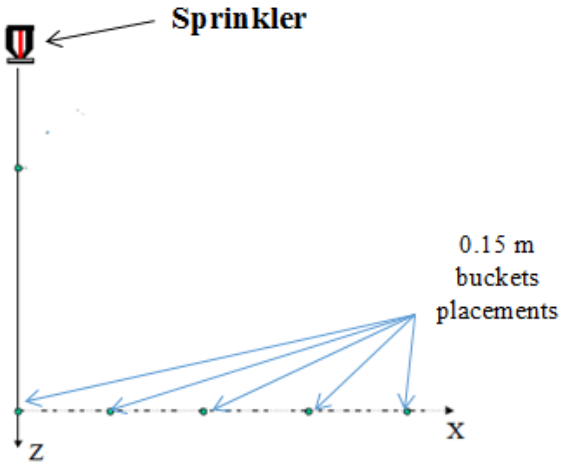

Figure 23 Radial water flux distribution[22]

To study the effect of the different flow rates, droplets' diameters and ceiling heights on the ADD, the ADD was calculated using a PDPA on an annulus with a radius of 1.29 m (same as Area II used in [3]) with its center placed exactly below the axis of the spray. A simple sketch showing the methodology is presented in Figure 24.

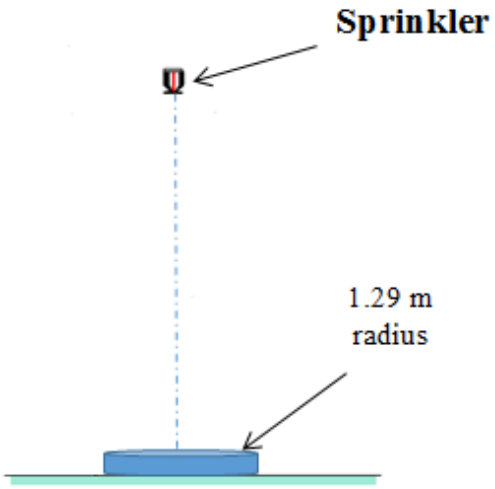

Figure 24 ADD measurements

A uniform and structured mesh has been used in the whole domain with a mesh size of 0.20 m. A sensitivity analysis was done to ensure the used size was acceptable; a simulation with cell size of 0.10 m was done and as it is shown in Figure 25, the water flux was not noticeably affected by increasing the cell size from 0.10 m to 0.20 m. Only an error of less than 5 % was noticed at the center at R= 0 m.

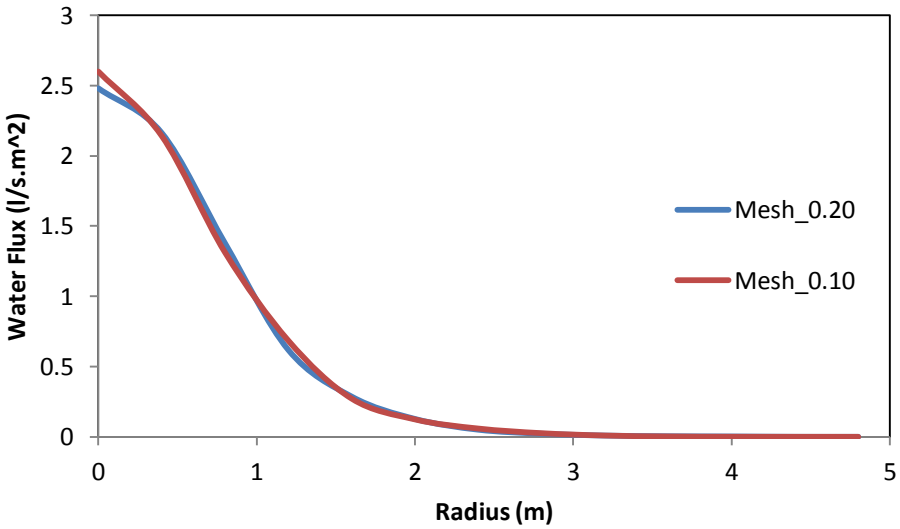

Figure 25 sensitivity analysis for the cell size

To summarize, the default input parameters for the sprinklers used in this research were as the following:

Table 8 Sprinklers used parameters

Sprinkler Number	D_{V50} (mm)	Gamma_D	Flow Rate (l/s)	Particle Velocity(m/s)	Spray angle
1	1.500	2.5	1.90	7.5	154
2	1.050	2.5	3.16	12	156
3	0.850	2.5	4.42	15	152
4	0.680	2.5	6.26	19	144
5	0.600	2.5	7.58	23	144
6	0.510	2.5	9.48	28.8	144

The FDS's default value of the number of droplets to be tracked in the water spray is 5000 droplets, as the number of droplets to be tracked increase; the computational time is expected to also increase because more Lagrangian particles are introduced in the computational domain [23].

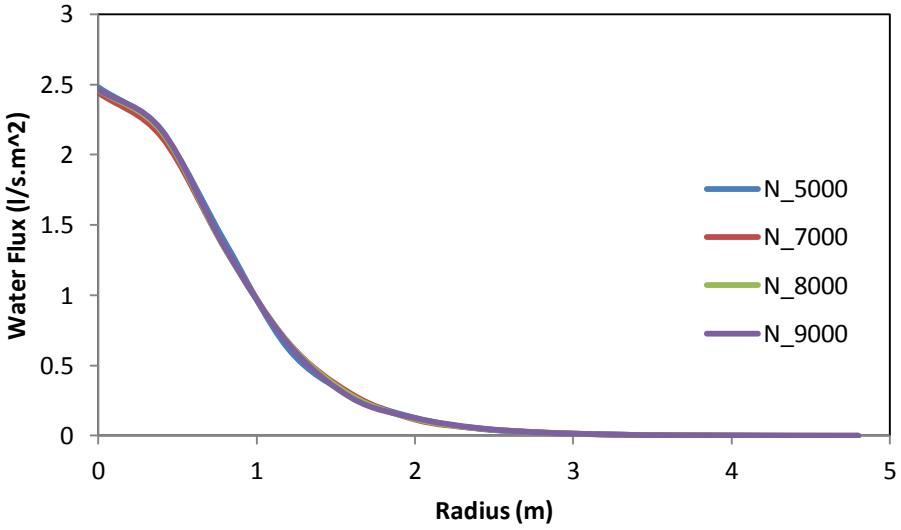

Figure 26 Sensitivity analysis for the number of tracked droplets

Based on that, a sensitivity analysis was done to investigate the effect of increasing the number of tracked droplets, in order to get the minimum reasonable value to be tracked, in [23] it was also mentioned that in

case of the two phase interaction the computational time could increase with decreasing the number of tracked droplets because of the longer time that might be needed to reach convergence in the numerical method when applying the two phases, however, because of the time limitations we decided to rely on the sensitivity analysis done in the water phase for the number of particles and to apply the same number of particles when doing the interaction simulations. As show in Figure 26 the increased number of tracked particles did not affect the water flux calculations. So the default value of 5000 number of particles was used in all the simulations.

3.3. Water phase results

3.3.1. Water flux FDS vs. water flux experimental

The radial distribution of the water flux was measured experimentally in [3] for the flow rates (1.88 l/s, 3.15 l/s, 4.42 l/s and 6.23 l/s) under the 3.0 m ceiling. A comparison was done between the provided experimental data and the calculated water flux by the FDS using the previously mentioned domain and parameters but with the angle set 2. As shown in Figure 27, the FDS was able to perfectly capture almost the same water flux values from 0.75 m to 2.5 m radius for the 1.91 l/s and 3.16 l/s, there was a bit of deviation with the increase of the flow rate up to 6.26 l/s. The FDS computed higher water flux values from 0.15 to 0.75 m radius for all of the flow rates with an average of deviation of 25 % from the experimental data. The experimental data was, however, higher by almost 25 % from 0 to 0.15 m radius. This analysis shows that by a simple modification to the spray angle we were able to take the water jets near the axis of the sprinklers into account and get good data compared to the experiments.

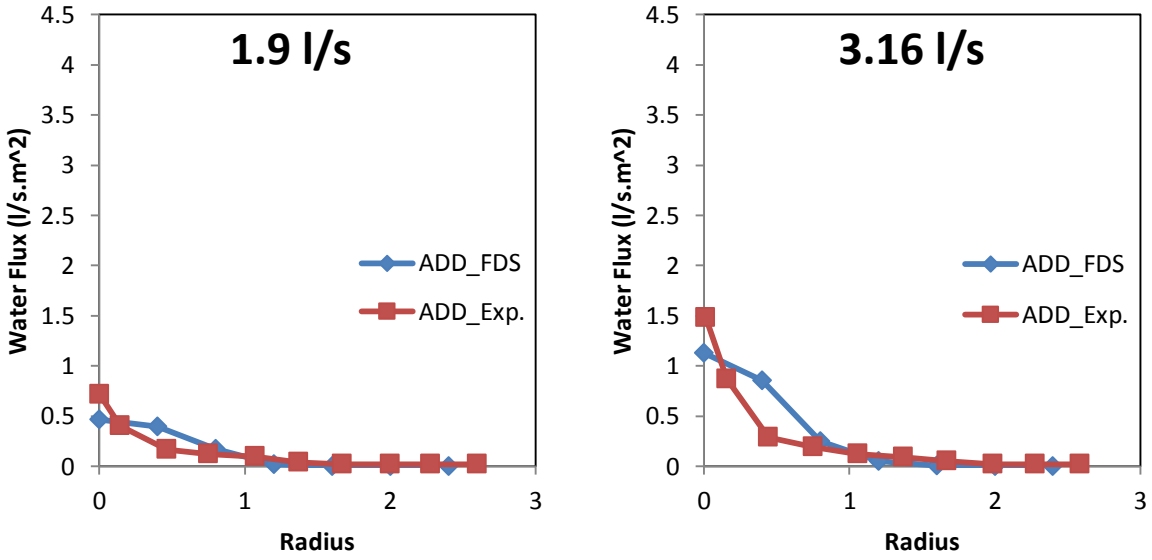

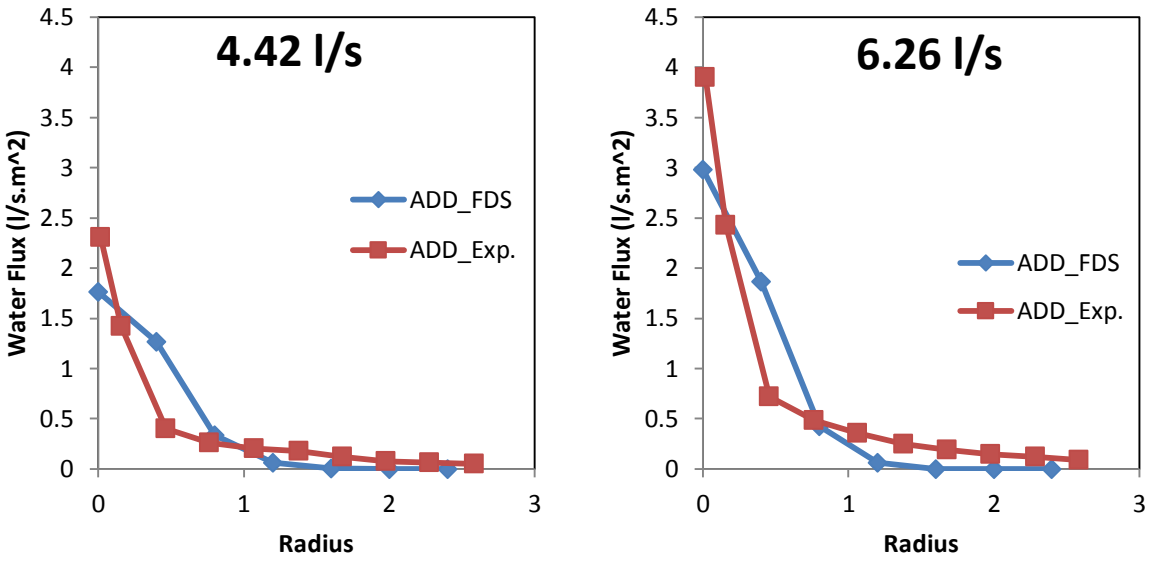

Figure 27 Radial water flux distribution (experimental vs. computational) (3.0 m ceiling)

As our upcoming research will be done by angle set 1, it was essential to show the water flux using angle set 2 and discuss the effect of the discharge angle on the water flux values. As it is shown in Figure 28, the effect of doubling the angle appears to reach its extreme at the center of the sprinkler spray, the deviation between the values of the water flux at the sprinkler axis is too low at low flow rate of 1.9 l/s, however, it goes to up to 70 % when the spray angle is doubled at high flow rates e.g. 3.15 l/s, 4.42 l/s and 6.23 l/s.

All in all, it is clear that by doubling the spray angle the water flux at the area near to the axis up to 0.75 m is highly affected. Based on that, we decided to use angle set 1 in our simulations to have less water flux without fire at the axis and then we can easily capture the effect of having fires below the sprinkler on both the ADD and the PR. It is also important to note that, with double angle the flow rate is still the same and the water flux was having a bit higher values for the double angled sprays from 1.0 m radius up to 4 m away from the axis and therefore it compensate the deviation at the axis and to deliver the same flow rate but on wider area.

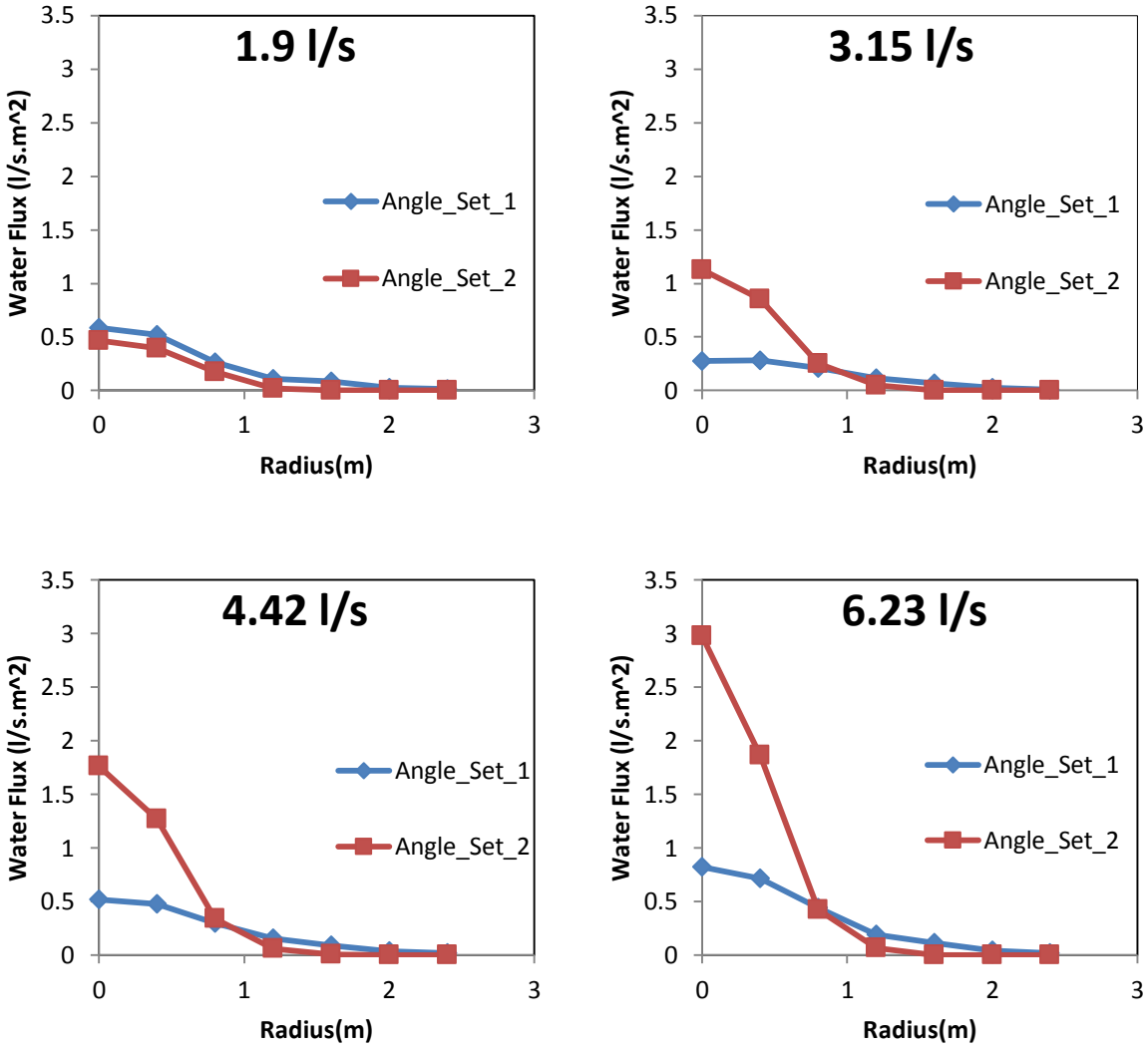

Figure 28 Radial water distribution vs. the spray angles (3.0 m ceiling)

3.3.2. ADD vs. flow rates (FDS and computational [4])

In this section a comparison between the ADD values calculated by the FDS (using angle set 1 and 2) and the computational results found in [4] will be presented for both the ceiling height 3.0 m and 6.0 m.

As shown in Figure 29, when the spray angle is doubled the ADD received on a 1.29 m radius annulus under the ceiling increased almost linearly with the increase of the flow rate which is depend less on the ceiling height. It was also noted that using angle set 2 gives results more matching to that done in [4] under the 6.0 m ceiling height, however, when using angle set 1 the results is almost the same for the computational work in [4] under the 3.0 m ceiling height. This variation is most probably because of the modifications done by Nam et al. to their simulation work to match that of the experiments. It was also noted that, the effect of the spray angle is almost constant depend less on the flow rate or the ceiling height for the same target (e.g. the target here is 1.29 m radius).

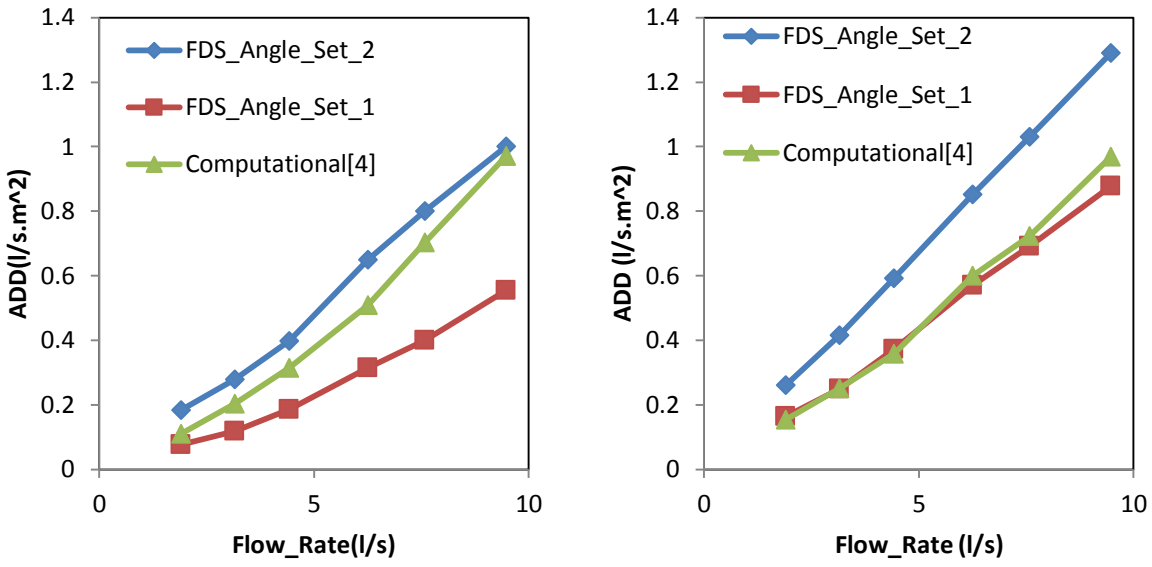

(a) (b)

Figure 29 ADD vs. Flow rate for two spray angles compared to the computational results in [4] ((a) ceiling height= 6.0m and (b) 3.0 m)

3.3.3. ADD vs. drop size

After doing some comparisons using the experimental and computational results in [3 & 4], from now on the used angles in our FDS simulations will be angle set 1, droplet sizes, discharge speeds and flow rates were mentioned in table 8 (if nothing else was mentioned).

To study the effect of the drop size independently on the ADD and the PR later, the ADD was calculated with different values for the volumetric median drop size (D_{V50}), the D_{V50} was increased by 25 and 50 % than the default value mentioned before (where d_o is the default drop size and d is the increased drop size). The simulations were done using only one flow rate of 3.6 l/s as in [4] for both the 3.0 m and 6.0 m ceilings. As shown in Figure 30, the FDS simulations almost did not show any effect of increasing the drop size at 3.0 m ceiling; however, at 6.0 m the FDS is showing a reasonable trend of decreasing ADD with the increase of the drop size. This decrease in the ADD is probably due to the fact that at constant velocity the larger drops usually spread farther away from the axis than that with smaller sizes.

Figure 31 shows that the ADD values under the 3.0 m ceiling is higher than that under the 6.0 m ceiling, it also shows that the difference between the ADDs under 3.0 m and 6.0 m ceiling decreases as the flow rate increase. That is explained in [4], as by decreasing the flow rate the size of the droplets increase so the water flow spray at low flow rate looks like a cone which means that by increasing the height the target area of radius 1.29 m will capture less amount of water. However, for high flow rates the water flow spray looks more like a bell which means by increasing the amount of water captured by the target area will not be so sensitive to the ceiling height and will almost capture the same amount of water.

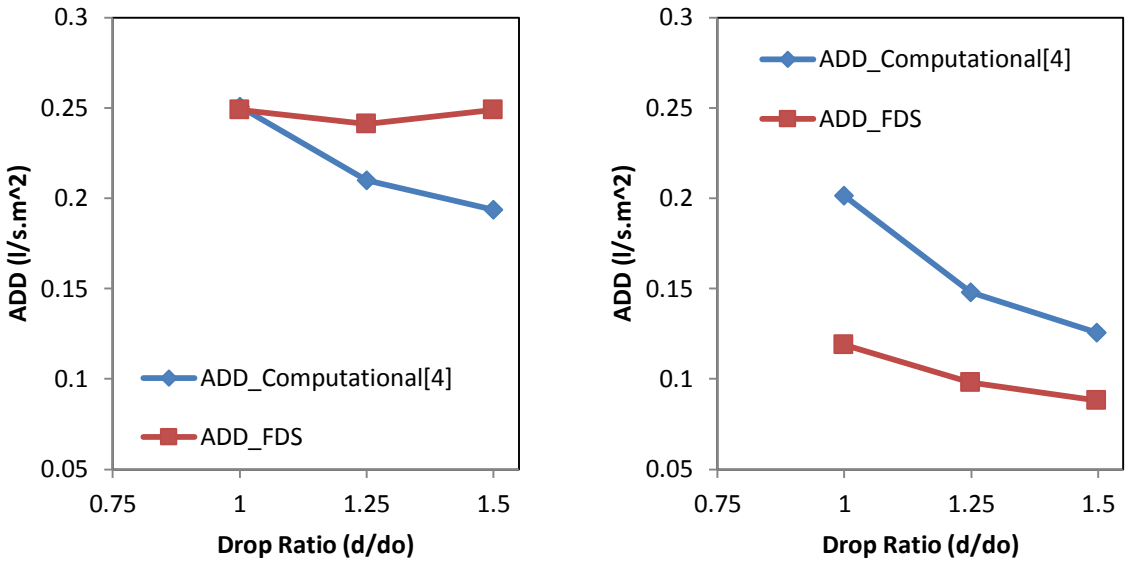

Figure 30 ADD vs. drop size at flow rate = 3.15 l/s (3.0 m ceiling (a) and 6.0 m ceiling (b))

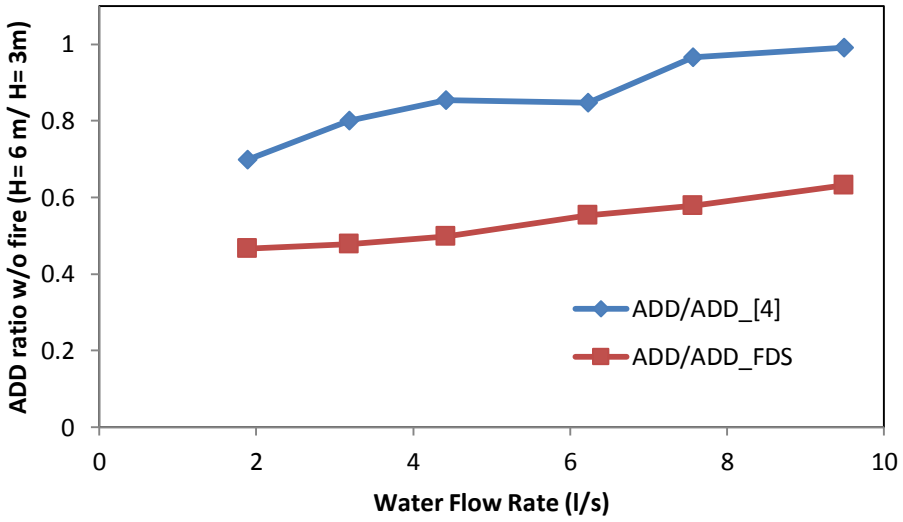

Figure 31 Ratio of ADDS without fire between 3.0 m ceiling and 6.0 m ceiling heights

3.3.4. Input sensitivity on the velocity radial distribution

The penetration capabilities of the sprinklers were well explained in [24] by Ebrahimzadeh, S. as a competition between the momentum of the upward fire plume and the downward sprinkler spray and the winner of this competition determines whether the fire extinguishment is possible. The momentum value

is based on the velocity value so it was important to study the effect of some input parameters on the velocity field.

In this section, a sensitivity to the effect of the following inputs on the velocity radial profile of the flow were investigated for the case with flow rate of 3.16 l/s under 6.0 m ceiling:

- Increase of the mean droplet size by 1.25 and 1.5 times.
- Using angle set 2.
- Changing the default inner spray angle from zero to 4°.

The sensitivity study was done on two heights namely the far field and the near field, the far field is assumed to be 2.0 m from the floor and the near field is 4.0 m from the floor.

- Far field:

As shown in Figure 32, It was interesting to monitor how the velocity decreases at the axis when using larger drop sizes, the default seems to be higher than that with 1.25 d_o and the 1.5 d_o cases respectively, yet, this deviation demolish radially till it almost vanishes from 1.0 m onwards. Using half of the discharge angle seems to have the highest impact on velocity at the axis as it almost doubled, however, the difference between the half and default angle decreases till it vanishes at 1.0 m radially then the trend is switched where the velocity of the default angle will start to show higher values than that with the half angle which means that at the axis the case with half angle gives higher momentum, while radially, the default angle spray seems to have higher momentum. By changing the inner angle from zero to 4°, the velocity decreased extremely (which is expected) at the axis and the peak value for the velocity is shifted from being one value at the center to two values at around 0.7 m radially and then the velocity trend switch where that with inner angle is 4° will be a bit higher than the default case and this difference demolish at 4.0 m.

- Near field:

It is clear in Figure 33, the same trends are observed however the numerical differences are smaller which means that by moving further from the sprinkler spray the effect of these parameters increases.

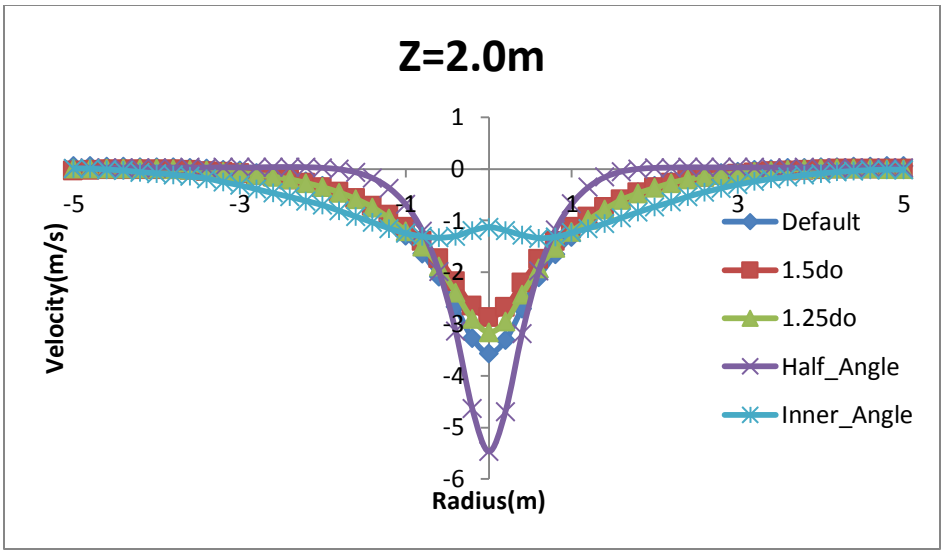

Figure 32 Far field radial velocity distribution

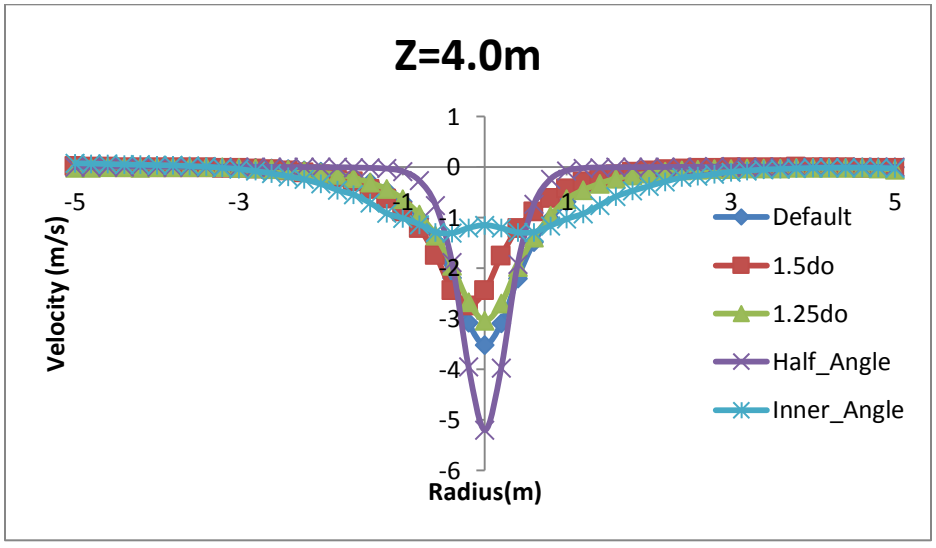

Figure 33 Near field radial velocity distribution

4. Interaction between the gas phase and the sprinkler sprays (water phase)

Six different flow rates were investigated in order to put hands on the effect of changing the water flow rate of a specific sprinkler on the sprinkler's penetration capabilities. To increase the flow rate, the operational pressure of the sprinkler will increase, yet, the droplets size will decrease. As mentioned in [21] the droplet size is reduced by increasing the pressure based on an empirical correlation. The reduction in the drop size will decrease the penetration capabilities, however, when the flow rate increase the spray momentum will also increase due to the increase in the velocity of the water spray. Based on that, it is interesting to study the balance between the effect of the increased flow rate on both the drop size and momentum by studying the effect of the flow rate variation on the penetration capabilities. The PR will only show the balanced relation between the momentum and the drop size, however, it won't show the effect of each parameter separately, and that's why later an analysis for the momentum and the drop size effect will be done.

In the hot air plume-water spray interaction simulations, the same sprinklers described at chapter 3 were used, also the comparisons were done using the hot air described in model B. Although one of the main goals behind this research was to use hot air injection instead of pool fires in the interaction simulations, it was necessary to re-do some of the interaction simulations using pool fires in order to ensure that we are getting the same results or at least comparable results. In addition to that, it was interesting to do sensitivity analysis to some parameters in our simulations to check its effect on the end results namely the PR.

4.1. Numerical modeling and set up

The setup of the interaction simulations was based on the ceiling height as a main controller for the domain size. The domain of the 3.0 m ceiling height was 5.0 m X 5.0 m X 3.0 m (Width X Depth X Height) while the domain of the 6.0 m ceiling height was 10 m X 10 m X 6.0 m (Width X Depth X Height), the reason behind increasing the floor area is the larger radial water distribution noticed in case of higher ceiling, the hot air was injected on 1 m^2 area (square) with its center placed exactly under the sprinkler's axis. To study the penetration performance the ADD values were calculated over a circle of radius 1.29 m with its center aligned directly under the sprinkler's axis. The radius of 1.29 m was chosen as the radius value chosen in [4] to be able to compare the data in case needed. Figure 34, gives a general view for the setup with 6.0 m ceiling height, where the blue flow presents the water spray and the red flow presents the hot air. It is also important to note that, for the interaction simulations whether using hot air or combustion pool fires the sprinklers' starting time was after 10 seconds from the beginning of the hot air or fire simulations start. Both of the hot air and combustion simulations showed steady state values around the 10 seconds. However, the PR and ADD values were taken after at least 40 seconds from the sprinklers starting time to ensure steady state values. Some of the upcoming simulations were repeated more than one time to ensure reaching convergence. The repeated results, however, showed typical values and there was no sense to keep repeating all the simulations more than one time. Also, sensitivity for the domain size for both the 3.0 m and the 6.0 m was done to ensure that the domain size is not affecting the results.

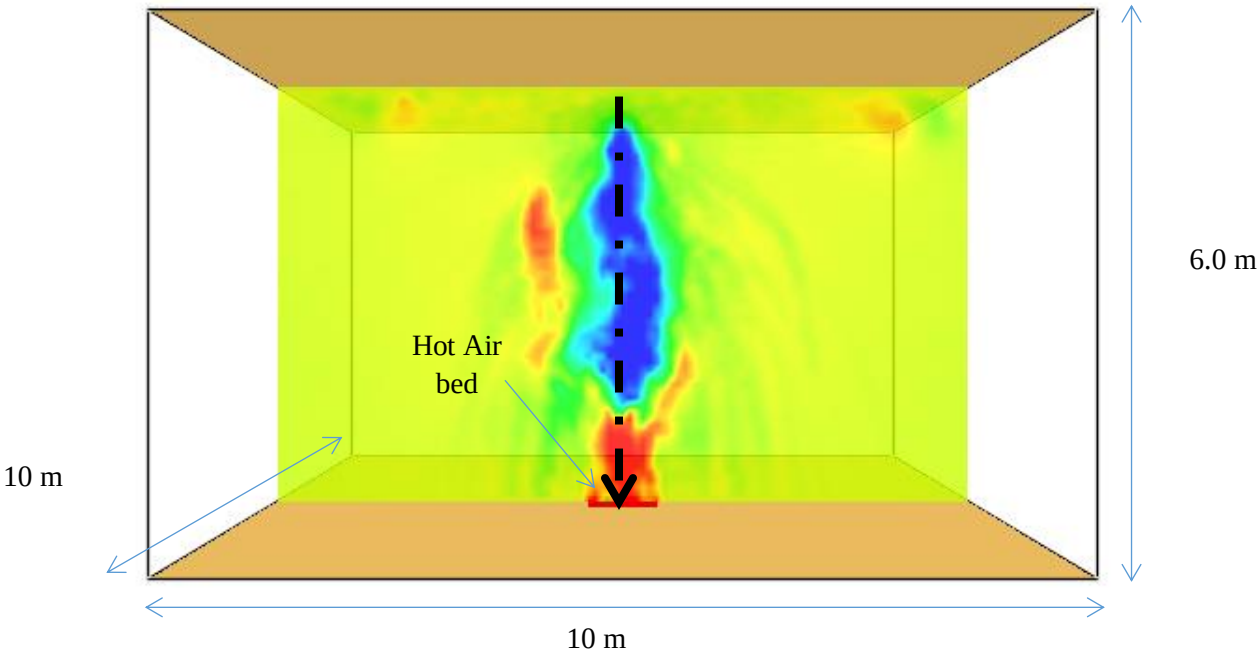

Figure 34 Domain for interaction simulations (6.0 m ceiling)

The cell size used for all the interaction simulations was 0.10 m and a cell size sensitivity analysis was done to ensure that the cell size is not affecting the results. In Figure 35, the sensitivity analysis was done for the 3.0 m ceiling height interaction simulation for the 1000 kW hot air plume case using 0.06 m cell size. As shown in Figure 35, the ADD values vs. the flow rates did not change with finer mesh size, which means that the used cell size of 0.1 m is reasonable:

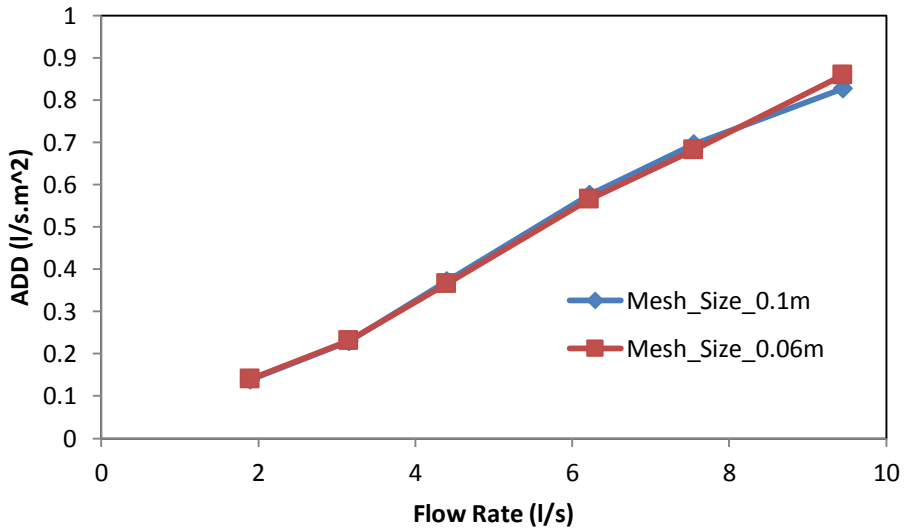

Figure 35 Sensitivity analysis for the cell size

It was also important to prove that simulating the pool fire by injecting the hot air was giving the same results as when using the hot air plumes. Based on that, the ADD values were computed for the six different flow rates and the three heat release rates fires under the 3.0 m ceiling. In addition to that, the ADD values for the six different flow rates were computed for the combustion simulation and hot air simulation for the 1000 kW under the 6.0 m ceiling. The following figures from Figure 36 to Figure 39 show that there was almost no deviation in the data between the simulations done using the hot air and those using the combustions model.

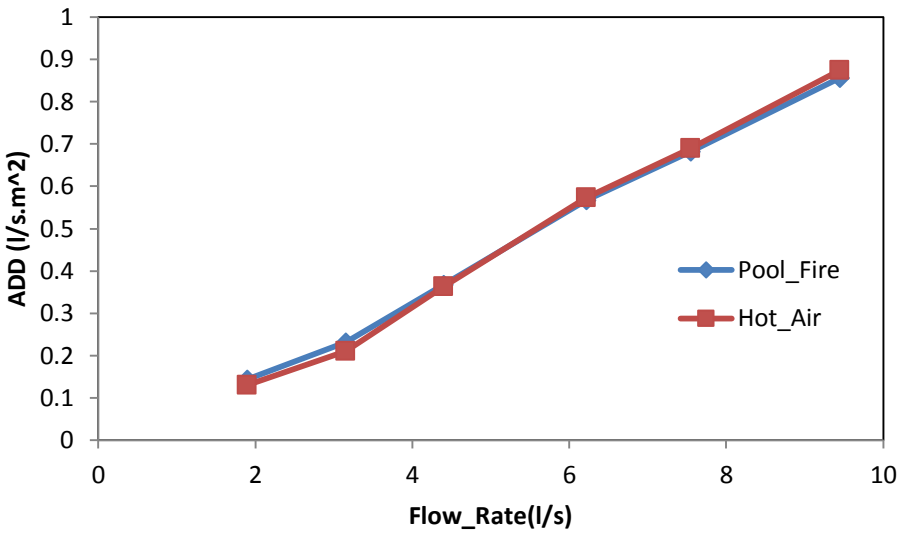

Figure 36 1500 kW fire 3.0 m ceiling

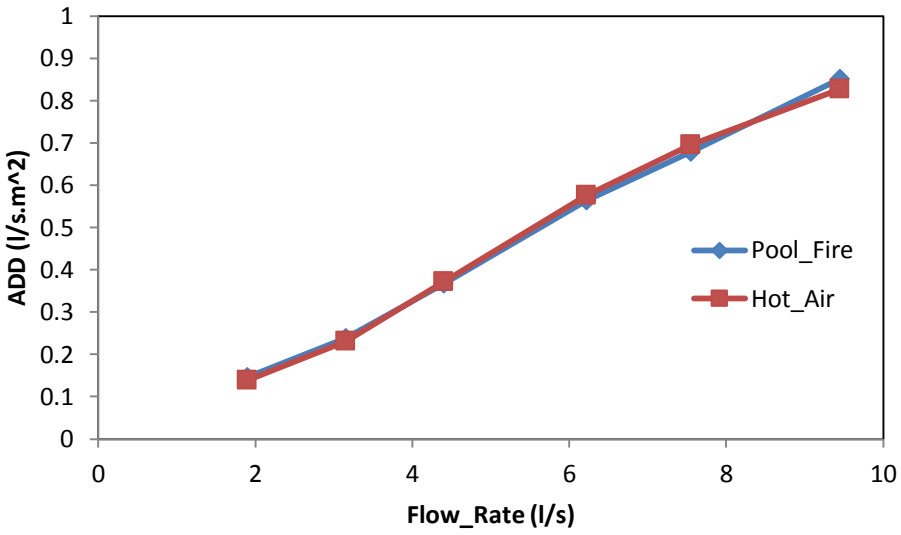

Figure 37 1000kW fire 3.0 m ceiling

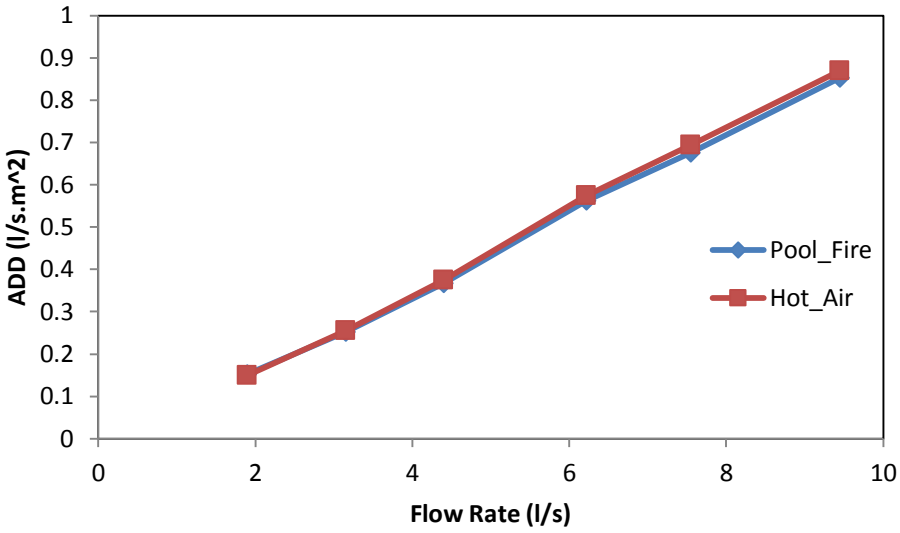

Figure 38 500 kW fire 3.0 m ceiling

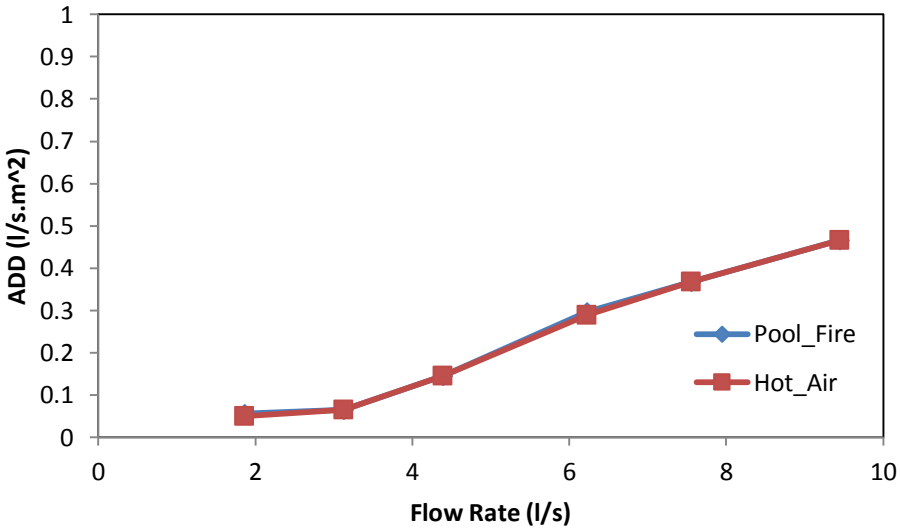

Figure 39 1000 kW fire 6.0 m ceiling

Also a cell size sensitivity analysis for the interaction simulations using pool fires was done. As presented in Figure 40, to ensure that using 0.10 m cell size for the interaction case using pool fires is reasonable. To ensure that, two simulations were done using 0.10 m and 0.05 m cell sizes. It was found that, the results using 0.10 m cell size is almost exactly the same as 0.05 m cell size.

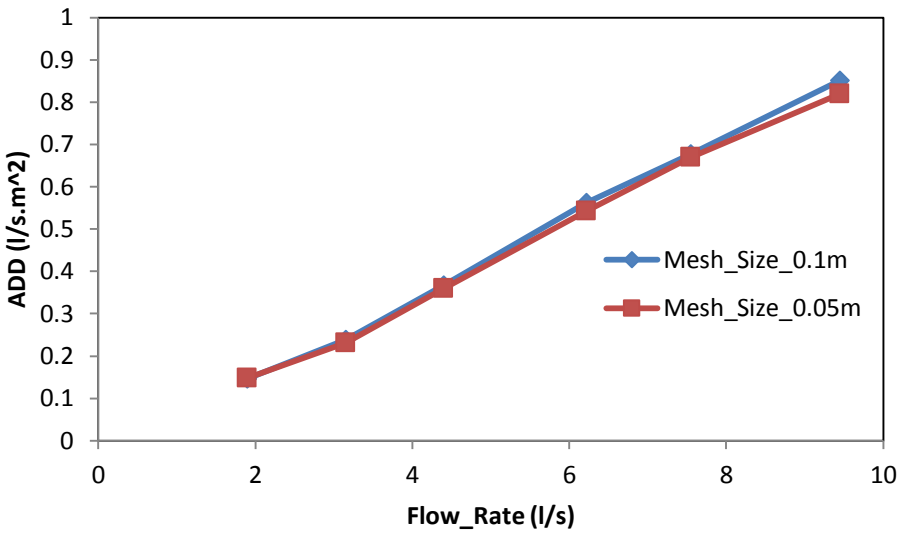

Figure 40 cell size sensitivity analysis

4.2. Interaction simulations results

The ADD and PR values of the six flow rates were computed for the three fires simulated by the hot air namely 500 kW, 1000 kW and 1500 kW using model B, under both of the two main celling's heights namely (6.0 m and 3.0 m) and an extra ceiling height of 8.0 m.

4.2.1. 6.0 m celling height

It was found that, the ADD of a specific sprinkler increases as the flow rate increase for a given fire and decreases with the increase of the fire size at fixed flow rate as shown in Figure 41. Based on that, the ADD is not the precious parameter to compare between sprinklers as the ADD is just showing the amount of water reached the floor or the burning surface.

Based on that, it was found to be critical to compute the PR which shows exactly how much is the amount of water that will reach the floor or the burning surface in case of fire compared to the amount of water reached the floor without the presence of fire. So for all the coming results and data the ADD will be the amount of water that reached the floor (the same level of the hot air injector / pool fire) on a circle of 1.29 m and the PR will be the ratio between the ADD in case of fire and the ADD in the case without fire.

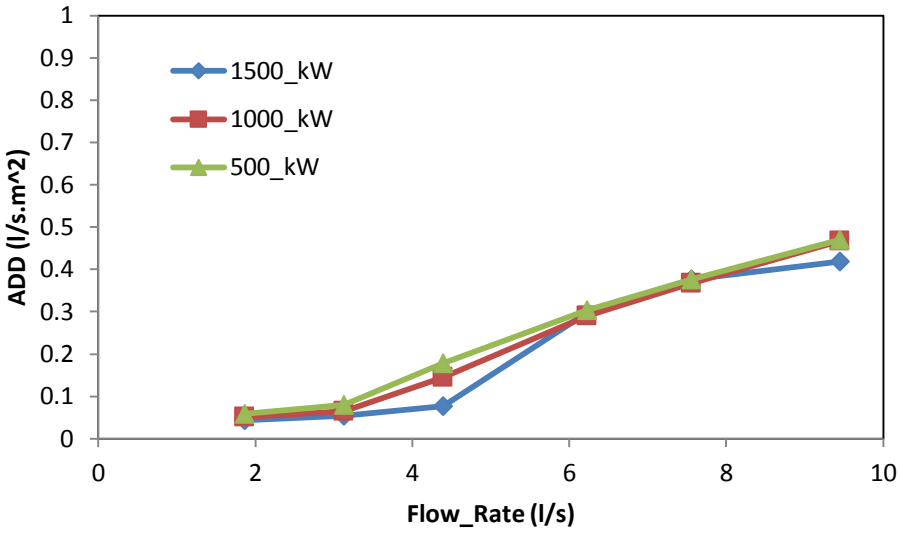

Figure 41 ADD vs. Water Flow Rate below 6.0 m ceiling

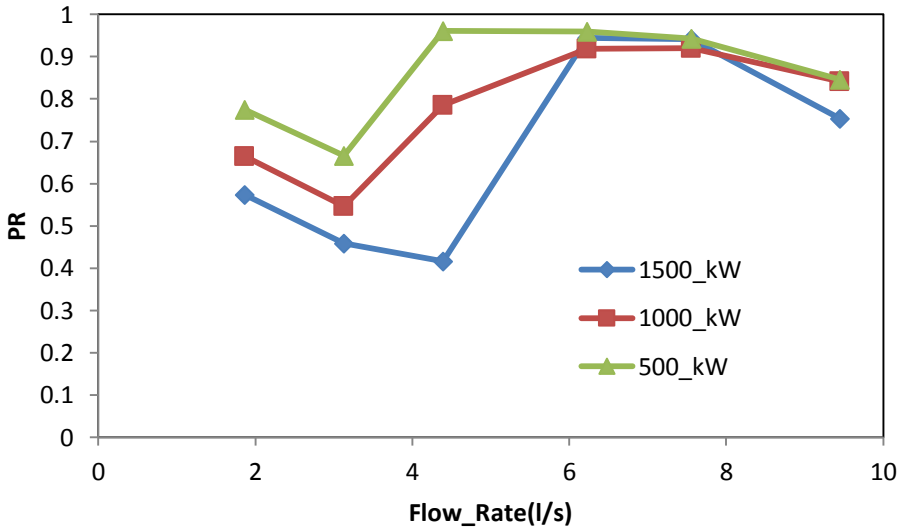

Figure 42 PR vs. Water Flow Rates below 6.0m ceiling

As shown in Figure 42, for the 500 kW and the 1000 kW the PR decreases with the increase of the flow rate up to 3.16 l/s, the PR, however, increases again till it reaches its highest value (near unity) at 4.42 l/s for the 500 kW and at 6.26 l/s for the 1000 kW, the PR then decreased again at higher flow rate of 9.48 l/s. For the 1500 kW fire, the PR decreases with the increase of the flow rate up to 4.42 l/s, the PR starts to increase after that, till it reaches almost unity at 6.26 l/s and then the PR decreased again at higher flow rate of 9.48 l/s.

All in all, the penetration ratio was found to be at its optimal operating value at 4.42 l/s for the 500 kW and to be 6.26 l/s for both the 1000 and 1500 kW. The same trends were found in [4], however, the optimum operating flow rates were a bit higher that is probably because of using fires with higher momentum (velocity) for the corresponding HRR. Based on that, in this specific case it's recommended to use a sprinkler with a flow rate of 6.26 l/s to get the highest PR for the whole range of fires.

There are many different factors that affect the value of the optimal operating value for example [4]:

- The fire size as it is shown that the optimal operation flow rate value increases with the increase of the fire size (probably the velocity of the plume).
- The droplet size.
- The flow momentum.
- The ceiling height.

First of all, the decrease in the PR between the flow rate of 1.90 to 3.16 l/s at 500 kW and 1000 kW and that between the flow rate of 1.90 to 4.42 l/s kW at 1500 kW fire is expected to be due to the decrease in the drop size with the increase of the flow rates. It is also expected that by having higher optimal flow rates values that the decrease in the drop size affects the PR value more significant when the fire size increase.

The effect of the drop size was the dominate value probably till the least PR values were reached at 3.16 l/s for the 500 kW and 1000 kW and at 4.42 l/s for the 1500 kW fire. The effect of the spray momentum is expected to dominate after that and helps the penetration ratios to boost with the increase of the flow rate. Based on the pervious analysis, it was interesting to study the sensitivity of the previously mentioned factors on the PR values, an analysis to check the effect of the drop size, the momentum and the ceiling height on the PR values will be done in the upcoming sections respectively.

4.2.1.1. Penetration Ratio vs. drop sizes

To separately check the effect of the drop size on the PR values, the drop size of the spray 3.16 l/s was increased by 50% and 25% with all the other parameters are kept constant. The flow rate of 3.16 l/s was chosen for two the reasons first its computational time is less than most of the other flow rates in addition to that it was also chosen for this sensitivity analysis at [4], so we found it could be interesting to compare our outcomes with something done already in the literature. As shown in Figure 43, the ADD was computed for the three different fire sizes with water flow rate of 3.16 l/s also it was computed to the water only case. The d is the drops' median size and the d_o is the default value that was used previously in the research, the values of the two other sizes were d= 1.5 d_o and d= 1.25 d_o. It was also shown that, the ADD for the water only case was noticeably decreasing with the increase of the droplet median size, this could be explained as mentioned before to be due to the ability of the larger drops to spread away further than smaller ones when both are injected with the same velocity. Figure 44 shows the effect of the drop size on the PR values and that the PR increases with the increase of the drop size. It was also noticed that, these founding verifies the conclusions and founding in [4].

Based on the pervious founding, it was important to quantify the effect of the flow momentum on the PR values. In the next section, the same flow rate of 3.16 l/s will be investigated with 25 and 50 % increase in the spray momentum.

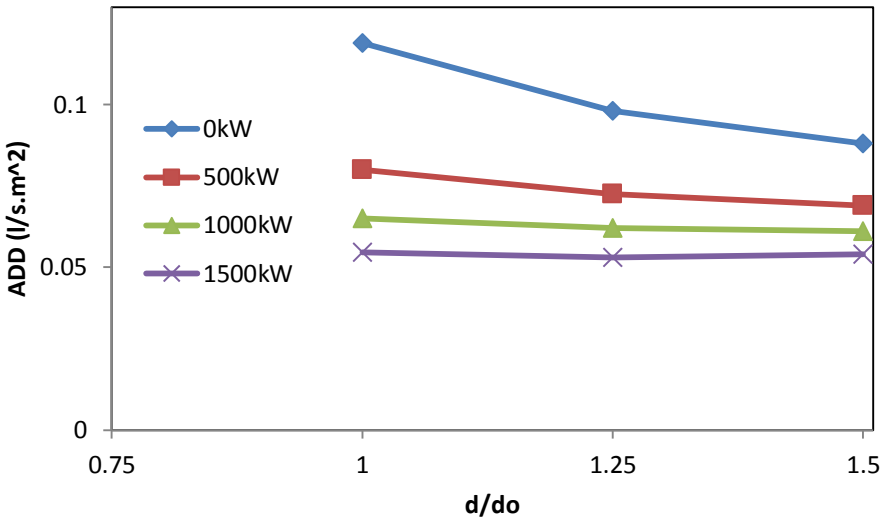

Figure 43 ADD vs. drop size at flow rate =3.16 l/s

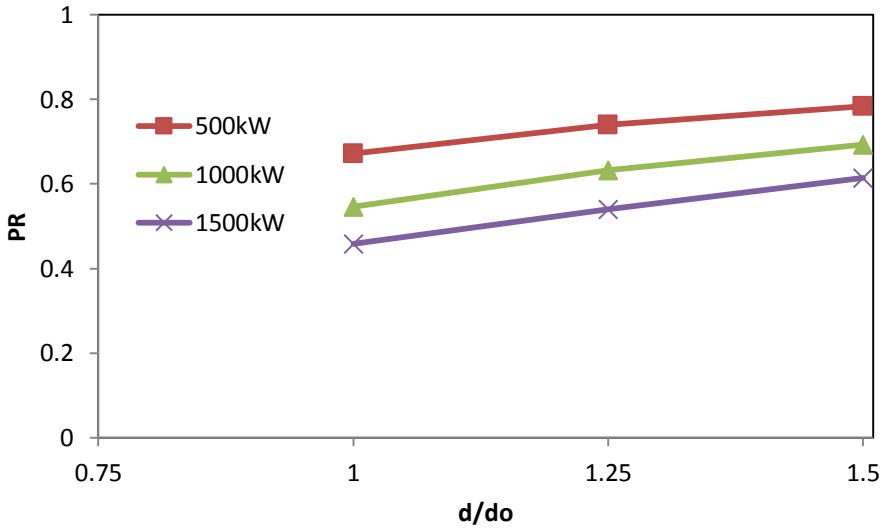

Figure 44 PR vs. drop size flow rate =3.16 l/s

4.2.1.2. Penetration Ratio vs. Spray momentum

To separately check the effect of the spray momentum on the penetration ratio at 3.6 l/s water flow rate, the spray momentum was increased to 25 % and 50 % of its default value. The increase of the spray momentum was computed by increasing the discharge speed by the needed percentage.

The Spray momentum is actually based on the following relation [4]:

$$T \alpha \int_A \boldsymbol{\rho v_z v_z . dA_m} \text{ (Equation 35)}$$

Where, ρ is the water density, v_z is the axial directional velocity vector and A_m is the area where the momentum will be measured. Based on equation 35 the spray momentum increases linearly with the increase of the velocity.

As shown in Figure 45 (where M is the water momentum value, Mo is the default momentum value for the corresponding case), the ADD values for the case of no fire and for the case of fire of 500 kW decreases with the increase of the momentum that is probably due to the increase in velocity which lead the water drops to be move further away from the center.

The ADD for the 1000 kW and 1500 kW is almost constant with different momentum values despite the slight decrease in the ADD for the 1000 kW at 1.25Mo momentum, this was almost the same trend found in [4]. Figure 46 shows that the PR values is almost constant with respect to the momentum (velocity) value, which proves that the effect of the momentum value on the PR value is too low compared to the effect of the drop size and this also verify the finding in [4].

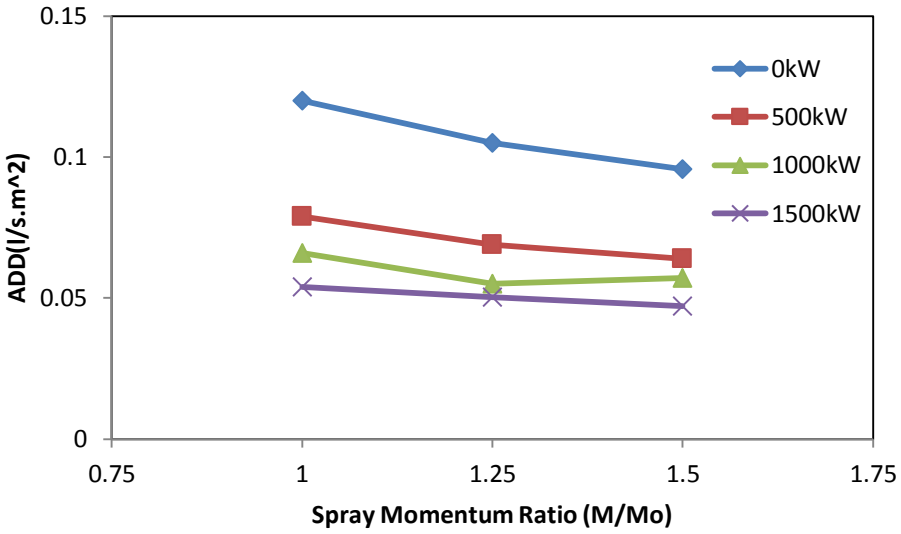

Figure 45 ADD vs. spray momentum flow rate= 3.16 l/s

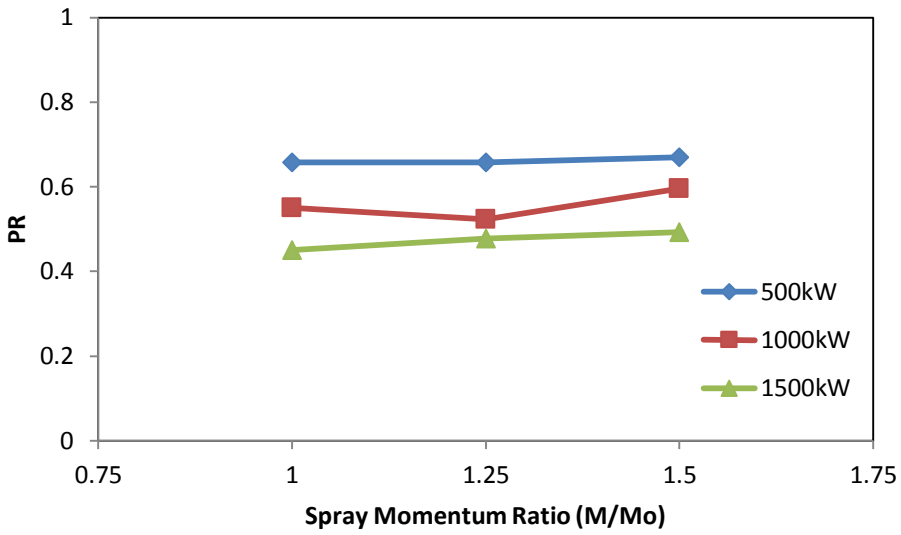

Figure 46 PR vs. spray momentum flow rate= 3.16 l/s

4.2.2. 3.0m celling

To study the effect of the ceiling height on the PR, the same cases were tested again but with a 3.0 m ceiling height. As it is presented in Figure 47, the ADD values are very close depend less on whether there is fire or not and even depend less on the fire size. However, there was a small variation in the results between the flow rate of 1.90 l/s to 4.42 l/s and the results is almost identical from 4.42 to 9.48 l/s. Figure 48 is showing the PR values against the flow rate values, as expected the PR value reached unity from the flow rate of 4.42 l/s for both the 1000 kW and 1500 kW, yet, it reached unity earlier for the 500 kW at flow rate of 3.16 l/s.

Based on that, the best operating flow rate is 3.16 l/s for the 500 kW and 4.42 l/s for the 1000 kW and 1500 kW. It is again proved that, the bigger the fire, the higher the optimum flow rate value. It is also interesting to show that the optimum flow rate decreased with the ceiling height decrease, the optimum operating flow rate for the 500 kW at 6.0m ceiling was 4.42 l/s however, it was found to be 3.16 l/s for the 3.0 m and the optimum flow rate for the 1000 and 1500 kW was found to be 6.26 l/s for the 6.0 m ceiling and it decreased to 4.24 l/s at 3.0 m ceiling height. It is recommended in this case (3.0 m) to use a flow rate of 4.42 l/s to achieve the heights penetration ratio while covering a range of fire sizes from 500 kW to 1500 kW. It was also found that, the penetration ratio increased steeply with the decrease of the ceiling height that was basically due to the increase of the ADD value on the same area.

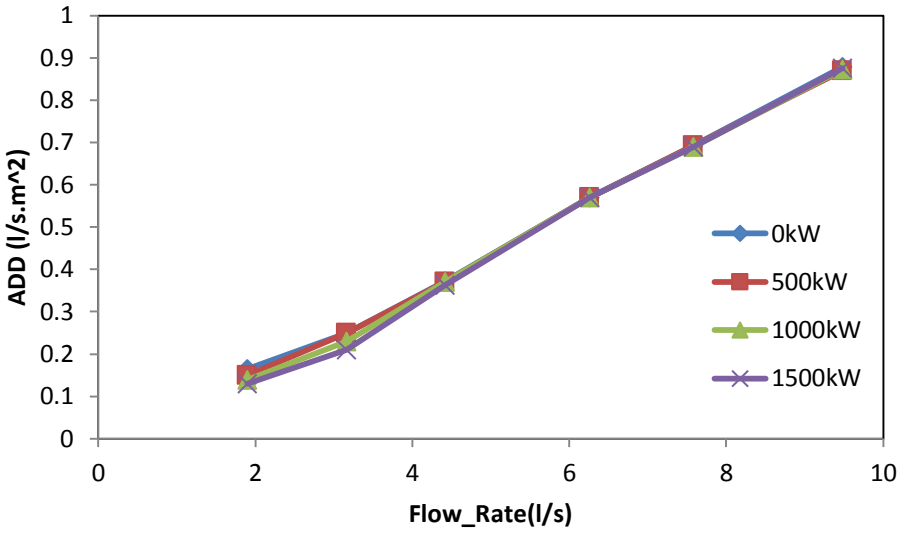

Figure 47 ADD vs. flow rates below the 3.0 m ceiling

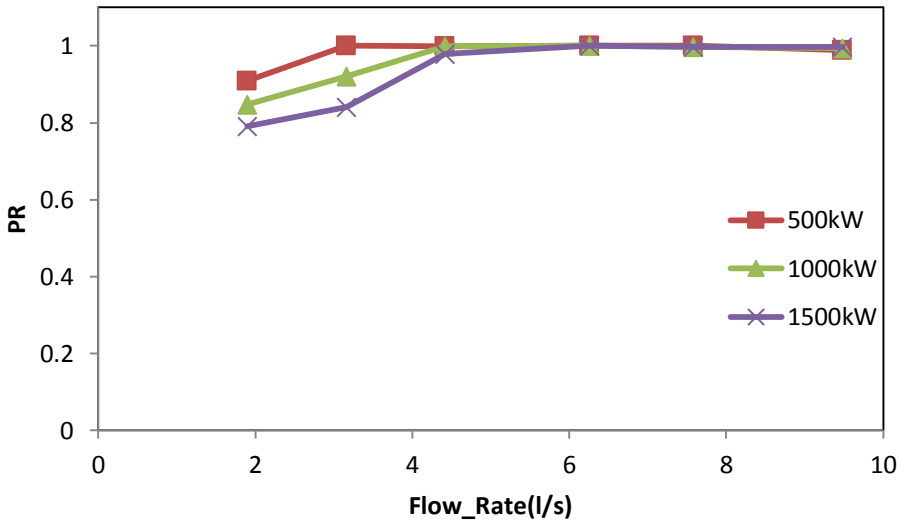

Figure 48 PR vs. flow rates below the 3.0 m ceiling

Due to the extremely high ADD and PR values found for the 3.0 m ceiling case, it was interesting to do one more sensitivity analysis for the effect of the ceiling height by running some simulations at a ceiling height of 8.0 m to cover broader range of ceiling heights.

4.2.3. 8.0 m ceiling

Couple of cases was computed with 8.0 m ceiling height, the first case was without fire and the second case was with a hot air plume of 1000 kW. The idea behind these simulations was to put hands on the effect of the ceiling height on the ADD and the PR values as mentioned before. The values of the 8.0 m

ceiling were compared to the corresponding cases of 6.0 m ceiling and 3.0 m ceiling. As shown in Figure 49, the ADD values of the 3.0 m height are much higher than that of the 6.0 m and 8.0 m in the case of no fire. Figure 50 shows that the ADD in case of 1000 kW increases with the ceiling height decrease. Which again verify the findings in the previous analysis and the findings in [4]. Figure 51, is showing how the PR values are sensitive to the ceiling height, the figure also shows that the flow rate corresponding to the lowest PR value increase with the increase of the ceiling height, where the water flow rate corresponding to the lowest PR value is 1.9 l/s, 3.16 l/s and 4.42 l/s for the ceiling heights 3.0 m, 6.0 m and 8.0 m respectively. Also the optimum operating flow rate value increases with the increase of the ceiling height, where the optimum value for the 3.0 m ceiling height is 4.42 l/s and for the 6.0 m and 8.0 m is 6.26 l/s.

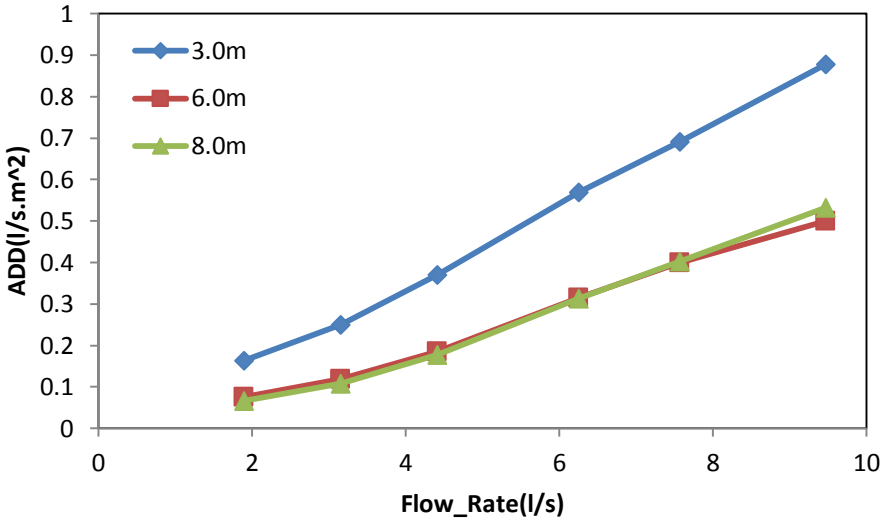

Figure 49 ADD vs. flow rate at 3.0m 6.0m and 8.0m ceiling height

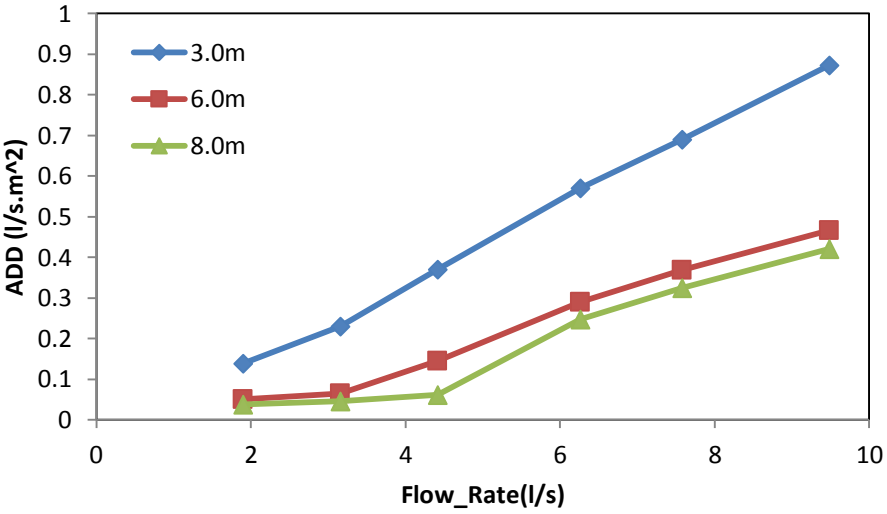

Figure 50 ADD vs. Flow rate with 1000 kW hot air plume at 3.0 m, 6.0 m and 8.0 m ceiling height

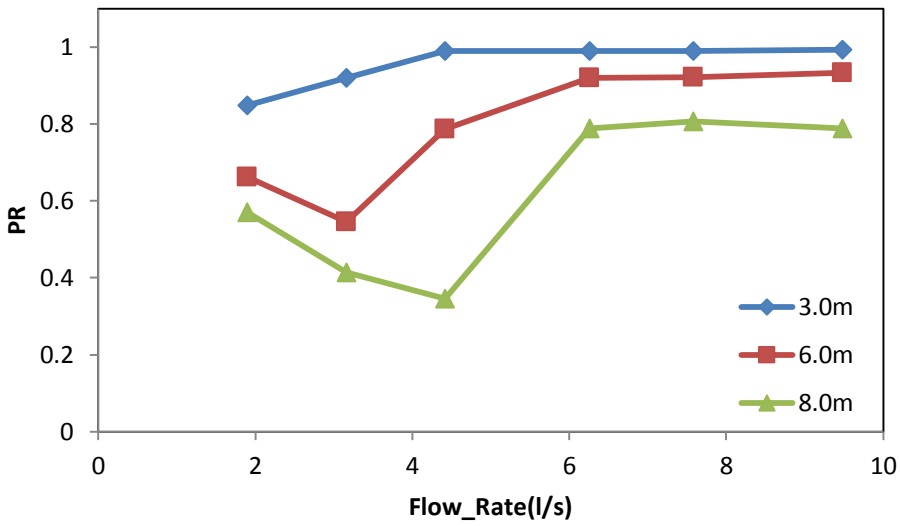

Figure 51 PR vs. flow rate with 1000 kW hot air plume at 3.0 m, 6.0 m and 8.0 m ceiling height

4.2.4. Target's area and spray angle sensitivity analysis

4.2.4.1. Target's area vs. the ADD and PR

We also found it interesting to examine the sensitivity of the size of the target area on the predicted optimum flow rate value. Based on that, we decided to do some simulations by changing the target's area where we are computing the ADD, we changed it to be the exact area of the hot air plume boundary 1 m^2 (0.564 m radius) and area I in [4] of 1.5 m^2 (0.69 m radius). We did the simulations using the three ceiling heights, the six flow rates and only the hot air plume of 1000 kW.

4.2.4.1.1. Actual Delivered Density

As shown in Figure 52, Figure 53 and Figure 54 the ADD values are higher for the areas with smaller radii, the reason is probably the fact that the ADD is usually higher near the axis with its peak value at the axis. Based on that, it was expected to have higher ADD values in case of no fire for the areas with smaller radial distances away from the axis. It is also showing that this fact is verified independent on the ceiling the height.

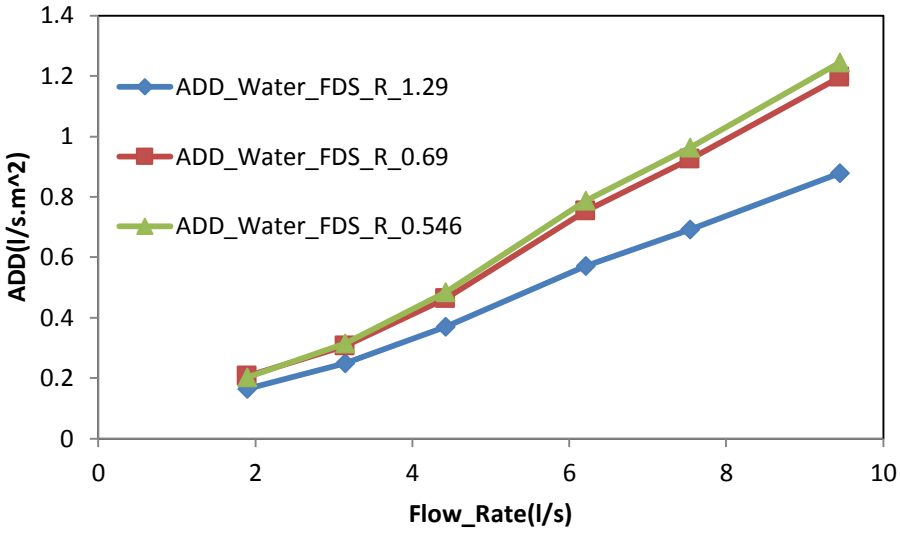

Figure 52 ADD vs. Flow Rate for three different target areas at 3.0 m ceiling

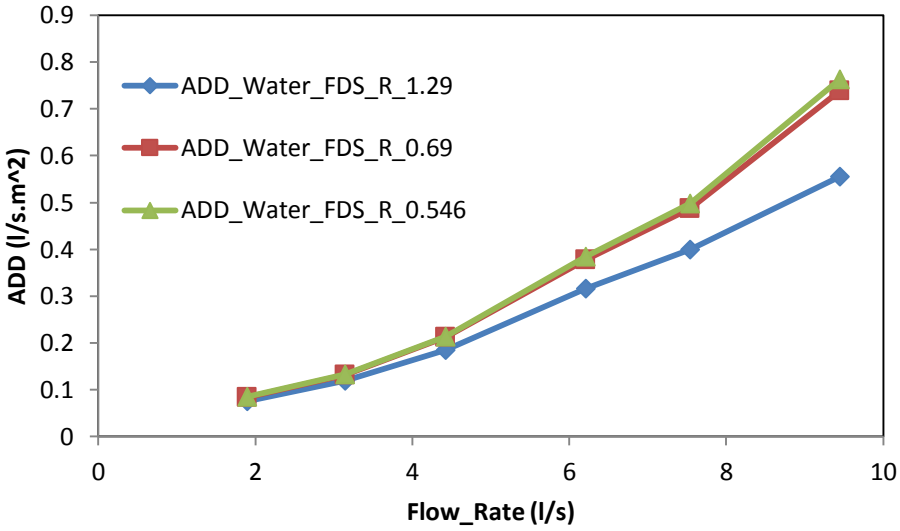

Figure 53 ADD vs. Flow Rate for three different target areas at 6.0 m ceiling

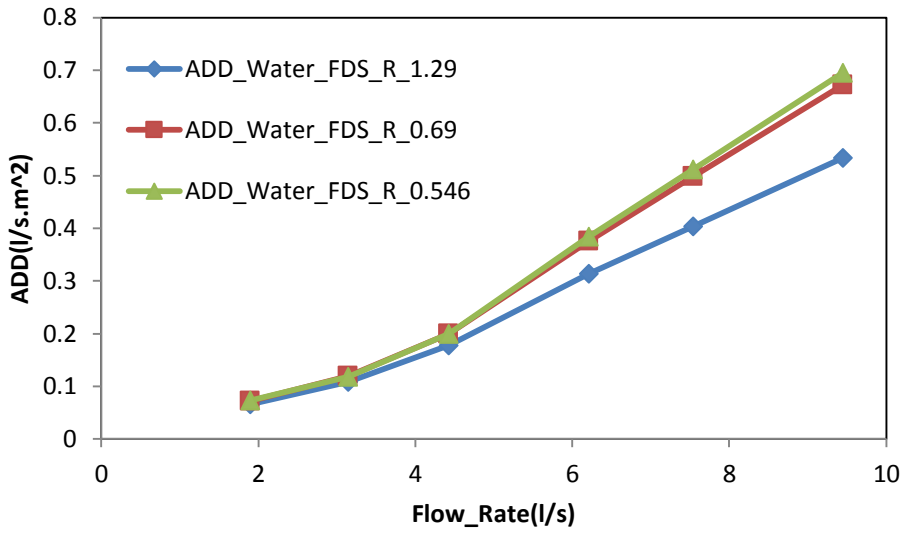

Figure 54 ADD vs. Flow Rate for three different target areas at 8.0 m ceiling

However, the deviation in the ADD values between the different target areas is decreasing and is approaching to zero with the increase of the ceiling height and deceasing of the flow rate. As shown in Figure 55 the ratio between the ADD values on the 1.29 m radius over that of 0.546 m radius is increasing and approaching to unity with the increase of the ceiling height for the same flow rate. That is probably because as the ceiling height increase the angle of spray that affects a specific area decrease, which means that the portion of flow rate taken by the trajectories just near by the axis is increasing among the total number of trajectories affecting a specific area by increasing the ceiling height. Assuming that, the effect of the water jets near the axis is between the discharge angle of 0 (where 0 is the center of the sprinkler orifice) and 4°. Therefore, by a simple sketch done in Figure 56 to calculate the water flow angle (α) used in reaching the 1.29 annulus radius in both of the two cases 3.0 m and 6.0 m, we can use the following relation:

$$\tan \alpha = \frac{\boldsymbol{opposite\ side}}{\boldsymbol{adjacent\ side}} \quad \textit{(Equation 36)}$$

Where the opposite side is the radius of the annulus (1.29 m) and the adjacent side is the ceiling height (3.0 m and 6.0 m). As it is shown in Figure 56, α_1 is smaller than α_2 and with simple calculations, the 4° are considered 30 % of the trajectories used in the 6.0 m ceiling (α_1) to cover an area with 1.29m radius, while it only considered 15 % of the trajectories used in the 3.0 m (α_2). Based on that, the effect of the water jet along the axis is doubled when the ceiling increased from 3.0 m to 6.0 m. Therefore, for the 6.0 m ceiling, the difference in the ADD between the two targets is small because of the dominating effect of the high water flow rates at the axis and this effect decreased by decreasing the ceiling height so the difference between the two targets is more obvious at 3.0 m.

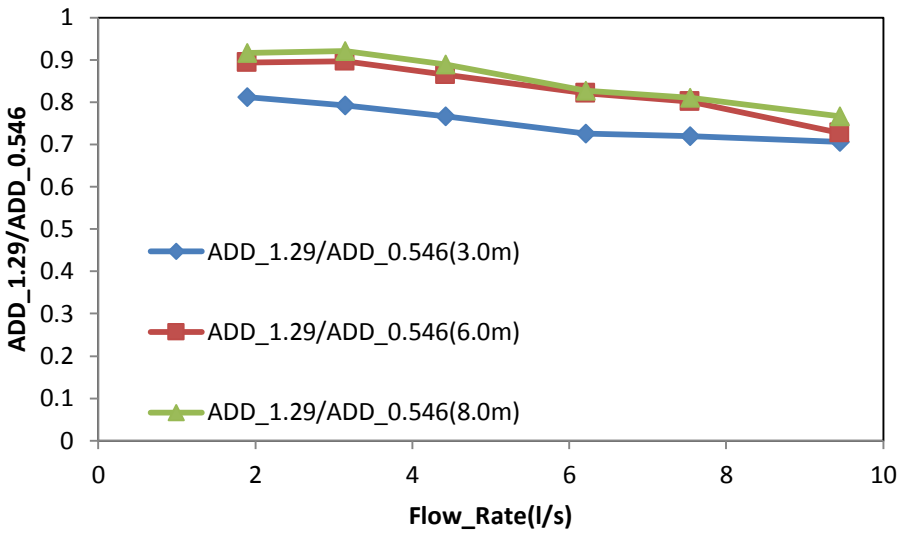

Figure 55 ADD ratio vs. Flow Rate for three different ceiling heights

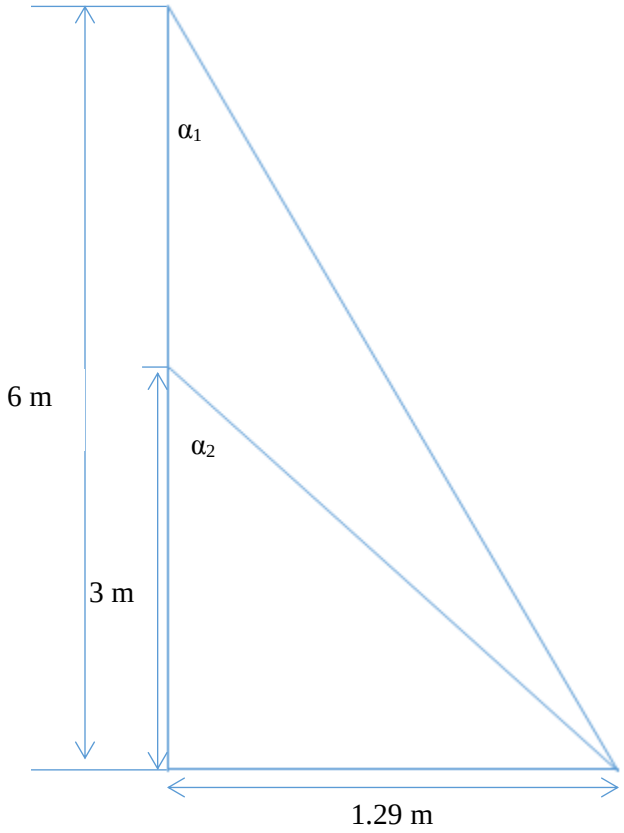

Figure 56 Flow angles vs. ceiling height

4.2.4.1.2. Penetration Ratio

The penetration ratio was also computed for the same previously mentioned cases by adding a hot air plume of 1000 kW and 500 kW. Since we got the same output trends from the 1000 kW and 500 kW simulations, only the 1000 kW simulations will be shown here.

As shown in Figure 57, Figure 58 and Figure 59 the PR values are lower when the target area is less and the fire (hot air plume) covers a bigger portion of the area. That is definitely expected and is probably due to the hot air with high momentum moving upward which collides with the downward droplets and whether evaporate it, push it further away from the hot air bed (target) or just let it pass. By increasing the portion of the hot air (with high momentum moving upward) in the targeted area, the amount of water drops that evaporate and pushed further away will increase which leads to lower PR values.

That concept can also conclude why the optimum flow rate increased from 4.42 l/s for the 1.29 radius area to 7.58 l/s for the 0.546 and 0.69 m radius areas for the 3.0 m ceiling as shown in Figure 57.

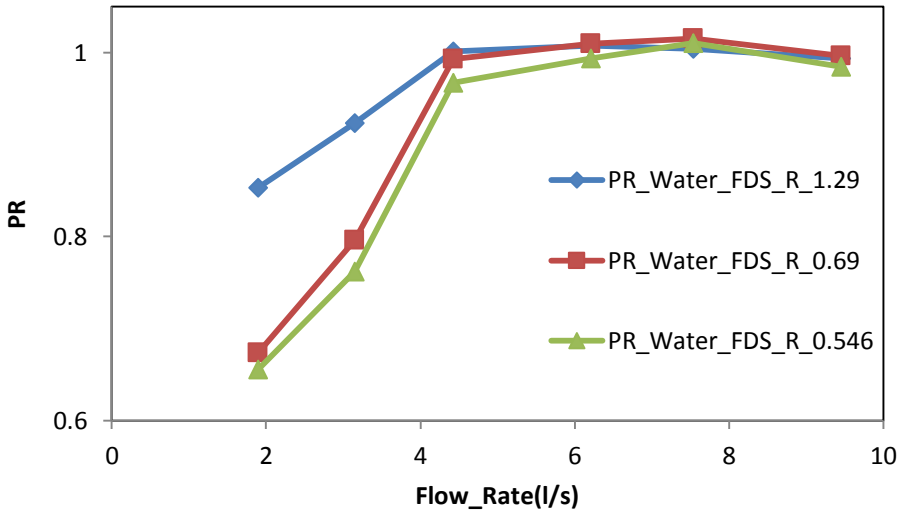

Figure 57 PR vs. Flow Rate on three different areas under 3.0 m ceiling

For the 6.0 m and 8.0 m ceilings the same optimum flow rate was found for the three different areas. That could be due to the loss in momentum of the hot air on higher heights and then when the interaction happens between the water drops and the hot air plume; the water drops dominates relatively easier than that of 3.0 m ceiling. Based on that, the target area factor seems to demolish with the increase of the ceiling height or decreasing the momentum of the hot air.

It was noted that, when the target area is 1.29 m radius the optimum flow rate increases with the increase of the height and when the target area was exactly the fire area, the optimum flow rate decreases with the increase of the height.

Please also note that the scale of the PR in Figure 57 was changed to be able to show the difference in PR especially for the flow rates between 4.42 to 7.58 l/s as by using the same scales used in Figure 58 and Figure 59 it was not clear how the PR value changes with the flow rate.

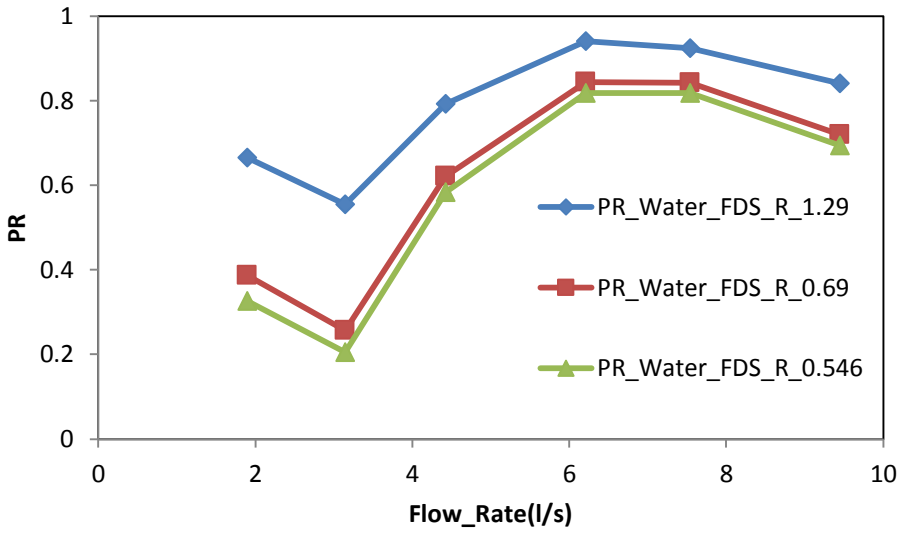

Figure 58 PR vs. Flow Rate on three different areas under 6.0 m ceiling

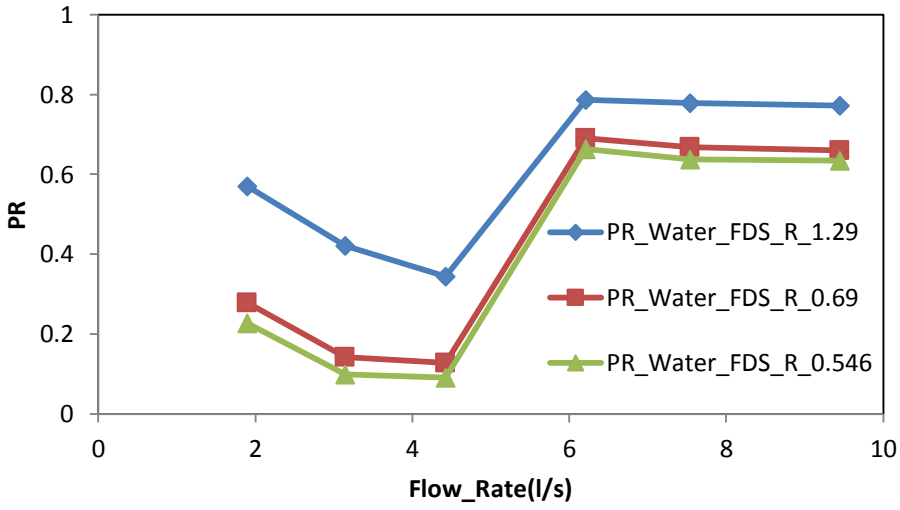

Figure 59 PR vs. Flow Rate on three different areas under 8.0 m ceiling

4.2.4.2. PR vs. spray angle

As mentioned before in the water phase section, by decreasing the spray angle the ADD increase extremely near the axis. In this section we tried to quantify the effect of the spray angle on the optimum spray flow rate for the same target area. It was found that, by decreasing the spray angle to the half of its value the penetration ratio will increase for the same flow rate, however, the optimum flow rate will decrease. As it is presented in Figure 60, Figure 61 and Figure 62 for heat release rates of 500 kW, 1000 kW and 1500 kW respectively, the PR increased by decreasing the spray angle and the optimum flow rate decreased by decreasing the spray angle. For the 500 kW plume the optimum flow rate changed from 4.42 l/s to 3.16 l/s and for the 1000 and 1500 kW plume the optimum flow rate changed from 6.26 l/s to 4.42 l/s.

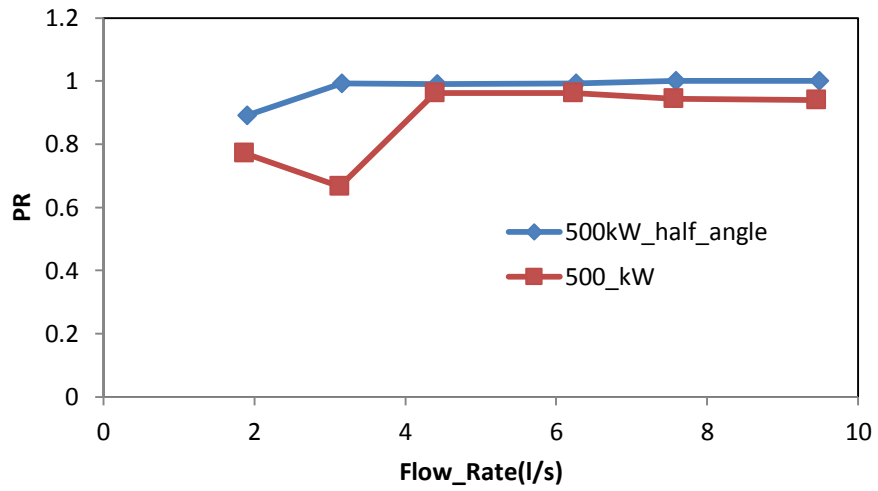

Figure 60 PR vs. Flow rate at 500 kW plume

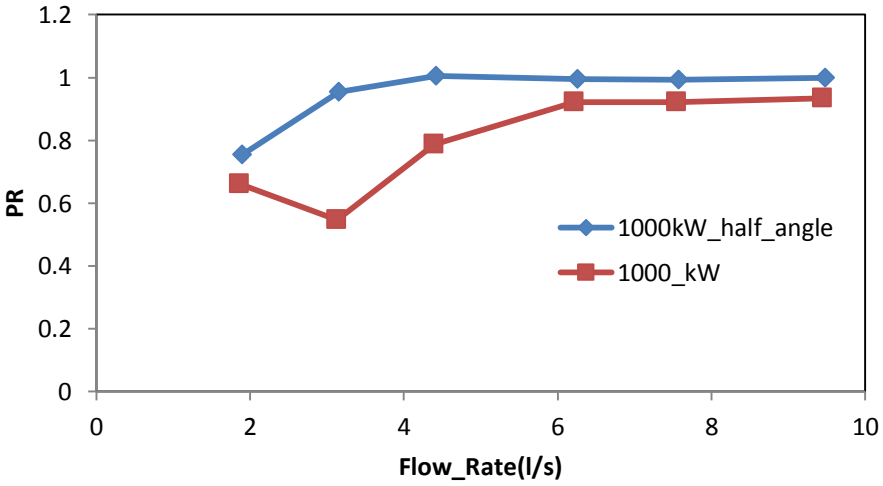

Figure 61 PR vs. Flow rate at 1000 kW plume

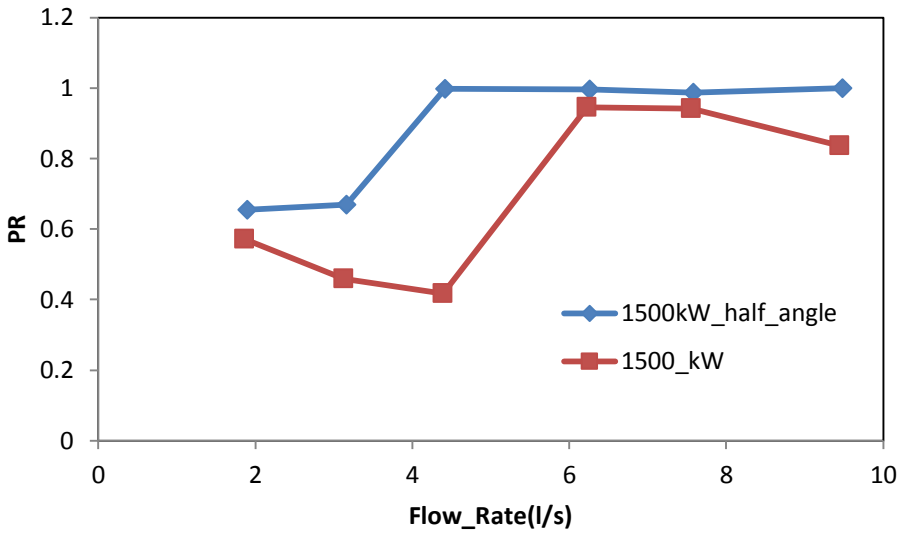

Figure 62 PR vs. Flow Rate at 1500 kW

4.2.5. Spray-Plume interaction boundary sensitivity analysis

As defined in [24], the spray- plume interaction boundary is the boundary between the downward spray momentum and the plume upward momentum. In this research we followed the same concept in [24] to determine the interaction boundary as the location where the downward flow of air entrained with the water spray and the upward hot air plume collide and form a stagnation plane where both of the two water and air flows meet.

In this section a sensitivity analysis for the location of the interaction boundary will be presented based on the fire size, spray angle, droplet size and flow rate.

4.2.5.1. Fire size

As shown in Figure 63 (where the average velocity vector flow field is presented for the 6.0 m ceiling domain and for the three heat release rates 500, 1000 and 1500 kW using a constant water flow rate of 3.16 l/s) that the boundary layer gets closer to the water spray when the size of the fire is increased. At 500 kW the boundary was at Z= 3.2 m, for 1000 kW the boundary was at Z= 4.4 m and for 1500 kW it reached Z= 5.0 m.

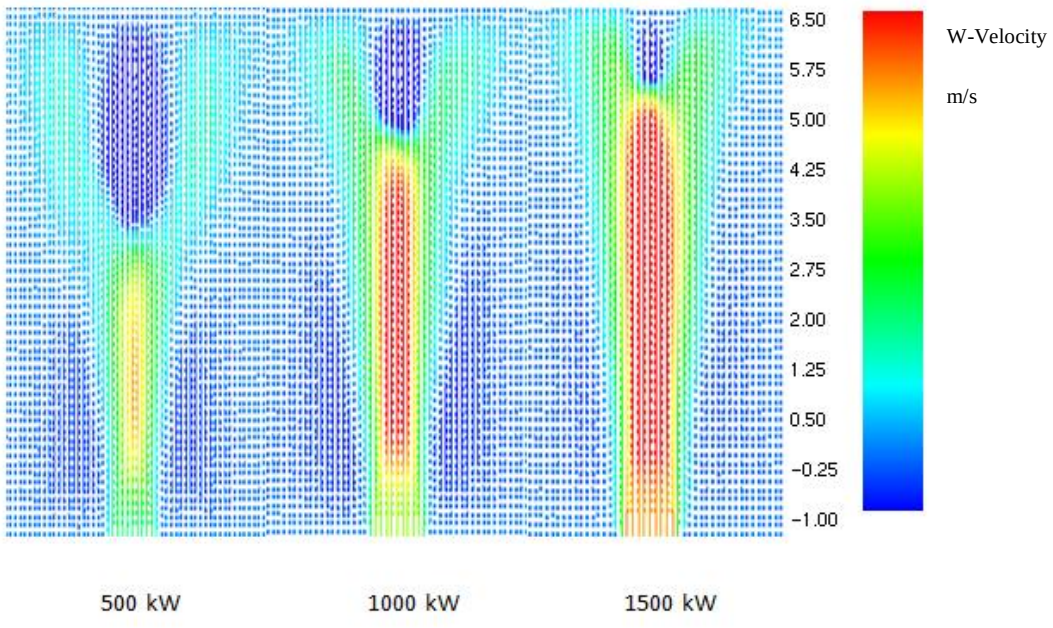

Figure 63 Velocity vector fields comparison based on the fire size

4.2.5.2. Spray angle

As it is shown in figure 64, the distance of the boundary layer for the interaction between the spray and the plume from the sprinkler is at least doubled when the spray angle decreased to half of its value. That was expected after the analysis done before where the flow rate per unit area for at the axis of the spray was almost doubled when decreasing the spray angle value to half of its value. This sensitivity analysis was done using the flow rate of 1.90 l/s under 3.0 m ceiling.

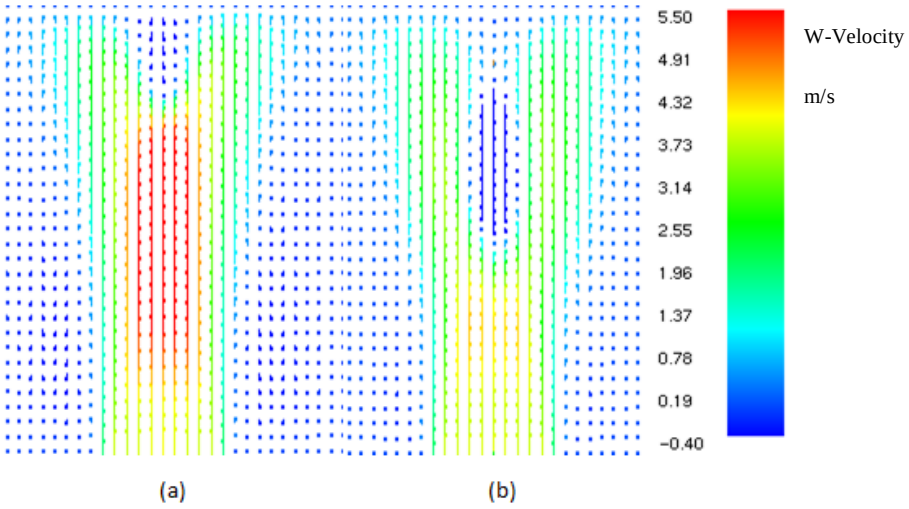

Figure 64 Velocity vector fields comparison based on the spray angle (Angle.1 (a) and Angle.2 (b))

4.2.5.3. Droplet size

As presented in Figure 65 (the average velocity vector fields for the 6.0 m ceiling cases with 1000 kW plume), the size of the droplet affects the boundary layer for the interaction between the spray and the hot air plume. As the spray's droplet diameter increase the boundary layer slightly approaches to near the sprinkler, that trend is opposite to the PR trend where the PR increase with the increase of the droplet size, it however, confirm the trend of the ADD in case of fire where it was found that at this case the ADD decreased very slightly with the increase of the droplet size at 1000 kW.

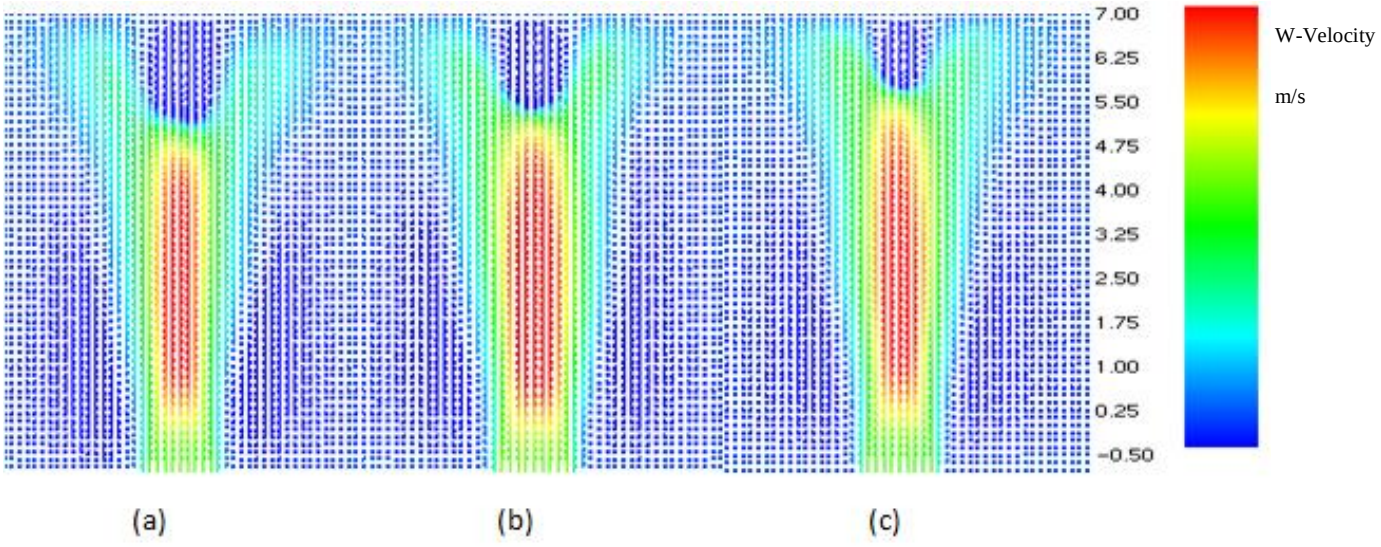

Figure 65 Velocity vector fields comparison based on the droplet size (Do(a), 1.25Do(b) and 1.5Do(c))

4.2.5.4. Water flow rate effect

Figure 66 (a, b, c, d, e and f) for the flow rates (1.90, 3.16, 4.42, 6.26, 7.58 and 9.48 l/s) respectively (for the 1500 kW case under 6.0 m ceiling height), presents the effect of the increase of the water flow rate on the position of the boundary layer.

As it is clear that the boundary layer moved away from the sprinkler position with the increase of the flow rate and also there was a great displacement when the flow rate increased from 4.42 to 6.26 l/s, as these velocity patterns are for the 1500 kW case under 6.0 m ceiling it was noticed that the great displacement happened exactly when the flow rate increased from that corresponding to the lowest PR value (4.42 l/s) to the optimum flow rate value (6.26 l/s) .This means that the optimum flow rate can be determined visually by using the smoke view.

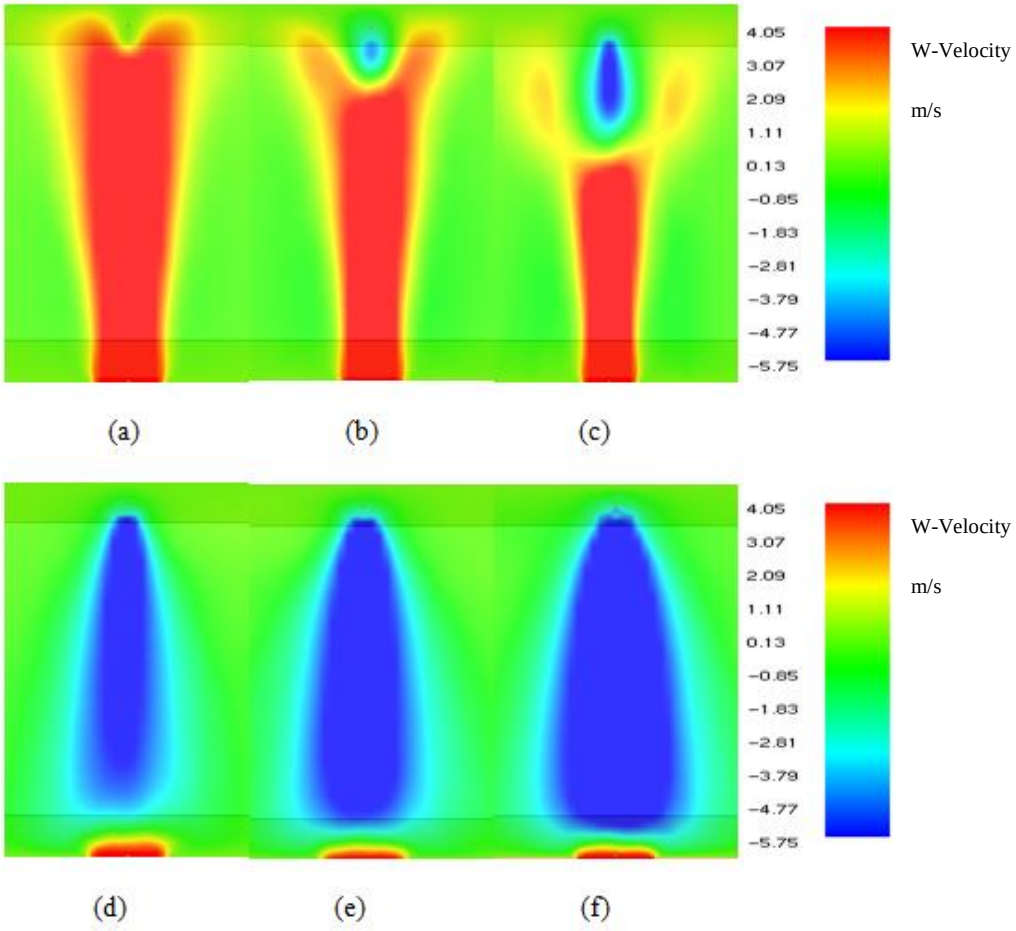

Figure 66 Average velocity flow field for the six different flow rates

5. Computational time

One of the main goals of this research was to substitute the combustion pool fires by hot air plumes, not only to decrease the computational time but also to propose a methodology that can be used in the experimental work as well. Doing experiments using the hot air instead of the real pool fires will be cheaper, easier and safer as well. Based on that, we highly recommend doing experimental work to validate the hot air models proposed in the gas phase section. If there is a good matching between our findings (data) and the experimental ones, there should be a great reduction in the experimental cost and also some of the computational work when using the hot air plumes. In this section an overview of the computational times for the previously mentioned simulations will be provided for both the gas and water phase.

5.1. The computational time for the gas phase only

As shown in Figure 67, the computational time for the combustion pool fire and all the hot air cases is almost the same at 100 kW, so it is recommended to just use the pool fire simulations in case of studying the pool fire solely at low HRRs. The computational time starts to increase with the increase of the HRR, for the 500 kW the computational time when using the hot air with Deardroff model only is 35 % less than that of the pool fire, when using the SEM the computational time increases by 24 % however, it is still less than the combustion pool fire by 25 %.For the 1000 kW, the computational time deviation between the hot air using Deardroff and that of the combustion pool fire increased to around 55 % less time when using only Deardroff and up to 30 % less when using Deardroff + SEM, yet, the deviation between using Deardroff only and Deardroff with SEM increased to 55 % extra computational time. For the 1500 kW, the deviation between the case of using Deardroff and that of the combustion pool fire increased to 60 % less computational time (when using Deardroff only) and the deviation between the Deardroff with SEM and that of the combustion pool fire decreased to 12 % less computational time (when using Deardroff + SEM) and also the deviation between using SEM and only Deardroff decreased to 45 % more computational time (when adding the SEM).

5.2. Computational time for the two phases

The computational time at the 3.0 m ceiling height was computed using the four heat release rates using both combustion pool fire and hot air (model B with SEM). As shown in Figure 68 (where CTF is the Computational Time using combustion pool Fire and CTA is the Computational Time using hot Air in the interaction simulations), the computational time using the combustion pool fires is lower than that of using the hot air at high heat release rates namely 1000 kW and 1500 kW with deviations up to - 80 %. While at lower HRR the deviation decreased to a maximum of - 10 % at 500 kW. The computational time for using hot air is lower than that of using the combustion pool fires at lower HRRs as shown for the 100 kW, with a decrease of computational time up to 32 %.

So to summarize this section:

- When simulating pool fires only, it is better to use the combustion pool fires at lower HRR like 100 kW as the computational time is the same as that for the hot air. However, for higher heat release rates, it is much cheaper to use the hot air modeling.
- When simulating the smoke – water interaction for high heat release rates more than or equal 500 kW it is better to use the combustion pool fire simulations as it gives lower computational time for this range of heat release rates. However, for heat release rates less than 500 kW it is cheaper to use the hot air models.
- Doing experiments using model A and B to simulate real fires could be possible as it is proved computationally to be possible and giving good reasonable out puts.
- Also it is good to note that, couple of simulation using the dynamic Smagorinsky turbulence model in the interaction simulations showed very high computational time, so it was decided not to go further into the analysis of the computational time using Smagorinsky's model. It seems to give much higher computational times but it cannot be verified by only couple of simulations and more simulations could be done in future work to verify it on a long range of heat release rates and water flow rates.

Despite the pervious analysis, we found by the end of this research that the combustion pool fire simulations cannot give reasonable data expect with a cell size of at least 0.10 m. However, the hot air simulations were found to give reasonable data which can be considered as cell-size independent with a maximum error of 9 % when we used 0.15 m cell size. As shown in Figure 69, the cell size of 0.20 m is far from that of the 0.10 m, however, the 0.15 m cell size is showing good match with an acceptable error.

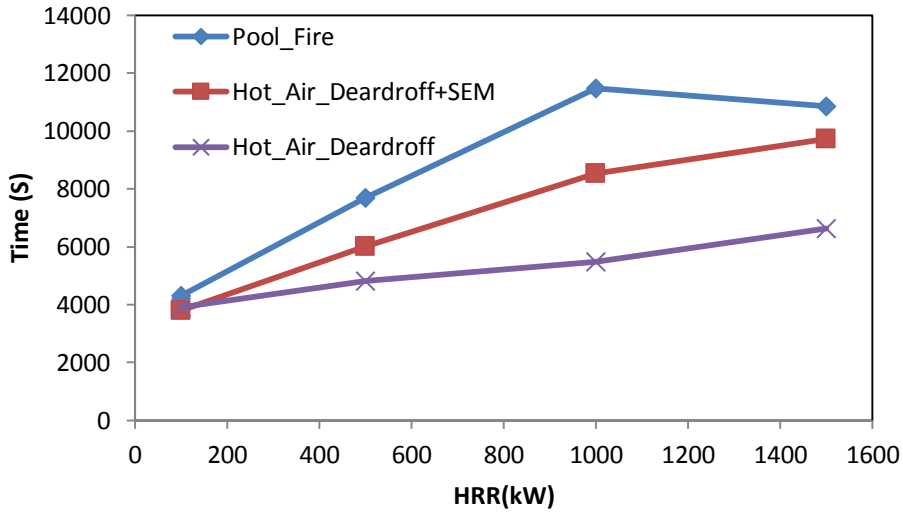

Figure 67 Computational time vs. HRR

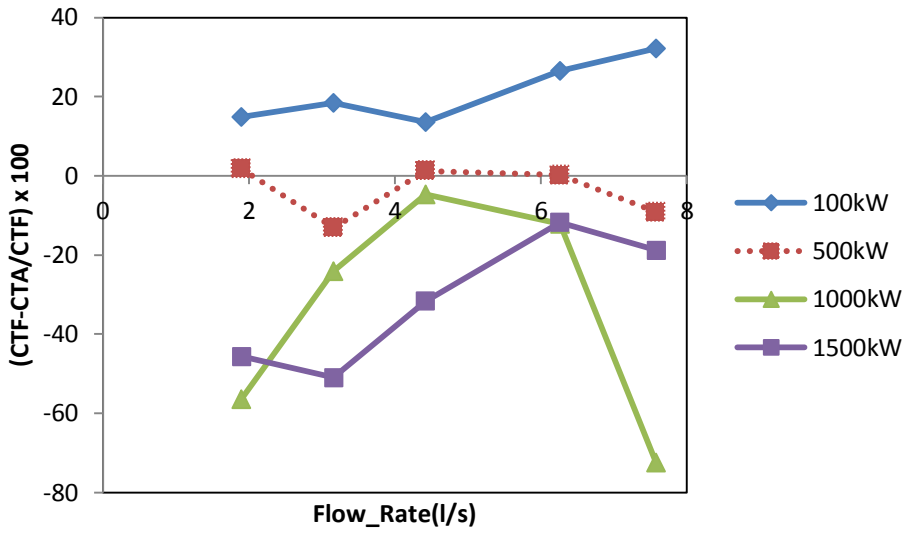

Figure 68 Ratio between the computational time using pool fires and hot air with SEM at ceiling of 3.0 m height

We also did a sensitivity analysis to ensure that using the cell size of 0.15 in the interaction simulations is acceptable and as shown in Figure 70, the cell size of 0.15 m is showing very good performance compared to the finer cell sizes. Based on that, we could have use 0.15 m cell size for the interaction simulations between the hot air and the water sprays but we could not do that for the combustion simulations. This comes as a strong point in the benefit of the hot air models, more investigation is needed indeed to ensure that the 0.15 m cell size is working perfectly and then it could be concluded that the hot air can work with much cheaper and faster simulations when compared to the combustion simulation for both cases gas phase only and the interaction between the gas and water phases.

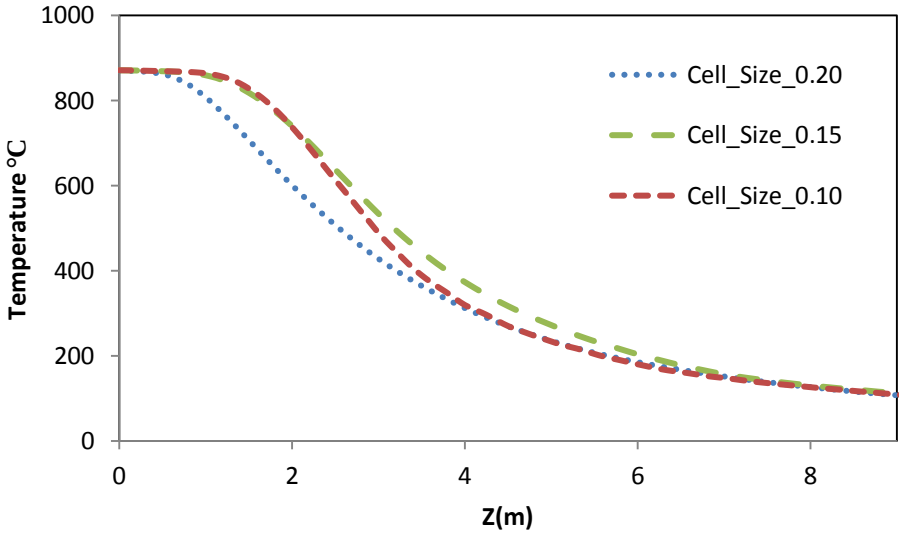

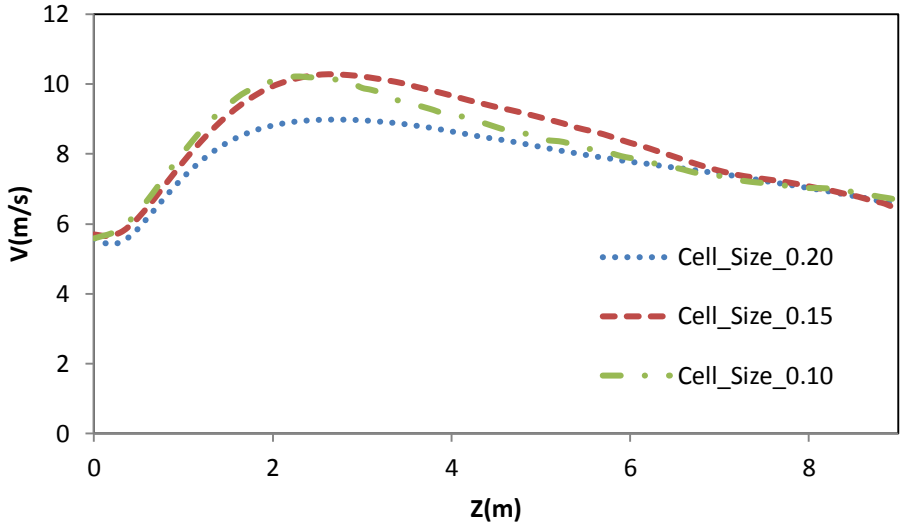

Figure 69 Cell_Size_Senstivity_Analysis_Hot_Air_500kW

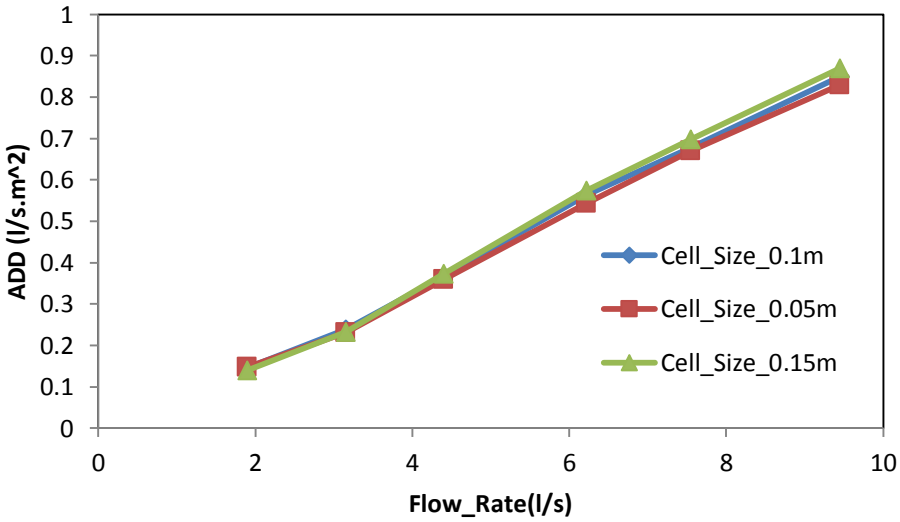

Figure 70 Cell Size Analysis for 1000 kW hot air_ spray interaction

6. Conclusions and discussions

6.1. Gas phase (hot air)

To substitute the heptane pool fire simulations with hot air simulations, two hot air models were discussed in this research to estimate the boundary conditions for the velocity and temperature at the inlet of the hot air flows. The first one was proposed by O Mégret and the second one was developed in this research, where the two models were named as model A and model B respectively. Model A is showing Froude numbers higher than that of Model B at the inlet conditions for the following Heat Release Rates (HRRs): 500, 1000 and 1500 kW. Lower value of Froude number means that this flow tends more toward the buoyancy driven flows which is more like real fires. Based on that, it was expected that model B will give better results than model A when compared to the combustion pool fires. It was also found that, using the default Deardroff turbulence model only will not help the hot air models to perform like the combustion simulations with respect to the velocity and temperature values along the z-axis. It was also found that using the Synthetic Eddy Method (SEM) to generate some synthetic turbulence at the boundary of the hot air flow was essential and gave very promising results. The sensitivity analysis shows that the number of eddies used in the SEM did not have any noticeable effect on the velocity or the temperature flow field and can be decreased down to 100 eddies, which have a positive impact on the computational time by decreasing it. Also a sensitivity analysis for the eddy length scale was done and showed primarily that it is not the most sensitive parameter when using the SEM in this case.

It was found for the three fire sizes that, both of the two models under estimate the temperature before and at the flame height, however, model B is showing less deviation from the combustion simulations than model A. It was also noted that, both of the two models match each other after 1.0 m from the flame height and match the combustion simulations after 2.0 m from the flame height.

For the velocity profiles, the two models are matching each other from the flame height onwards independent on the fire size. Specifically speaking; for the 500 kW fire, the velocity profiles before and after the flame height is well predicted by both of the two model, however, both of the two models are overestimating the velocity after the flame height by 18 and 13 % for the 1000 and 1500 kW fires respectively.

A comparison with experimental work for another hydrocarbon fuel (Propane) with total heat release rate (HRR) of 39 kW was done using model B. Model B predicted the temperature and velocity very well at the flame height and up to three times the flame height. Yet, after the flame height model B underestimated the temperature and overestimating the velocity by a maximum deviation of 30 %. However, both of the two simulations for velocity and temperature seem to be very promising, not only because of the low HRR of the propane experiments so we covered wider range of heat release rates but also because the model is compared to real experimental work not simulations or empirical correlations. This means that, it can give good results experimentally, therefore, that opens the door in front of doing some experiments' validations for this model. In addition to that, all the pervious simulations were done for the heptane pool fires, while this comparison was done with propane burners, which also show a good positive point toward model B, as it can also cover different hydrocarbon fuels.

The radial profile of the velocity using model B was compared to the velocity radial profile using the combustion simulations in both far and near fields and it shows perfect matching for the whole range of heat release rates [500, 1000 and 1500 kW] and for both near and far fields.

6.2. Water phase

Numerical simulations were conducted to investigate the performance of the ESFR sprinkler sprays with (1.90, 3.16, 4.42, 6.26, 7.58 and 9.48 l/s) flow rates, under two ceiling heights namely (3.0 and 6.0 m). The sprinkler spray model was described by assigning the water particle size, particle discharge speed and the spray angle. It was possible by changing the spray angle to assign near similar ADD values of the sprinkler spray used in [4] under both the 6.0 m and 3.0 m ceiling heights. However, based on the fact that there won't be direct numerical comparisons with the simulations in [4] because of the modified pool fire they used; it was found to just keep the simulations with angle set 1 as default for all the simulations. The water flux was computed radially and the ADD was computed over an area of 5.23 m^2 (1.29 m radius). The following was found in this section:

- The calculations seem to be insensitive to the changes in the number of tracked droplets in the Lagrangian approach and the default value of 5000 can be used.
- The effect of the spray angle on the water flux seems to have its extreme effect at the spray axis.
- The spray angle seems to have constant effect based on the ceiling height variation for the same target.
- The ADD value increased with the increase of the flow rate.
- The ADD value over a 1.29 m radius circle under the 6.0 m ceiling was less than that for the 3.0 m ceiling; however, this difference decreases as the flow rate increases.
- To independently study the effect of the drop size and the momentum, two simulations were done by increasing the default value of the drop size by 1.25 and 1.5 times at constant momentum and increase of the momentum by 1.25 and 1.5 times at constant drop size. It was found that, increasing the drop size shows a decrease in the ADD which was only significant under 6.0 m ceiling and was not showing any effect under the 3.0 m ceiling height. The momentum increase was done only under the 6.0 m ceiling height and it showed that the ADD decrease with the increase of the momentum.
- A sensitivity analysis for the sprinkler's parameters on the radial velocity distribution was done, to know which parameter affects the radial velocity of the sprinkler spray the most. This sensitivity analysis was done on two fields' far field and near field. The changed parameters were (the droplet size, the total angle and the inner angle).It was found that, the spray angles has the most influence on the velocity at the axis and radially where the velocity increased to the double at the axis when the total angle is decreased to the half, however, this influence vanishes at around 1.0 m from the axis and then the trend is switched, where the smaller angle is showing slightly lower velocity. That means that the larger angle is having higher momentum radially while the smaller angle is having higher momentum at the axis. On the other hand, when the inner angle is changed from 0 to 4° the velocity decreases at the axis to near zero and the velocity creates two peaks on the two sides of the axis instead of one

peak at the axis. The velocity at the two peaks reached the same velocity of the 0 inner angle flows for the same radial position and then is showing to be slightly higher radially. Additionally, The velocity is decreasing at the axis when using higher drop size, yet, the influence of the drop size on the velocity decreased till it vanishes around 1.0 m away from the axis. The same findings where observed in the near field however the effect seems to be less.

6.3. Spray-smoke interaction

In this section the main concern was given to the Penetration Ratio (PR) capabilities for different sprinklers. First, few simulations were done to ensure that the same results are captured using pool fire simulations and hot air simulations and it was found to be perfectly matching. Six flow rates sprinklers, two ceiling heights and three fire sizes were used as main parameters in this analysis. Then a sensitivity analysis for the effect of the drop size, momentum and the spray angle was investigated. In addition to that, an extra ceiling height of 8.0 m was investigated to cover a wider range of ceiling heights. The following were found in this section:

- The ADD of a specific sprinkler increases as the flow rate increases for a given a fire and decreases as the fire size increase for a given flow rate.
- The flow rate corresponding to the minimum penetration ratio increases as the fire size increases, that means, the drop size effect on the penetration capabilities increases as the fire size increase.
- The PR value increases as the drop size increases, also the PR increases with the increase of the momentum, however, the increase in the PR capabilities due to the increase of the momentum of the water flow from a specific sprinkler is less than that due to the increase of the drop size. The same trend was found in [4].
- The optimum operational flow rate value increases with the increase of the ceiling height, where the optimum value for the 3.0 m ceiling height is 4.42 l/s and for the 6.0 m and 8.0 m is 6.26 l/s.
- The ADD and the PR increases with the decrease of the ceiling height. In [4] it was found that, the ADD increases with the decrease of the ceiling height as well, however, the PR decreases with the decrease of the ceiling height (with some exceptions), that could be because of the fire source in [3 and 4]. That's why in this research we broaden the range of the ceiling heights used to ensure that the founded trends are precise.
- The ADD values without fires are higher for the target areas with smaller radii, probably because the ADD is usually higher near the axis. This fact was verified under the three ceiling heights. However, the deviation in the ADD values between the different target areas is decreasing and is approaching to zero with the increasing of the ceiling height and decreasing the flow rate.
- The PR was found to be lower when the target area is of smaller radii and the fire (hot air plume) covers a bigger portion of the area, which is expected to be due to the big portion of high momentum air in the target area. The effect of the target area was more obvious at the 3.0 m ceiling where higher optimum flow rates were observed. This effect seems to demolish

with the ceiling height increase as the same optimum operational flow rate was found for the 6.0 and 8.0 m ceiling heights.

- It was noted that, when the target area is 1.29 m radius the optimum flow rate increases with the increase of the height and when the target area was exactly the fire area, the optimum flow rate decreases with the increase of the height
- It was found that, by decreasing the spray angle to the half of its value the penetration ratio will increase for the same flow rate, however, the optimum flow rate will decrease.
- The boundary layer of the interaction between the two flows gets closer to the sprinkler when the fire size is increased.
- The boundary layer position gets almost double its distance far from the sprinkler when the spray angle is doubled.
- The boundary layer position gets closer to the sprinkler position when the droplet size is increased. Based on what was previously mentioned, the increase of the drop size will decrease the ADD, increase the PR and make the interaction boundary layer approaches more towards the sprinkler position.
- There will be a big displacement in the position of the boundary layer when the flow rate increased from the flow rate corresponding to the lowest PR to the optimum flow rate and the optimum flow rate can easily be determined by the smoke view visualization.

All in all, the simulations show that there is always an optimal flow rate to give the highest penetration ratio for a specific range of flow rates, fire sizes and under a specific ceiling height. Where in this research it is 6.26 l/s for the 6.0 m ceiling and 4.42 l/s for the 3.0 m ceiling .It was also proved that the rate the PR increase by increasing the drop size is higher and more significant than that by increasing the spray velocity (momentum).

6.4. Computational time

In this section the computational time were investigated to give a general sense about how expensive is it to run each case using hot air with the default Deardroff turbulent model only, hot air with the default Deardroff model + SEM and the combustion pool fire simulations using the same cell size of 0.10 m. The following points were noted:

- When only doing pool fire simulations, the 100 kW simulations for all of the three cases is giving the same computational time. The computational time starts to increase with the increase of the HRR where the difference between the Hot air simulations and the pool fire simulations also increases with the increase of the HRR. The computational time of the hot air plumes + SEM was less than the combustion pool fire simulations by 25 %, 30% and 15% at heat release rates of 500 kW, 1000 kW and 1500 kW respectively.
- When comparing the computational time of using the hot air + SEM and the combustion in the interaction simulations, it was found that at high heat release rates the combustion pool fires is showing lower computational times and the difference decreases by the decrease of the heat release rate till it almost reach zero at 500 kW. Then the hot air + SEM is showing faster computational time less than the 500 kW.

- Based on this cell size and these simulations, it can be recommended to use the hot air models especially in the small fire sizes.
- Another sensitivity analysis for the cell size was done using cell size of 0.15 m for the hot air simulations + SEM and it was found to give reasonable outputs with an error less than 9 % of that with 0.10 m cell size, that means, the hot air simulations could have been done using the 0.15 cell size. However, the combustion pool fires cannot be simulated with cell size of less than 0.10 m, therefore, even in the case of bigger fires in case of interaction simulations the computational time for the hot air models will be lower because it can be simulated using bigger cell sizes.

All these computational simulations are still in need to be validated by bench mark experimental work. Also all the conclusions and findings in this research should not be taken for granted or used for design purposes. However, these findings are seen as promising results and indeed it should be investigated experimentally later.

7. Acknowledgment

This thesis was done in the last semester of my master program. The International Master of Science in Fire Safety Engineering (IMFSE) is a joint program between three full partner universities namely (Ghent university, Lund university and the university of Edinburgh) and three associated partner universities namely (University of Maryland, University of Queensland and ETH Zurich).

First of all, I would like to thank the IMFSE scientific board for offering me admission to this program and all the scientific staff of the IMFSE in Ghent University, Lund University and the University of Edinburgh for all the interesting lectures and knowledge I was offered during this master.

I would like to thank my promoter and supervisor prof. Bart Merci for hosting me in his research group for an internship last year and then for my master thesis work this year.

I would like to take the opportunity to express my deep gratitude for the support and help I got from my promoter and supervisor dr. Tarek Beji. This thesis work would have never been done without your guidance, aid and encouragement.

I would also like to thank all my IMFSE class mates with whom I have shared the last two years of my life.

Lastly, I would love to thank my parents, brothers and sister for all the support and encouragements they offered me in the last two years, despite the fact that I was hundreds of miles away from home; they were always in contact to share their love. Without you I would have never been doing what I am doing now.

I want to end my acknowledgment with Richard Feynman (Nobel Prize winner)'s quote "I don't know anything, but I do know that everything is interesting if you go into it deeply enough"

8. References

1. Anthony D. Putorti (2004), Simultaneous Measurements of Drop Size and Velocity in Large-Scale Sprinkler Flows Using Particle Tracking and Laser-Induced Fluorescence. NIST GCR 04-861
2. Takieddin, S. (2016), Numerical Investigation of Spray-Plume Interactions. *Master Thesis, Ghent, Ghent University*.
3. Nam, S.(1996) Development of Computational Model Simulating the Interaction between a Fire Plume and Sprinkler Spray, *Fire Safety Journal*, 26(1): 1-33.
4. Nam, S.(1999) Numerical Simulation of the Penetration Capability of Sprinklers Sprays, *Fire Safety Journal*, 32: 307-329
5. Marshall, A.W. and Di Marzo, M. (2004) Modeling Aspects of Sprinkler Spray Dynamics in Fire, *Process Safety Environmental Protection*, 82(B2): 97–104
6. Zhou, X. (2015) Characterization of interaction between hot air plumes and water sprays for sprinkler protection, *Proceedings of the Combustion Institute*, 35:2723-2729.
7. O.Mégret, O. Vauqelin (2000) A model to evaluate tunnel fire characteristics. *Fire Safety Journal*, 34: 393-401.
8. McCaffrey (1979) Purely Buoyant Diffusion Flames: Some Experimental Results. National Bureau of Standards, NBSIR79-1910.
9. Kung, H.C. and Stravrianides, P. (1982) Buoyant Plumes of Large Scale Pool Fires. *Proceedings of the Combustion Institute*, 19: 905-912.
10. Merci, B. and Beji, T. (2016) Fluid Mechanics Aspects of Fire and Smoke Dynamics in Enclosures. Taylor and Francis Group, London, UK.
11. Koseki H, Hayasaka H. (1989) Estimation of Thermal Balance in Heptane Pool Fire. *Journal of Fire Sciences*.7: 237-250
12. Babrauskas, V.(1983) Estimating Large Pool Fire Burring Rates. *Fire Technology Journal*. 19: 251-261.
13. Koseki H, Yumoto T.(1988) Air Entrainment and Thermal Radiation from Heptane Pool Fires. *Fire Technology*. 24: 33-47.
14. Drysdale D. (2011) An Introduction to Fire Dynamics. Wiley, New York, 2011.
15. Baum, H.R., McGrattan, K.B. & Rehanm, R.G. (1997) Three Dimensional Simulations of fire plume. *Fire Safety Science proceedings of the fifth International Symposium*.
16. Ma, T.G. & Quintiere J.G. (2003) Numerical Simulation of Axi-symmetric Fire Plumes: Accuracy and Limitations. *Fire Safety Journal*. 38(5):467-492
17. Jarrin, N. (2008) Synthetic Inflow Boundary Conditions for the Numerical Simulations of Turbulence. *PhD Thesis. Manchester, the University of Manchester*.
18. Gengembre, E., Cambray, P., Karmed, D. & Bellet J.C. (1983) Turbulent Diffusion Flames with Large Buoyancy Effects. *Combustion Science and Technology*. 41: 55-67.
19. Zukoski, E.E., Kubota, T. and Cetegen, B. (1981) Entrainment in Fire Plumes, *Fire Safety Journal*. 3: 107
20. H.M.I. Mahmud, K.A.M. Moinuddin and G.R. Thorpe., 2012. Characterization of a water-mist spray: Numerical modeling and experimental validation. *18th Australasian Fluid Mechanics Conference Launceston, Australia.*

21. Ren, N., Blum, A., Zheng, Y., Do, C. and Marshall, A., 2008. Quantifying the Initial Spray from Fire Sprinklers. *Fire Safety Science* 9: 503-514.
22. Sheppard, D.,(2002) ‘‘Spray Characteristics of Fire Sprinklers,’’ *PhD Thesis NIST GCR 02-838*, Northwestern University, USA.
23. Beji, T., Ebrahimzadeh, S., Maragkos, G. and Merci, B, 2017. Influence of the particle injection rate, droplet size distribution and volume flux angular distribution on the results and computational time of water spray CFD simulations. *Proceedings of 12 th international Symposium on fire safety science.*
24. Ebrahimzadeh,S., 2016. Extensive Study of the Interaction of a Hot Air Plume with a Water Spray by Means of CFD Simulations. *PhD thesis*, Ghent University, Belgium.
25. Fire Dynamics Simulator Technical Reference Guide, *NIST Special Publication* 1018-1 Sixth Edition.
26. Fire Dynamics Simulator User’s Guide, *NIST Special Publication* 1019 Sixth Edition.

9. Appendix

1. FDS input file for combustion pool fire (500 kW)

```
&HEAD CHID='Combustion_500', TITLE='Combustion_500' /
&MESH IJK=50,50,100, XB=0, 5,0,5,0,10/

&TIME T_END=60/

&RADI RADIATIVE_FRACTION = 0.30, RADIATION=.FALSE. /

&REAC ID                ='Heptane',
    SOOT_YIELD          = 0.0037,
    CO_YIELD            = 0.0010,
    C                   = 7.,
    H                   = 16.,
    O                   = 0.
    HEAT_OF_COMBUSTION  = 44580./

&MATL ID                = 'Heptane LIQUID'
    EMISSIVITY          = 1.
    NU_SPEC             = 1.
    SPEC_ID             = 'Heptane'
    CONDUCTIVITY        = 0.14
    SPECIFIC_HEAT       = 2.24
    DENSITY             = 675./

&SURF ID                = 'Heptane POOL'
    STRETCH_FACTOR      = 1
    CELL_SIZE_FACTOR    = 1
    COLOR               = 'ORANGE'
    MATL_ID(1,1)        = 'Heptane LIQUID'
    BACKING             = 'EXPOSED'
    THICKNESS           = 0.100/

&SURF ID='Heptane POOL', MLRPUA=0.0160 /

&OBST XB= 2, 3, 2, 3, 0.000, 0.10, SURF_IDS='Heptane POOL','INERT','INERT'/

&VENT MB='XMIN', SURF_ID='OPEN' /
&VENT MB='XMAX', SURF_ID='OPEN' /
&VENT MB='YMIN', SURF_ID='OPEN' /
```

```
&VENT MB='YMAX', SURF_ID='OPEN' /
&VENT MB='ZMAX', SURF_ID='OPEN' /
&SLCF PBY=2.5, QUANTITY='TEMPERATURE'/
&SLCF PBY=2.5, QUANTITY='W-VELOCITY'/
&SLCF PBY=2.5, QUANTITY='U-VELOCITY'/
&TAIL/
```

2. FDS input file for hot Air model A, 500 kW

```
&HEAD CHID='Smoke_Model_A_500', TITLE='Smoke_Model_A_500' /

&MESH IJK=50,50,100, XB=0,5,0,5,0,10.0/

&TIME T_END=60 /

& RADI RADIATION=.FALSE./

&SURF ID='HOT_AIR', VEL= -2.17 , TMP_FRONT= 531,COLOR='RED'/

&VENT XB= 2.0, 3.0,2.0, 3, 0.0, 0.0 , SURF_ID='HOT_AIR',N_EDDY= 1000,L_EDDY=0.1,
VEL_RMS=1.86/

&VENT MB='XMIN', SURF_ID='OPEN' /
&VENT MB='XMAX', SURF_ID='OPEN' /
&VENT MB='YMIN', SURF_ID='OPEN' /
&VENT MB='YMAX', SURF_ID='OPEN' /
&VENT MB='ZMAX', SURF_ID='OPEN' /

&SLCF PBY=2.5, QUANTITY='TEMPERATURE'/
&SLCF PBY=2.5, QUANTITY='W-VELOCITY'/

&TAIL /
```

3. FDS input file for hot air model B, 500 kW

```
&HEAD CHID='Smoke_Model_B_500', TITLE='Smoke_Model_B_500' /

&MESH IJK=50,50,100, XB=0,5,0,5,0,10.0/
```

&TIME T_END=60 /

&RADI RADIATION=.FALSE./

&SURF ID='HOT_AIR', VEL= -2, TMP_FRONT=871,COLOR='RED'/

&VENT XB= 2.0, 3.0,2.0, 3, 0.0, 0.0 , SURF_ID='HOT_AIR',N_EDDY= 1000,L_EDDY=0.1, VEL_RMS=1.86/

&VENT MB='XMIN', SURF_ID='OPEN' /
&VENT MB='XMAX', SURF_ID='OPEN' /
&VENT MB='YMIN', SURF_ID='OPEN' /
&VENT MB='YMAX', SURF_ID='OPEN' /
&VENT MB='ZMAX', SURF_ID='OPEN' /

&SLCF PBY=2.5, QUANTITY='TEMPERATURE'/
&SLCF PBY=2.5, QUANTITY='W-VELOCITY'/

&TAIL /

4. FDS input file for water phase to calculate the radial water flux (3.0 m ceiling and flow rate 3.16 l/s)

&HEAD CHID='ESFR_2'/
&MESH IJK=50,50,15,XB=-5,5,-5,5,0,3/

/&TIME T_END=0.0/
&TIME T_END=60/
&MISC TMPA=20./
&RADI RADIATION=.FALSE./

/====================SPRAY=========

&SPEC ID='WATER VAPOR'/

&PART ID='waterdrops', SPEC_ID='WATER VAPOR', DIAMETER= 1050, GAMMA_D = 2.5/

&PROP ID='spr_FM', PART_ID='waterdrops', OFFSET=0.20, FLOW_RATE=189, PARTICLE_VELOCITY= 12, SPRAY_ANGLE= 0,78, PARTICLES_PER_SECOND=5000./

&DEVC XYZ=0,0,2.6, PROP_ID='spr_FM', ID= 'Spr', QUANTITY= 'TIME', SETPOINT= 0./

```
/==================================OPEN BOUNDRY CONDITIONS=========

&VENT MB='XMIN', SURF_ID='OPEN'/
&VENT MB='XMAX', SURF_ID='OPEN'/
&VENT MB='YMIN', SURF_ID='OPEN'/
&VENT MB='YMAX', SURF_ID='OPEN'/
&VENT MB='ZMIN', SURF_ID='OPEN'/

/===============Water Flux Measurements==============

&PROP ID='pdpa_flux', PART_ID='waterdrops', QUANTITY='PARTICLE FLUX Z',
PDPA_RADIUS=0.15, PDPA_START=10., PDPA_END=60./

&DEVC XYZ=0.0,0,0, QUANTITY='PDPA', PROP_ID='pdpa_flux', ID='PF-1' /
&DEVC XYZ=0.4,0,0, QUANTITY='PDPA', PROP_ID='pdpa_flux', ID='PF-2' /
&DEVC XYZ=0.8,0,0, QUANTITY='PDPA', PROP_ID='pdpa_flux', ID='PF-3' /
&DEVC XYZ=1.2,0,0, QUANTITY='PDPA', PROP_ID='pdpa_flux', ID='PF-4' /
&DEVC XYZ=1.6,0,0, QUANTITY='PDPA', PROP_ID='pdpa_flux', ID='PF-5' /
&DEVC XYZ=2.0,0,0, QUANTITY='PDPA', PROP_ID='pdpa_flux', ID='PF-6' /
&DEVC XYZ=2.4,0,0, QUANTITY='PDPA', PROP_ID='pdpa_flux', ID='PF-7' /
&DEVC XYZ=2.8,0,0, QUANTITY='PDPA', PROP_ID='pdpa_flux', ID='PF-8' /
&DEVC XYZ=3.2,0,0, QUANTITY='PDPA', PROP_ID='pdpa_flux', ID='PF-9' /
&DEVC XYZ=3.6,0,0, QUANTITY='PDPA', PROP_ID='pdpa_flux', ID='PF-10' /
&DEVC XYZ=4.0,0,0, QUANTITY='PDPA', PROP_ID='pdpa_flux', ID='PF-11' /
&DEVC XYZ=4.4,0,0, QUANTITY='PDPA', PROP_ID='pdpa_flux', ID='PF-12' /
&DEVC XYZ=4.8,0,0, QUANTITY='PDPA', PROP_ID='pdpa_flux', ID='PF-13' /
==================================================================

&  TAIL/
```

5. FDS input file for calculating the ADD at a target area of 1.29 m, 0.69 m and 0.56 m radius (6.0 m ceiling and water flow rate of 3.16 l/s)

```
&HEAD CHID='ESFR_2'/
&MESH IJK=50,50,30,XB=-5,5,-5,5,0,6/

/&TIME T_END=0.0/
&TIME T_END=60/
&MISC TMPA=20./
&RADI RADIATION=.FALSE./
```

/====================SPRAY=========

&SPEC ID='WATER VAPOR'/

&PART ID='waterdrops', SPEC_ID='WATER VAPOR', DIAMETER= 1050, GAMMA_D = 2.5/

&PROP ID='spr_FM', PART_ID='waterdrops', OFFSET=0.20, FLOW_RATE=189, PARTICLE_VELOCITY= 12, SPRAY_ANGLE= 0,78, PARTICLES_PER_SECOND=5000./

&DEVC XYZ=0,0,5.6, PROP_ID='spr_FM', ID= 'Spr', QUANTITY= 'TIME', SETPOINT= 0./

/==================================OPEN BOUNDRY CONDITIONS=========

&VENT MB='XMIN', SURF_ID='OPEN'/
&VENT MB='XMAX', SURF_ID='OPEN'/
&VENT MB='YMIN', SURF_ID='OPEN'/
&VENT MB='YMAX', SURF_ID='OPEN'/
&VENT MB='ZMIN', SURF_ID='OPEN'/

/===============Water Flux Measurements==============

&PROP ID='pdpa_flux', PART_ID='waterdrops', QUANTITY='PARTICLE FLUX Z', PDPA_RADIUS=1.29, PDPA_START=10., PDPA_END=60./

&DEVC XYZ=0.0,0,0, QUANTITY='PDPA', PROP_ID='pdpa_flux', ID='PF-1' /

&PROP ID='pdpa_flux_2', PART_ID='waterdrops', QUANTITY='PARTICLE FLUX Z', PDPA_RADIUS=0.69, PDPA_START=10., PDPA_END=60./

&DEVC XYZ=0.0,0,0, QUANTITY='PDPA', PROP_ID='pdpa_flux_2', ID='PF-2' /

&PROP ID='pdpa_flux_3', PART_ID='waterdrops', QUANTITY='PARTICLE FLUX Z', PDPA_RADIUS=0.564, PDPA_START=10., PDPA_END=60./

&DEVC XYZ=0.0,0,0, QUANTITY='PDPA', PROP_ID='pdpa_flux_3', ID='PF-3' /

& TAIL/

6. **FDS input file for the interaction simulation at 6.0 m ceiling height, hot air (model B) = 500 kW and flow rate = 3.16 l/s**

```
&HEAD CHID='ESFR_2'/
&MESH IJK=100,100,60,XB=-5,5,-5,5,0,6/

/&TIME T_END=0.0/
&TIME T_END=80/
&MISC TMPA=20./
&RADI RADIATION=.FALSE./

/====================SPRAY=========

&SPEC ID='WATER VAPOR'/

&PART ID='waterdrops', SPEC_ID='WATER VAPOR', DIAMETER= 1050, GAMMA_D = 2.5/

&PROP ID='spr_FM', PART_ID='waterdrops', OFFSET=0.20, FLOW_RATE=189, PARTICLE_VELOCITY= 12, SPRAY_ANGLE= 0,78, PARTICLES_PER_SECOND=5000./

&DEVC XYZ=0,0,5.6, PROP_ID='spr_FM', ID= 'Spr', QUANTITY= 'TIME', SETPOINT= 10/

/========================HOT AIR===============

&SURF ID='HOT_AIR', VEL= -2, TMP_FRONT=871,COLOR='RED'/

&VENT XB= -0.5, 0.5,-0.5, 0.5,0,0 , SURF_ID='HOT_AIR',N_EDDY= 1000,L_EDDY=0.1, VEL_RMS=3/

/==================================OPEN BOUNDRY
CONDITIONS=========

&VENT MB='XMIN', SURF_ID='OPEN'/
&VENT MB='XMAX', SURF_ID='OPEN'/
&VENT MB='YMIN', SURF_ID='OPEN'/
&VENT MB='YMAX', SURF_ID='OPEN'/

&SLCF PBY=0, QUANTITY='TEMPERATURE'/
&SLCF PBY=0, QUANTITY='W-VELOCITY'/

/===============Water Flux Measurments==============
```

&PROP ID='pdpa_flux', PART_ID='waterdrops', QUANTITY='PARTICLE FLUX Z', PDPA_RADIUS=1.29, PDPA_START=10., PDPA_END=80./

&DEVC XYZ=0.0,0,0, QUANTITY='PDPA', PROP_ID='pdpa_flux', ID='PF-1' /

&PROP ID='pdpa_flux_2', PART_ID='waterdrops', QUANTITY='PARTICLE FLUX Z', PDPA_RADIUS=0.69, PDPA_START=10., PDPA_END=80./

&DEVC XYZ=0.0,0,0, QUANTITY='PDPA', PROP_ID='pdpa_flux_2', ID='PF-2' /

&PROP ID='pdpa_flux_3', PART_ID='waterdrops', QUANTITY='PARTICLE FLUX Z', PDPA_RADIUS=0.564, PDPA_START=10., PDPA_END=80./

&DEVC XYZ=0.0,0,0, QUANTITY='PDPA', PROP_ID='pdpa_flux_3', ID='PF-3' /

==========

& TAIL/

7. Combustion simulations, hot air simulations and McCaffrey

500 kW:

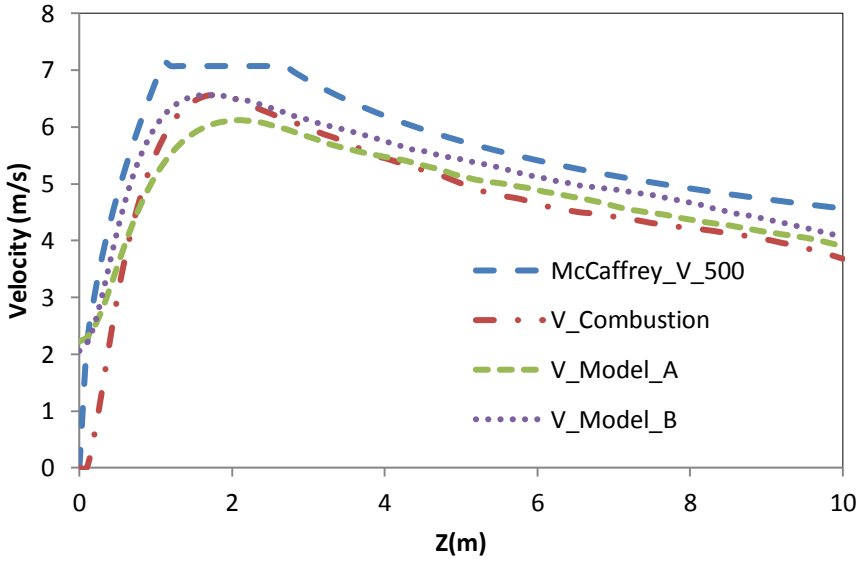

(a)

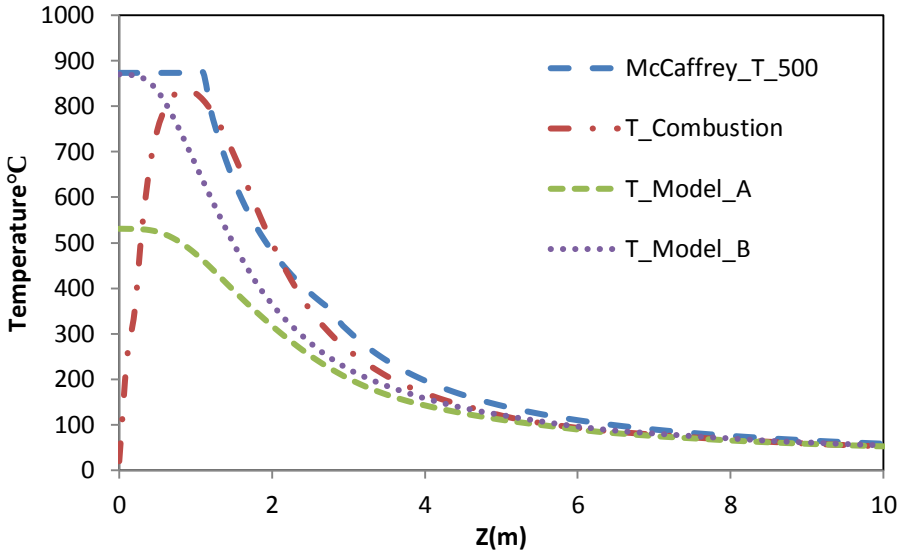

(b)

Velocity (a) and temperature (b) patterns averaged along the plume height for hot air and combustion simulations vs. McCaffrey correlations [$\dot{Q}_c = 500\ kW$]

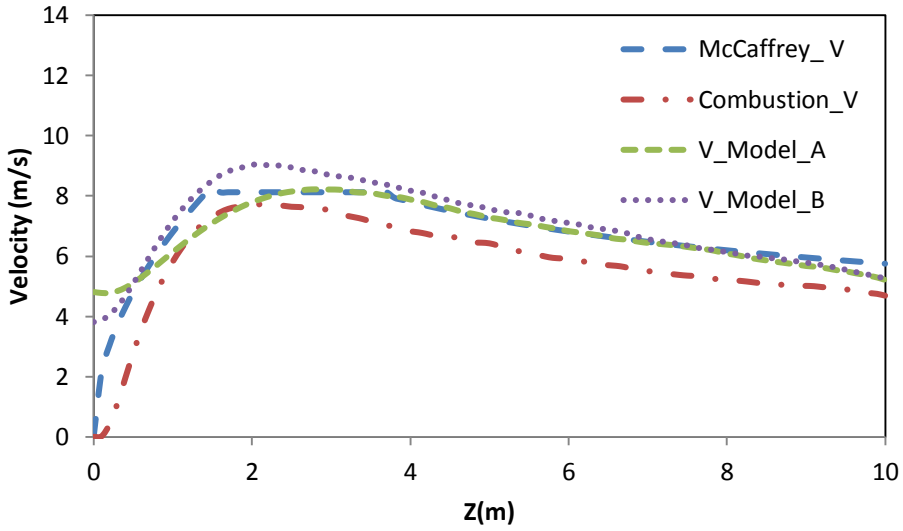

(a)

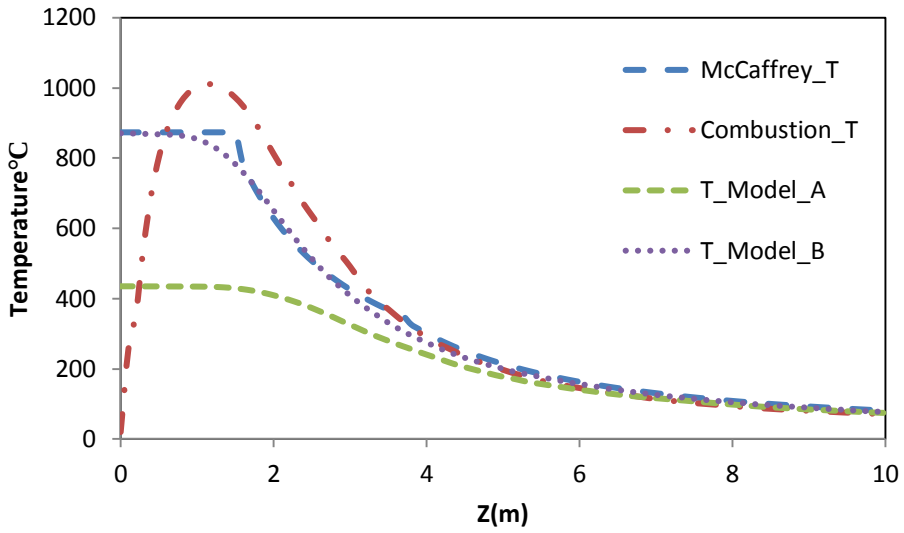

(b)

Velocity (a) and temperature (b) patterns averaged along the plume height for hot air and combustion simulations vs. McCaffrey correlations [$\dot{Q}_c = 1000\ kW$]

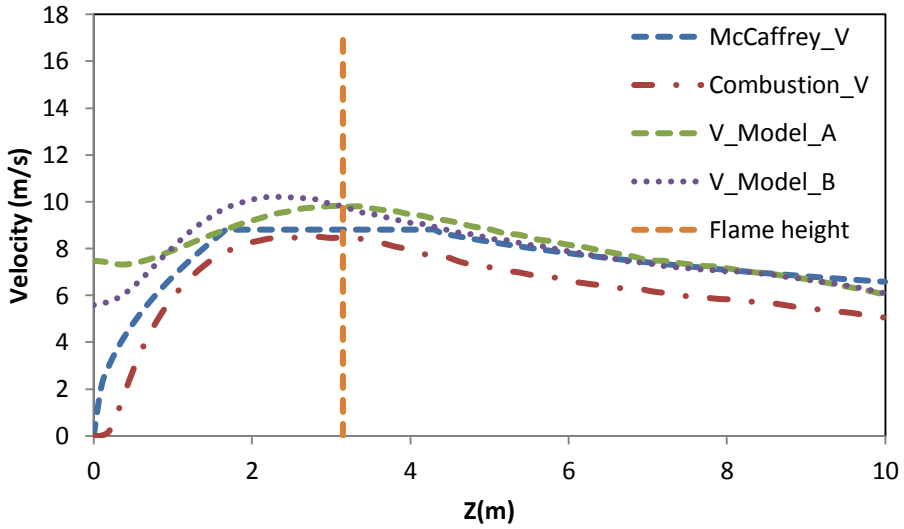

(a)

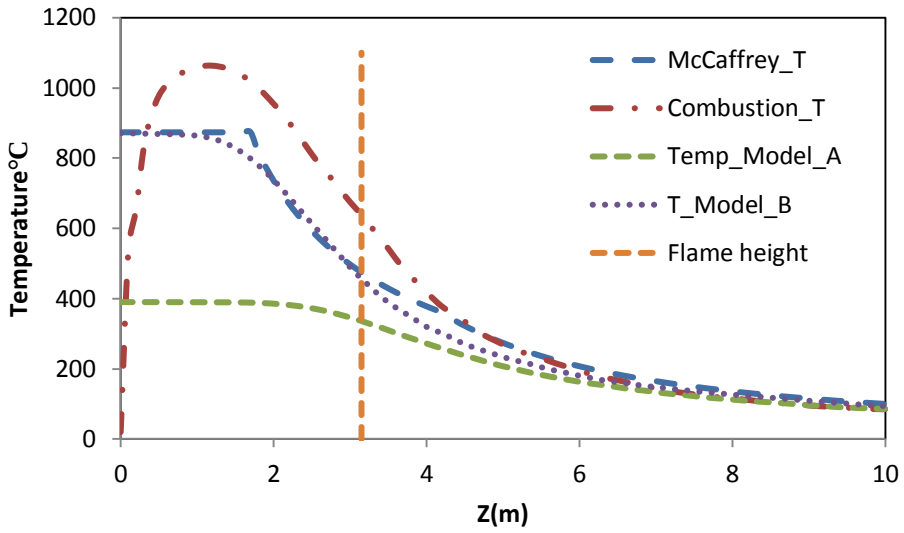

(b)

Velocity (a) and temperature (b) patterns averaged along the plume height for hot air and combustion simulations vs. McCaffrey correlations [$\dot{Q}_c = 1500\ kW$]